

T 1299

THE SPLIT HOPKINSON BAR METHOD
OF ROCK TESTING

by

Paul P. Wu

ProQuest Number: 10781676

All rights reserved

INFORMATION TO ALL USERS

The quality of this reproduction is dependent upon the quality of the copy submitted.

In the unlikely event that the author did not send a complete manuscript and there are missing pages, these will be noted. Also, if material had to be removed, a note will indicate the deletion.



ProQuest 10781676

Published by ProQuest LLC (2018). Copyright of the Dissertation is held by the Author.

All rights reserved.

This work is protected against unauthorized copying under Title 17, United States Code
Microform Edition © ProQuest LLC.

ProQuest LLC.
789 East Eisenhower Parkway
P.O. Box 1346
Ann Arbor, MI 48106 – 1346

T 1299

A thesis submitted to the Faculty and the Board of Trustees of the Colorado School of Mines in partial fulfillment of the requirements for the degree of Master of Science in Mining Engineering.

Signed: Paul P. Wu
Paul P. Wu

Golden, Colorado

Date: July 1, 1971

Approved: William A. Hustrulid
William A. Hustrulid
Thesis Advisor

Albert M. Keenan
Albert M. Keenan
Head of Department
Mining Engineering

Golden, Colorado

Date: Dec 8, 1971

ARTHUR LAKES LIBRARY
COLORADO SCHOOL OF MINES
GOLDEN, COLORADO

ABSTRACT

ARTHUR LAKES LIBRARY
COLORADO SCHOOL OF MINES
GOLDEN, COLORADO

The split Hopkinson bar has been used for about 20 years to study properties of rock and rock failure under dynamic loading conditions. The mathematical analysis needed to construct stress-strain curves from the measured waves requires that the rock specimen be very short compared to the wave length of the impact generated wave. In practice, specimens of several different lengths are often used with different length waves, always making the assumption that the specimen is "short" enough for the analysis to apply. This paper describes the results of a study on the effect of the stress-strain curves derived from strain wave measurements and the behavior of four common rock types under impact generated waves.

TABLE OF CONTENTS

	Page
INTRODUCTION	1
LITERATURE REVIEW.	4
Hopkinson Pressure Bar Device	4
Dynamic Behavior of Rock.	9
Dynamic Stress-Strain Curves.	9
Dynamic Strength of Rock.	10
Dynamic Modulus	12
Strain Wave Transmission and Fracture Mechanism.	13
THEORETICAL ANALYSIS	16
Average Stress and Average Strain	19
Average Strain Rate	23
Energy Loss in Specimen	24
COMPUTER SIMULATION OF THE SPLIT HOPKINSON BAR	25
EXPERIMENTATION.	38
Description of the Split Hopkinson Bar.	38
Testing Procedure	43
Data Reduction.	44
TESTS AND RESULTS.	52
Stress-Strain Behavior.	52
Strain Wave Transmission and Energy Loss in the Specimen	63
Fracture of Rock Under the Split Hopkinson Bar Test.	75

	Page
DISCUSSION	88
Dynamic Loading and Unloading Processes	88
Elastic Moduli for a Major and Minor Stress Cycle	95
Strain Rate Sensitivity of the Compressive Strength.	98
A Statistical Model of Strain Wave Transmission in the Specimen	104
Factors Influencing the Results	111
Uniformity of Stress Within the Specimen. . .	111
Loading History of the Specimen	115
Frictional End Effect	118
CONCLUSIONS.	119
APPENDIX I	121
APPENDIX II.	124
APPENDIX III	128
APPENDIX IV.	130
APPENDIX V	132
APPENDIX VI.	133
APPENDIX VII	135
BIBLIOGRAPHY	139

LIST OF FIGURES

Figure	Page
1. Forces acting on element of an elastic rod.	17
2. A rock specimen sandwiched between the ends of the steel bars	20
3. A diagrammatic representation of the trans- mitted and reflected waves produced by a wave incident at the steel-rock interface.	27
4. Reflected and transmitted strain-time curves calculated using plane wave theory for specimens of various lengths assuming a given incident waveform	30
5. Comparison of stress-strain curves derived from the strain waves of figure 4 with the given value (E_R).	31
6. The effect of neglecting the time (Δt) required for a wave to traverse the specimen on the derived stress-strain curves.	33
7. Comparison of derived stress-strain curves for a given specimen length and various incident wave lengths	34
8. Comparison of derived stress-strain curves for a given specimen length and various incident wave lengths	35
9. Split Hopkinson bar apparatus	39
10. Diagrammatic representation of a split Hopkinson bar	41
11. Oscilloscope pictures of the recorded strain- time waves (Colorado Red Granite and Yule Marble)	45
12. Oscilloscope pictures of the recorded strain- time waves (Indiana Limestone and Gray Sandstone).	46

Figure	Page
13. Analysis of strain waves for a typical experiment.	49
14. Derived average stress-strain curve (specimen G-104).	51
15. Dynamic stress-strain curves for Gray Sandstone using a 1-in. striker at increasing striking velocities.	53
16. Dynamic stress-strain curves for Indiana Limestone for successive impacts using several striker lengths	54
17. Dynamic stress-strain curves for Colorado Red Granite for successive impacts using a 5-in. striker	56
18. Experimental static and dynamic stress-strain curves for Colorado Red Granite	57
19. Experimental static and dynamic stress-strain curves for Yule Marble.	58
20. Experimental static and dynamic stress-strain curves for Indiana Limestone.	59
21. Experimental static and dynamic stress-strain curves for Gray Sandstone	60
22. Correlation of the incident energy, maximum stress and percent energy loss with the number of consecutive strikes-specimen G-121, length = 1.045 in.	72
23. Correlation of the incident energy, maximum stress and percent energy loss with the number of consecutive strikes-specimen G-221, length = 1.568 in.	73
24. Correlation of the incident energy, maximum stress and percent energy loss with the number of consecutive strikes-specimen G-321, length = 2.011 in.	74
25. Longitudinal cross section of Colorado Red Granite specimen loaded in the static testing machine (SL-101, 1-in. long).	77

Figure	Page
26. Longitudinal cross section of Colorado Red Granite specimen loaded in the static testing machine (SL-102, 1-in. long).	78
27. Longitudinal cross section of Colorado Red Granite specimen loaded in the static testing machine (SL-103, 1-in. long).	79
28. Longitudinal cross section of Colorado Red Granite specimen loaded in split Hopkinson bar (DL-104, 1-in. long).	81
29. Longitudinal cross section of Colorado Red Granite specimen loaded in the split Hopkinson bar (DL-107, 1-in. long).	82
30. Longitudinal cross section of Colorado Red Granite specimen loaded in the split Hopkinson bar (DL-155, 1.5-in. long).	83
31. Longitudinal cross section of Colorado Red Granite specimen loaded in the split Hopkinson bar (DL-158, 1.5-in. long).	84
32. Transverse cross section of Colorado Red Granite specimen loaded in the split Hopkinson bar (G-103, 0.25-in. from the impacted end)	85
33. Standard stress-strain curves for static and dynamic loading	89
34. Idealized force-displacement curves for components of testing system (Wawersik, 1968).	92
35. A complete force-displacement curve for Tennessee Marble (Wawersik, 1968)	94
36. Directions of movement around major and minor stress cycles (Cook and Hogson, 1965)	97
37. A schematic diagram of the statistical stress distribution in the specimen.	101
38. Energy transmission in Tennessee Marble, 5.0-in. striker (Hakalehto, 1967)	106
39. Total recovered strain energy in Colorado Red Granite	107

Figure	Page
40. Incident and average stress-time waves.	109
41. Observed strain-time wave on the specimen surface	113
42. Comparison of an average strain-time wave with a measured strain-time wave.	114
43. Loading history of the specimen	116
44. Wheatstone bridge circuit	131
45. Elastic constants for bar material (stainless steel cylinder) under static loading	132
46. Diagrammatic representation of the static testing apparatus	134
47. Diagrammatic representation of the resonant frequency apparatus	137

LIST OF TABLES

Table	Page
1. The energy consideration of an incident sinusoidal stress pulse related to specimen length and stress pulse length	37
2. Dynamic and static Young's modulus for four rock types.	62
3. Dynamic and static uniaxial compressive strength values	64
4. Analysis of the energy content in strain waves. .	66
5. Energy loss in specimen subjected to multiple impact-specimen G-121, length = 1.045 in.	69
6. Energy loss in specimen subjected to multiple impact-specimen G-221, length = 1.568 in.	70
7. Energy loss in specimen subjected to multiple impact-specimen G-321, length = 2.011 in.	71
8. Calculations of dynamic Young's modulus from the resonant frequencies.	138

ACKNOWLEDGMENTS

The author wishes to thank Dr. William A. Hustrulid for his suggestions, guidance, and encouragement throughout this research. Appreciation is extended to Dr. Hormuzd Rassam, Prof. Niles E. Grosvenor, and Dr. B. W. Paulding for their advice and assistance.

The author is indebted to Colorado School of Mines Research Foundation for sponsoring this research (Grant F-6908), and is grateful for the support provided by the National Defense Education Act of 1958.

Special thanks are extended to Mr. Earl Dickens for directing the construction of the split Hopkinson bar in the CSM instrument shop. Mr. Raymond Frahm, research technician in the Department of Mining, assisted in the development of the electronic instrumentation.

LIST OF SYMBOLS

Symbol	Unit	Definition
A	(in) ²	cross-sectional area of the steel bar or specimen
A ₀	(lb)(in) ⁻²	maximum stress amplitude of an assumed elastic sine wave
a	(in)	radius of the steel bar or specimen
C	(in)	average crack length
c	(in)(sec) ⁻¹	longitudinal wave velocity in the steel bar or specimen
c ₁	(in)(sec) ⁻¹	longitudinal wave velocity in the first media
c ₂	(in)(sec) ⁻¹	longitudinal wave velocity in the second media
c _r	(in)(sec) ⁻¹	longitudinal wave velocity in the specimen
c _s	(in)(sec) ⁻¹	longitudinal wave velocity in the steel bar
E	(lb)(in) ⁻²	Young's modulus of the steel bar or specimen
E _{ab}	(millivolt)	input voltage of the Wheatstone bridge system
E _{cd}	(millivolt)	output voltage of the Wheatstone bridge system
E _i	(in)(lb)	energy incident upon first bar-specimen interface
E _l	(in)(lb)	energy loss in the specimen
E _{mv}	(in)(lb)	energy used in the motion of the rock fragments

Symbol	Unit	Definition
E_0	(in)(lb)	all forms of energy losses other than E_{sf} and E_{mv}
E_R	(lb)(in) ⁻²	Young's modulus of the rock specimen
E_r	(in)(lb)	energy reflected back into first steel bar
E_s	(lb)(in) ⁻²	Young's modulus of the steel bar
E_{sf}	(in)(lb)	energy used in creation of new fracture surface
E_{sp}	(in)(lb) ⁻²	specific fracture energy of the rock specimen
E_T	(in)(lb)	total energy contained in an elastic wave
E_t	(in)(lb)	energy transmitted into second steel bar
F	-	strain gage factor
$F_{1(Net)}$	(lb)	net applied force across specimen-bar interface 1
$F_{2(Net)}$	(lb)	net applied force across specimen-bar interface 2
$F(S; \sigma)$	-	the probability that the local stress in the specimen exceed the local strength S
f_b	(sec) ⁻¹	longitudinal resonant frequency including pole pieces correction
f'_b	(sec) ⁻¹	measured longitudinal frequency from resonant frequency method
$f(\sigma; \bar{\sigma})$	-	a probability density function of variable σ , $\bar{\sigma}$ is the statistical average stress
I	(milliamp)	current through the gages in Wheatstone bridge circuit
K	-	a material constant defined by equation (4-6)

Symbol	Unit	Definition
KE	(in)(lb)	kinetic energy contained in an elastic wave
l	(in)	length of the specimen
n	-	number of reflections in the specimen
m	-	resistance ratio between fixed resistors in the Wheatstone bridge circuit
PE	(in)(lb)	potential energy contained in an elastic wave
R	(ohms)	total gage arm resistance for the Wheatstone bridge circuit
S	(lb)(in) ⁻²	local strength of rock specimen or Griffith's critical fracture stress
s	(millivolt) ⁻¹	sensitivity of the Wheatstone bridge system
t	(sec)	time variable
t_1	(sec)	period of the incident wave
t_2	(sec)	period of the reflected wave
u	(in)	longitudinal displacement in the steel bar or specimen
u'	(in)	longitudinal displacement contributed from the incident strain wave at specimen-bar interface 1
u''	(in)	longitudinal displacement contributed from the reflected strain wave at specimen-bar interface 1
$u_{1(Net)}$	(in)	net longitudinal displacement at specimen-bar interface 1
$u_{2(Net)}$	(in)	longitudinal displacement contributed from the transmitted strain wave at specimen-bar interface 2 or net longitudinal displacement at specimen-bar interface 2

Symbol	Unit	Definition
V_b	$(\text{in})(\text{sec})^{-1}$	calculated longitudinal bar velocity including lateral inertial correction
V_b'	$(\text{in})(\text{sec})^{-1}$	calculated longitudinal bar velocity from resonant frequency method
v	$(\text{in})(\text{sec})^{-1}$	particle velocity in the steel bar or specimen
W'	(gms)	weight of both pole pieces used in measure the resonant frequency of the specimen
W	(gms)	weight of specimen
X	(in)	distance measured along the axis of the steel bar
α	-	frictional coefficient between specimen and bars
γ	$(\text{lb})(\text{in})^{-1}$	specific surface energy of the rock
γ'	$(\text{gms})(\text{in})^{-3}$	specific weight of specimen
Δl	(in)	portion of the steel bar which contains the elastic wave
Δm	$(\text{lb})(\text{sec})^2(\text{in})^{-1}$	mass of a portion of the steel bar which contains the elastic wave
Δt	(sec)	time required for the wave to travel through specimen of length l
ϵ	-	longitudinal strain
ϵ_i	-	incident longitudinal strain amplitude
ϵ_r	-	reflected longitudinal strain amplitude
ϵ_t	-	transmitted longitudinal strain amplitude
$\bar{\epsilon}$	-	longitudinal average strain across a specimen of length defined by equation (3-15)

Symbol	Unit	Definition
$\dot{\epsilon}_{avg}$	-	average strain rate in a specimen of length defined by equation (3-20)
ζ	(in)	radial displacement of the steel bar
λ	(in)	wave length of an assumed elastic sine wave
μ	-	Poission's ratio of the steel bar
ξ	(in)	longitudinal displacement at the end of the steel bar
$\dot{\xi}$	(in)(sec) ⁻¹	partical velocity at the end of the steel bar
π	-	a mathematical constant equals 3.14159...
ρ	(lb)(sec) ² (in) ⁻⁴	mass density of the steel bar of specimen
ρ_1	(lb)(sec) ² (in) ⁻⁴	mass density of the first media where an elastic wave travels through
ρ_2	(lb)(sec) ² (in) ⁻⁴	mass density of the second media where an elastic wave enters
ρ_r	(lb)(sec) ² (in) ⁻⁴	mass density of the rock specimen
ρ_s	(lb)(sec) ² (in) ⁻⁴	mass density of the steel bar
σ	(lb)(in) ⁻²	longitudinal stress in the steel bar or specimen
σ_i	(lb)(in) ⁻²	incident longitudinal stress amplitude
σ_r	(lb)(in) ⁻²	reflected longitudinal stress amplitude
σ_t	(lb)(in) ⁻²	transmitted longitudinal stress amplitude
$\bar{\sigma}$	(lb)(in) ⁻²	longitudinal average stress across a specimen of length defined by equation (3-18)

INTRODUCTION

A knowledge of the dynamic properties of rock is important both for the development of improved rock fragmentation methods (percussive drilling, rock blasting, etc.) as well as the improved design of structures constructed in or on rock subjected to dynamic loading. Although a large amount of applied research has been done in drilling and blasting, there is little information on the basic behavior of rock under dynamic loading conditions.

It is usually stated that rock can withstand much higher stresses and exhibits a higher elastic modulus under very short duration loads than under those applied over an extended period. The mechanism governing this rock behavior, however, is not fully understood. In this thesis some basic work concerning this phenomenon will be described.

A direct measurement of stress and strain while a specimen is being deformed under a transient loading cycle is not easily achieved. The methods such as the pulse or resonance techniques are often employed to determine elastic rock properties. Since the induced stress pulses are rather low in amplitude, the response of rock in the fracture range cannot be achieved by these methods.

Although several methods have been used to obtain dynamic rock properties at high stress level, the Hopkinson

split bar is perhaps the simplest one. The device consists basically of two cylindrical steel bars to which strain gages have been bonded, the specimen which is sandwiched between the bars, and the loading system. In many laboratories including that of the present author, the loading system consists of a striker which is accelerated down a long tube under the action of compressed air and impacts the end of the first steel bar. Quite a range of loading rates can be produced by merely changing striker length and controlling the velocity at impact. As the impact-produced strain wave $\epsilon_i(t)$ reaches the specimen, part of the wave is reflected $\epsilon_r(t)$ back into the bar and part is transmitted $\epsilon_t(t)$ into the second steel bar. From measurements of the incident, reflected, and transmitted waves and assuming plane wave theory to apply, one can construct stress-strain curves for the rock specimen. A comparison of these "derived" dynamic curves and dynamic constants with those obtained by other methods and static methods can then be made.

Although the technique described above is very attractive because of the relatively simple equipment required and the range of loading rate possible, difficulties have been found in deriving stress-strain curves. A detailed analysis of the averaging process used in the wave analysis method in the composition of dynamic stress-strain curves by an elastic model and computer simulation will be given.

In this investigation, the split Hopkinson bar technique was applied to the study of some common types of rocks. The loading pulse is of the order of 20-50 micro-seconds in duration, with peak stress amplitudes exceeding the fracture strength of rock. Studies were also made on the strain wave transmission and energy dissipation in the intact and partially failed rock specimens. Polished sections were prepared at a number of points in the failure region and an examination of the fracture patterns made.

LITERATURE REVIEW

Hopkinson Pressure Bar Device

In recent years the Hopkinson pressure bar has become an increasingly popular tool in the study of the dynamic response of materials. The device was introduced by Hopkinson (1914) to investigate the propagation of stress pulses on a laboratory scale and was later used to study the nature of the pressure-time relations when an explosive was detonated or when a projectile impinged on a hard surface.

Hopkinson's apparatus consisted of a cylindrical steel bar several feet in length and about an inch in diameter which was suspended horizontally by four threads so that it could swing in a vertical plane. At one end of the bar a short cylindrical pellet known as the time-piece was wrung on, and a transient pressure was applied at the other end (known as the firing end of the bar). The time-piece was of the same diameter and of the same material as the bar. The faces of the time-piece and the end face of the bar to which it was attached were ground flat. The time-piece was held to the bar by magnetic attraction or by smearing a little grease on the two ground faces.

When a bullet impinges on the firing end of such a bar, or when an explosive charge is detonated in contact with it,

a compression pulse travels down the bar. It is assumed that the diameter of the bar is small compared with the length of the pulse, and the material of the bar is not stressed beyond its proportional elastic limit. Such a compression pulse will be transmitted through the joint between the bar and the time-piece without change in form, and will then be reflected at the free end of the time-piece as a tensile pulse. This reflected tensile pulse will travel back through the tail of the incident compression pulse, and as soon as a net tensile force is built up across the joint between the bar and the time-piece, the latter will fly off with the momentum trapped in it. This momentum was measured by capturing the time-piece in a ballistic pendulum, and at the same time the momentum remaining in the bar could be determined from the amplitude of swing of the bar. A time-piece half the length of the pulse will trap all the momentum, leaving the bar at rest. The duration of the pulse can be obtained if (1) the minimum length of time-piece which leaves the bar undisturbed, and (2) the velocity of longitudinal waves in the material of the bar are known.

By measuring the momentum trapped in time-pieces of different lengths, the areas under the pressure-time curves for different intervals can be obtained. The precise shape of the pressure-time curve cannot, however, be deduced from such measurements since the points of commencement of the

different intervals are not known.

Davies (1948) devised a pressure bar which allowed a continuous measurement of the longitudinal displacement produced by the pressure pulse at the free end of the bar to be made.

According to one dimensional wave theory, the longitudinal stress σ is proportional to the particle velocity $\partial u/\partial t$, the relation being

$$\sigma = \rho C \frac{\partial u}{\partial t} \quad (2-1)$$

The free end of the bar has twice the particle velocity of any cross-section within the bar

$$\dot{\xi} = 2 \frac{\partial u}{\partial t} = 2 \frac{\sigma}{\rho C} \quad (2-2)$$

where

ξ is the longitudinal displacement at the end of the bar

$\dot{\xi}$ is the particle velocity at the end of the bar

C is the longitudinal wave velocity in the bar.

The displacement-time curve $\xi(t)$ can be obtained directly. By differentiating this curve a stress-time curve for the pulse can be determined. If the radial displacement ζ is measured at the same point along the bar and the definition of Poisson's ratio is used, one finds that

$$\zeta = \frac{\nu \sigma}{E} \quad (2-3)$$

where

a is the radius of the bar

ν is the Poisson's ratio

E is the Young's modulus.

The stress-time curve is found simply by multiplying the ordinate of the $(\zeta \cdot t)$ curve by the factor $E/\nu a$.

The form of the Hopkinson pressure bar presently, in most common use, is patterned after that first devised by Kolsky (1949). Here a short compressive specimen is sandwiched between two pressure bars and is loaded by a single pulse travelling through the system. The pressure bars in this arrangement are used both to (1) apply the load to the specimen, and (2) as transducers to measure the displacements and applied loads at the faces of the specimen in contact with the bars. This device is sometimes also known as a split Hopkinson bar.

Davies (1948) made a very complete theoretical study of the Hopkinson pressure bar in which he rather clearly defines its limits of application. The following are the assumptions on which the method is based.

(1) The waves propagated in the bar are elastic waves, i.e., the stress at every point in the bar must always lie within the region where the stress, strain curve is linear and reversible. With a given bar, this implies that there is an upper limit to the stress that can be measured with it, this limit being determined by the elastic and plastic properties of the material composing the bar.

(2) A pressure pulse is propagated without distortion. This assumption is only true when the wave-lengths of the elastic waves concerned in the propagation of the pulse are large compared with the lateral dimensions of the bar. When this condition is not fulfilled, the waves suffer dispersion and the form of the pulse is distorted as it travels along the bar.

(3) The pressure in the pulse is uniformly distributed over the cross section of the bar. This uniform distribution of pressure does occur provided that the duration of the pulse due to the applied pressure is not so small that dispersion is important and provided that the length of the bar is more than four diameters.

According to the limitations posted by Davies, various arrangements of specimen, bar, loading and measuring mechanisms are possible and have been employed. In Kolsky's work a specimen of geometry $a/l \ll 10$ (a is the radius of the specimen, l is the length of the specimen), and a pulse of sufficient length compared with the specimen length were used so that the difference in stress on the specimen faces could be neglected.

Allowance still had to be made for the inertial forces in the radial and tangential directions.

Davies and Hunter (1963) used a device similar to that of Kolsky's, but used a specimen having quite a different geometry. They used the criterion derived by Siebel (1923)

where α is the frictional coefficient between specimen and bars

$$2\alpha a/3l \ll 1 \quad (2-4)$$

so that frictional effects could be neglected. Hawkyard and Freeman (1954) have estimated α under conditions similar to those of the experiment to be between 0.02 and 0.06. Taking the larger of these values gives

$$a/l \ll 25 \quad (2-5)$$

Davies and Hunter in their work used this criterion and limited the minimum value of 'l' to be the same order as 'a' ($a/l \sim 1$). In addition to the radial and tangential forces of Kolsky's analysis the axial inertial forces must be considered.

Lindholm (1964) and Hakalehto (1967) used strain gages as a measuring device on both bars instead of the condenser transducers. In this way, the elastic strain-time curves in the steel bars are directly measured instead of the displacement-time curves.

Dynamic Behavior of Rock

Dynamic Stress-Strain Curves

The dynamic stress-strain behavior of rock was first reported by Attewell (1962). He used igneous and sedimentary specimens from less than 0.01-in. to 0.25-in. in length inserted in a split Hopkinson bar and subjected to high-

intensity stress pulses by means of explosive detonators. In his experiments, the displacement-time curves were measured by a parallel-plate capacitance gage and the curves were numerically differentiated to give the pulse amplitudes. The strains were obtained at 2-microsecond intervals. The stress-strain characteristics derived over a period of about 20 microseconds revealed that rocks develop considerable hysteresis and have little tendency to recover over the period of the pulse. He thus suggested a time-dependent visco-elastic model.

Hakalehto (1967) similarly used the split bar method to study the dynamic behavior of Tennessee marble (described as a pure calcite rock of very uniform grain size). The dynamic stress-strain curves were obtained using a short specimen (0.1-in. long) and two different lengths of strikers. No significant differences were found between the static and dynamic compressive strengths and the elastic moduli for the rock tested. He suggested that rock behaves similarly under static and dynamic loadings.

Dynamic Strength of Rock

The ultimate strength values of rock materials under impact loading are normally different from those under static loading. In addition, the strengths appear to increase with increasing strain rate. Attewell (1962) performed tests on thin sections of several igneous and sedimentary rocks and

found a much greater strength in dynamic compression than under simple static testing. Robertson (1955) also noted an increase in the yield strength of limestone compressed at impact loading rates.

The effect of the rate of application of load (or stress rate) on the strengths of two concretes having approximately static compressive strengths of 25 kpsi and 65 kpsi has been investigated by Wattstein (1953). A drop weight machine was used for the impact tests. The concrete was tested at stress rates ranging from 10 to 10^7 psi per second. The corresponding strain rates were of the order of 10^{-6} to 10 per second. He found that the compressive strength of each concrete increased with the rate of stressing.

Kumar (1968) measured the ultimate strengths of basalt and granite over a range of stress rates from 2×10 to 3×10^{10} psi per second (this corresponds to varying the elastic strain rates from 10^{-6} to 2×10^3 per second). He showed that the static strengths of basalt and granite were 27.5 and 29 kpsi, respectively, at the stress rate of 2×10 psi per second while their strengths at the stress rate of 3×10^{10} psi per second were 59 and 70 kpsi respectively.

Recent investigations in this field such as made by Friedman (1968) and Perkins et. al. (1969) similarly reported an increase in strength with increasing strain rates.

Attewell (1963) studied the tensile strength of rock rods subjected to tensile stress wave reflected from the

free end of the rock rod. He found that the apparent rock strength increased considerably under high loading rates, the differences being less pronounced for the harder igneous rocks which have a higher Young's modulus.

Bacon (1962) also reported that the dynamic tensile strength is one to four times the static tensile strength.

Dynamic Modulus

It is customary to measure the dynamic elastic modulus by the pulse technique (bar velocity), or resonance frequency method. The dynamic modulus obtained by these methods in which the stress amplitude of the applied sonic wave is relatively small. The values obtained in this way showed a slightly higher value than in the static case (Rinehart, et. al., 1961; Bacon, 1962). As will be shown later, the dynamic moduli obtained are actually an average value of a small stress-strain cycle at low stresses.

In impact loading of the specimen, a direct measurement of the stress-strain history of the specimen cannot be achieved. The average stress-strain curves are derived from wave analysis methods, the dynamic modulus thus obtained may not be the same as from other dynamic methods. A survey of the present literature showed a considerable scattering in the results. Since some of the methods used were not reported, disagreement between the results and those of the present author are expected.

The dynamic modulus obtained by Kumar (1968) for basalt (calculated as the ratio of average stress rate and average strain rate) was higher than obtained from the pulse technique. Friedman et. al. (1968) reported an increase in elastic modulus for Solenhofen limestone under split bar test over static loading. Perkins (1969) showed that tonalite was found to exhibit increased stiffness with increasing strain rate and decreasing temperature.

Strain Wave Transmission and Fracture Mechanism

When a transient pulse with a stress level above a critical value traverses a rock bar, energy is absorbed by fractures, grain cleavages, and in damage to grain to grain bonds. At low stress levels, little attenuation was found (Goldsmith et. al., 1966) as the stress pulse propagates in the rock bars. Attewell (1962) suggested that rocks do not behave truly elastically at high rates of strain and suggest that stress waves, when propagated through such media will be attenuated. He showed rocks to be frequently sensitive in attenuation, that is, there would appear to be a particular energy loss associated with a particular frequency within the composition of the wave.

Goldsmith et. al. (1966) observed the stress wave propagation in rock bars. No dispersion was found for any of the rock bars tested. Attenuation above certain stress levels was different for different rock types. Large grain

sizes were found to increase the attenuation. No plastic deformation was observed in any of the test bar failures.

In split Hopkinson bar experiments, the transmission of the stress wave through the specimen is complicated by the multiple reflections inside the specimens and possible energy loss between specimen-bar interfaces. Hakalehto (1967) studied the input and transmitted energy carried by the stress waves. He found that the amount of energy available to cause fracture growth depends on both the duration and the stress level of the impact waves. For a given input wave form, there exists a maximum amount of energy which can be transmitted through the rock specimen.

Miller (1966) has used a very short duration (5-microsecond) stress pulse (generated using under water discharge) to study the fracture of a heterogeneous brittle material. He found that the duration of the wave influenced the amount of energy required to fracture a unit volume of material. The specific fracture energy was the lowest for a high-amplitude, short-duration wave.

A limited number of investigations have been done on the dynamic nature of rock fracture mechanisms. Hakalehto (1967) studied the crack initiation and growth of Tennessee marble. He found that in dynamic loading fracture initiated in the same manner as in static loading, the cracks developing and extending in the direction of the wave. He also found that in dynamic testing the loading is more uniformly

distributed across the cross section of the specimen and the axial cracks are relatively longer.

A photographic study of rock specimens during loading in the split Hopkinson device was done by Friedman (1968). For Solenhofen limestone it was observed that in the sequence of events leading to gross failure of the specimens, macroscopic shear fracture developed before extension fractures. In tests on granite these shear lines were not visible.

THEORETICAL ANALYSIS

The particle displacement over the cross-section of a circular, elastic, isotropic bar loaded longitudinally is not generally uniform (both radial stress and strain are induced). However, when the wavelength of the disturbance is long compared with the diameter of the bar, a uniform stress distribution can be assumed over any cross section.

The one-dimensional theory of wave propagation in elastic rods can be derived considering a small element PQ of length Δx and cross-sectional area of the rod A (see figure 1). Assuming that the stress on the face passing through P is σ , the stress on the other face will be given by $\sigma + \frac{\partial \sigma}{\partial x} \cdot \Delta x$. If the displacement of the element is given by u , we have from Newton's second law of motion:

$$\rho A \Delta x \frac{\partial^2 u}{\partial t^2} = A \frac{\partial \sigma}{\partial x} \cdot \Delta x \quad (3-1)$$

where

x is the distance measured along the axis of the rod

t is the time variable.

For a linearly elastic material the stress and strain are related by Young's modulus.

$$\sigma = \epsilon E = \frac{\partial u}{\partial x} E \quad (3-2)$$

where ϵ is the strain.

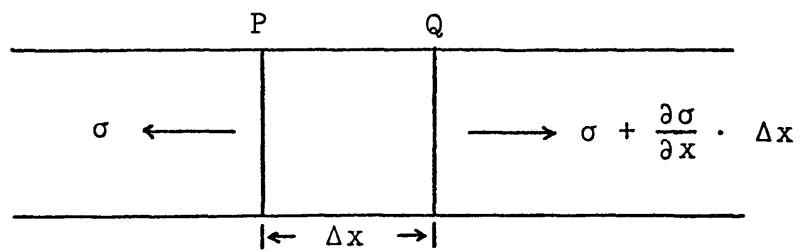


Figure 1. Forces Acting on Element of an Elastic Rod.

Equation (3-1) may be written as:

$$\rho \frac{\partial^2 u}{\partial t^2} = E \frac{\partial^2 u}{\partial x^2} \quad (3-3)$$

The general solution of this equation is:

$$u = f(x-ct) + F(x+ct) \quad (3-4)$$

where c is the longitudinal wave velocity ($c = \sqrt{E/\rho}$).

f and F are arbitrary functions depending on initial conditions (f corresponding to a plane wave travelling along the positive direction of the x -axis, and F to one in the direction opposite to this). When the wave motion is in the negative x direction

$$u = F(x+ct) \quad (3-5)$$

$$\frac{\partial u}{\partial x} = F'(x+ct) \quad (3-6)$$

$$\frac{\partial u}{\partial t} = cF'(x+ct) + c \frac{\partial u}{\partial x} \quad (3-7)$$

Since $\partial u/\partial t$ is the particle velocity v , and $\partial u/\partial x$ is the strain ϵ

$$v = c\epsilon \quad (3-8)$$

Integration of equation (3-7) gives

$$u = c \int_0^t \epsilon dt \quad (3-9)$$

Since all the strain wave measurements are made in the two steel bars, the material constants such as c are those of steel.

Average Stress and Average Strain

A diagrammatic representation of the split Hopkinson bar in the vicinity of the specimen is shown in figure 2. The strain waves $\epsilon_i(t)$ and $\epsilon_r(t)$ act on interface 1 and strain wave $\epsilon_t(t)$ on interface 2.

The net displacement of interface 1 in the direction of bar 2 is made up of contributions from both the incident and reflected waves. For the incident wave one obtains

$$u' = c \int_0^{t_1} \epsilon_i dt \quad (3-10)$$

Similarly for the reflected wave one finds

$$u'' = -c \int_0^{t_2} \epsilon_r dt \quad (3-11)$$

where:

t_1 = period of the incident wave

t_2 = period of the reflected wave ($t_2 \geq t_1$)

c = wave velocity in the steel bar.

The displacement has a positive or negative sign according to the direction of travel of the wavefront. Theoretically t_2 should be infinite; in practice, however, the strain amplitudes approach zero very rapidly as t_2 becomes large and the contribution for large t can be neglected. The net displacement of interface 1 is given by

$$u_{1(\text{net})} = u' + u'' = c \int_0^{t_2} (\epsilon_i - \epsilon_r) dt \quad (3-12)$$

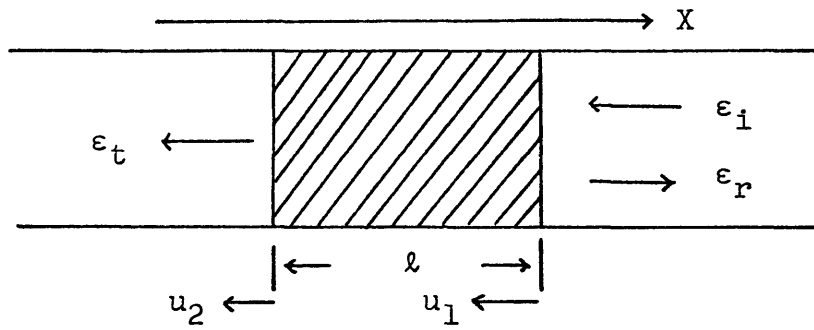


Figure 2. A Rock Specimen Sandwiched Between the Ends of the Steel Bars.

In equation (3-12) the integration limits on t are from 0 to t_2 for both ϵ_i and ϵ_r . This is permissible since ϵ_i is equal to zero during the time interval t_1 to t_2 .

The net displacement of interface 2 as a function of time is given by

$$u_2(\text{Net}) = c \int_0^{t_2+\Delta t} \epsilon_t dt \quad (3-13)$$

where:

Δt = time required for the wave to travel through specimen of length l ($\Delta t = l/c_r$).

The "average" strain ($\bar{\epsilon}$) in the specimen is then

$$\bar{\epsilon} = \frac{u_1(\text{Net}) - u_2(\text{Net})}{l} = \frac{c}{l} \int_0^{t_2+\Delta t} (\epsilon_i - \epsilon_r - \epsilon_t) dt \quad (3-14)$$

where:

$$\epsilon_i = 0 \text{ for } t > t_1$$

$$\epsilon_r = 0 \text{ for } t > t_2$$

$$\epsilon = 0 \text{ for } t < \Delta t$$

Letting

$$t = t_2 + \Delta t$$

equation (3-14) can be written in the more usual form

$$\bar{\epsilon} = \frac{c}{l} \int_0^t (\epsilon_i - \epsilon_r - \epsilon_t) dt \quad (3-15)$$

The net applied force across interface 1 is given by

$$F_1(\text{Net}) = EA (\epsilon_i + \epsilon_r) \quad (3-16)$$

Since the net force applied across interface 2 is given by

$$F_2(\text{Net}) = EA \epsilon_t \quad (3-17)$$

the average stress in the specimen ($\bar{\sigma}$) is given by

$$\bar{\sigma} = \frac{F_1 + F_2}{2A} = \frac{E}{2} (\epsilon_i + \epsilon_r + \epsilon_t) \quad (3-18)$$

To this point in the discussion, nothing has been specifically mentioned about the effect of specimen length on the validity of the analysis. The specimen length introduces a time delay ($\Delta t = l/c_r$) between the arrival of the waves at the two interfaces. As the length of the specimen approaches zero, or when the ratio of the incident wave length to specimen length is very large, the calculated stress and strain values approach those actually in the specimen.

On the other hand, for specimens in which the ratio of the incident wave length to specimen length is small, a meaningful "average" value does not exist. The determination of the ratios for which average values are meaningful will be performed in the next section.

If the length of specimen is considered to be infinitesimal, the time Δt with which the transmitted wave should be displaced from the incident and reflected wave is normally neglected. (All three waves are assumed to begin at $t = 0$, i.e., $\epsilon_t \neq 0$ for $t < \Delta t$.) It will be shown in the following section that this procedure can result in a very large error in the stress-strain relationship.

Although this discussion has been concerned with (1) the effects of specimen length, and (2) the way in which the

analysis is performed on the distribution of stress or strain over the length of the specimen, a nonuniform distribution can also result from either frictional restraint of the specimen at the boundaries or inertial restraint in both the axial and radial directions. The frictional or end effects are believed to be less than, or at most equal to that observed under static loading conditions. These can be minimized by choosing the specimens with appropriate geometry of length to diameter ratio and/or lubricating the bearing surfaces.

Average Strain Rate

The average strain rate ($\dot{\epsilon}_{avg}$) in a specimen of length l is defined as

$$\dot{\epsilon}_{avg} = \left(\frac{\partial u_1}{\partial t} - \frac{\partial u_2}{\partial t} \right) / l \quad (3-19)$$

from equations (3-12) and (3-13) we obtain

$$\dot{\epsilon}_{avg} = \frac{c}{l} (\epsilon_i - \epsilon_r - \epsilon_t) \quad (3-20)$$

It is noted that the average strain rate is inversely proportional to the specimen length. The values of ϵ_i , ϵ_r , and ϵ_t are all functions of time, and thus $\dot{\epsilon}_{avg}$ is also a function of time.

Energy Loss in the Specimen

The total energy (E_t) contained in an elastic wave is the sum of its kinetic energy (kE) and potential energy (PE)

$$E_T = kE + PE \quad (3-21)$$

where:

$$kE = \frac{1}{2} \Delta m v^2 = \frac{1}{2} \rho A \Delta l v^2 \quad (3-22)$$

and

$$PE = \frac{1}{2} \sigma \epsilon A \Delta l \quad (3-23)$$

Here Δl is the portion of bar which contains the elastic wave ($\Delta l = c \Delta t$).

Equation (3-21) can be rewritten as

$$E_T = \frac{1}{2} \rho c^3 A \int_0^t \epsilon^2 dt + \frac{1}{2} A E c \int_0^t \epsilon^2 dt \quad (3-24)$$

$$E_T = A E c \int_0^t \epsilon^2 dt \quad (3-25)$$

Assuming that

E_i = energy incident upon first bar-specimen interface

E_r = energy reflected back into first bar

E_t = energy transmitted into second bar.

The energy lost in the specimen (E_l) is

$$E_l = E_i - E_r - E_t \quad (3-26)$$

COMPUTER SIMULATION OF THE SPLIT HOPKINSON BAR

A computer simulation of the split Hopkinson bar was performed to investigate (1) the effect of the incident wave length to specimen length ratio, and (2) the effect of the way in which the strain waves are superimposed on the stress-strain curves of the rock specimen. The two steel bars were assumed to have a mass density (ρ_s), longitudinal wave velocity (c_s), and be of a sufficient length to avoid the necessity of considering reflections from their ends. The rock specimen having a mass density ρ_r , wave velocity c_r , and length l was assumed to have an elastic limit sufficiently large to avoid the possibility of rock failure under the applied loads.

In the analysis, the incident wave (σ_i) was assumed to be one half of a sine wave having a maximum amplitude A_0 and wave length λ . Mathematically this can be expressed as

$$\sigma_i = A_0 \sin \frac{\pi c_s}{\lambda} t \quad (4-1)$$
$$(0 \leq t \leq \frac{\lambda}{c_s})$$

As the incident wave meets interface 1, part of the wave is reflected and part is transmitted into the rock specimen. The part which is transmitted into the specimen upon reaching interface 2 is again partitioned into a

transmitted and a reflected wave. The process is shown in some detail in figure 3. The waves reflected and transmitted into the two bars are constructed by adding the various components at the proper time intervals. The general expressions for the reflection and transmission coefficients at an interface (incident wave travelling from the first to the second medium) are derived using plane wave assumptions and force and velocity continuity at the interface. These are

$$\frac{\sigma_t}{\sigma_i} = \frac{2\rho_2 c_2}{\rho_2 c_2 + \rho_1 c_1} \quad (4-2)$$

$$\frac{\sigma_r}{\sigma_i} = \frac{\rho_2 c_2 - \rho_1 c_1}{\rho_2 c_2 + \rho_1 c_1} \quad (4-3)$$

where:

σ_i = amplitude of incident wave

σ_r = wave reflected from the interface

σ_t = wave transmitted through the interface

ρ_1, ρ_2 = mass densities of the first and second mediums, respectively

c_1, c_2 = longitudinal wave velocities in the first and second mediums, respectively.

Equations (4-2) and (4-3) must be evaluated for the following combinations.

Media 1	Media 2
Steel bar 1	Rock
Rock	Steel bar 2
Rock	Steel bar 1

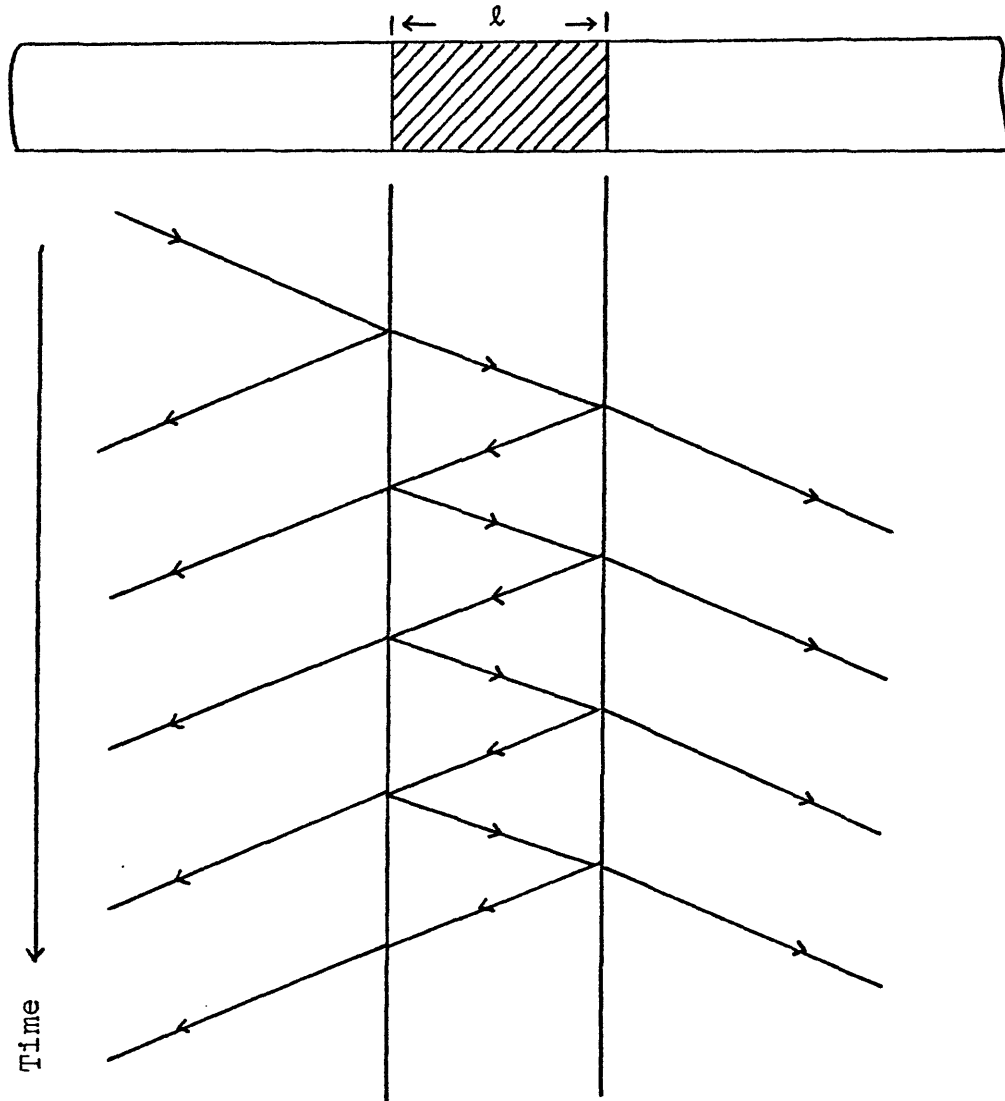


Figure 3. A Diagrammatic Representation of the Transmitted and Reflected Waves Produced by a Wave Incident at the Steel-Rock Interface.

For the sine wave described in equation (4-1), the expressions for the reflected (σ_r) and transmitted (σ_t) stress waves become

$$\sigma_r = A_0 k \sin \frac{\pi c_s}{\lambda} t + A_0 (1-k^2) \sum_{n=1}^{\infty} (-k)^{2n-1} \sin \frac{\pi c_s}{\lambda} \left(t - \frac{2n\ell}{c_r} \right) \quad (4-4)$$

$$\sigma_t = A_0 (1-k^2) \sum_{n=1}^{\infty} (-k)^{2n-2} \sin \frac{\pi c_s}{\lambda} \left\{ t - \frac{(2n-1)\ell}{c_r} \right\} \quad (4-5)$$

In equations (4-4) and (4-6)

$$k = \frac{\rho_r c_r - \rho_s c_s}{\rho_r c_r + \rho_s c_s} \quad (4-6)$$

n = number of reflections in the specimen.

The time at which the incident wave first arrives at the bar-specimen interface is taken as zero. Because of the many calculations required and the complexity of keeping track of all the waves, a computer program (Appendix I) was written to evaluate equations (4-4) and (4-5). In the cases discussed below, the following constants will be used.

$$\begin{aligned} n &= 20 \\ \rho_s &= 8.79 \times 10^{-3} \text{ slugs/in.}^3 \quad (\rho_s = 7.8 \text{ gm/cm}^3) \\ E_s &= 28 \times 10^6 \text{ psi} \quad (E_s = 1.97 \times 10^6 \text{ kg/cm}^2) \end{aligned}$$

The values of c_r and c_s are calculated using

$$c = \sqrt{\frac{E}{\rho}} \quad (4-7)$$

Figures 4 and 5 show the effect of varying the length of the rock specimen on the reflected and transmitted waves and on the calculated stress-strain curve for a given incident wave length* ($\lambda = 10$ in.). In figure 4 the transmitted waves are translated with respect to the incident and reflected waves for each specimen length by the appropriate value of Δt . Superimposed upon the calculated stress-strain results in figure 5 is the actual Young's modulus (E_R) assumed for the rock. The observed nonlinear behavior of the initial loading and final unloading portions of the derived curves is largely the result of nonuniform stress distribution along the specimen axis (i.e. it is a direct indicator of the appropriateness of the describing process in terms of "average" values). For curve C, the specimen length is only about one half of the wave length and the stress-strain curve obtained is obviously quite different from that specified (E_R). The results of figure 4 suggest that the analysis can be applied with reasonable accuracy for incident wave length to specimen length ratios greater than 5 to 1.

The first step in the processing of the experimental strain wave data is to determine the corresponding starting times of the various strain-time curves. Even though the

*The incident wave is given in terms of its length in the steel bar.

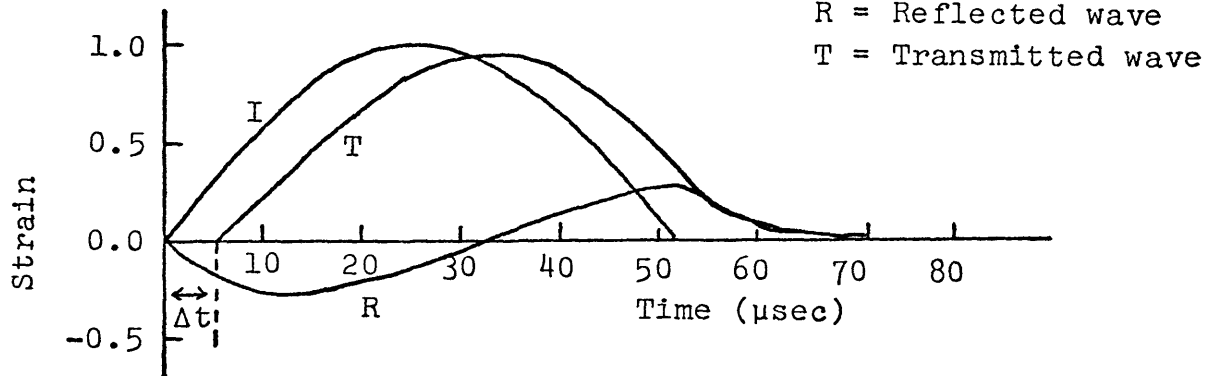
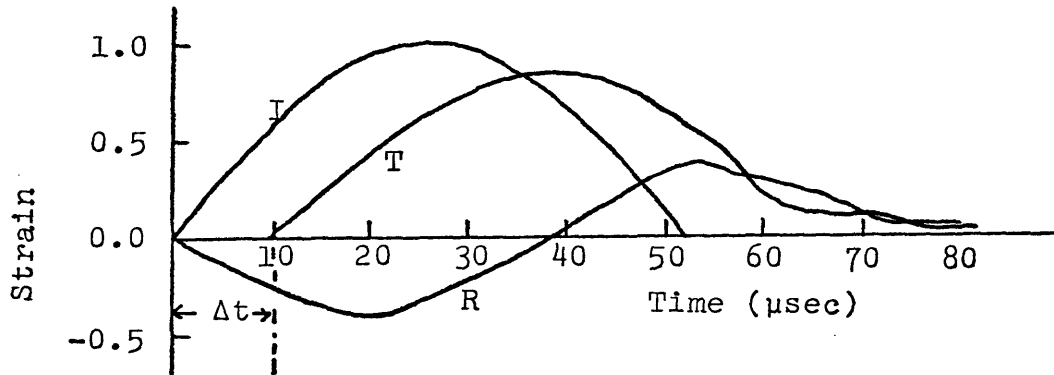
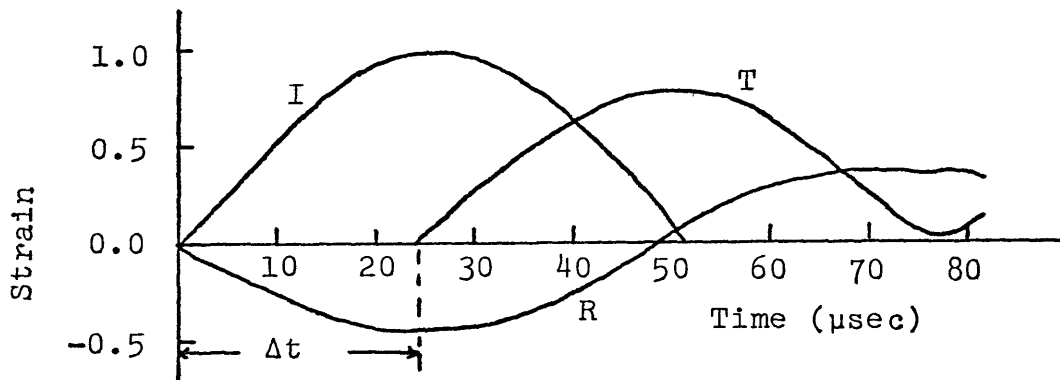
A. Specimen length $\ell = 1.0$ in.B. Specimen length $\ell = 2.0$ in.C. Specimen length $\ell = 5.0$ in.

Figure 4. Reflected and Transmitted Strain-Time Curves Calculated Using Plane Wave Theory for Specimens of Various Lengths Assuming a Given Incident Waveform. In this Example $A_0 = 1.0$, $\lambda = 10$ in., $\rho_r = 3.0 \times 10^{-3}$ slugs/in.³ (2.7 gm/cm³), and $E_R = 11 \times 10^6$ psi ($.774 \times 10^6$ kg/cm²).

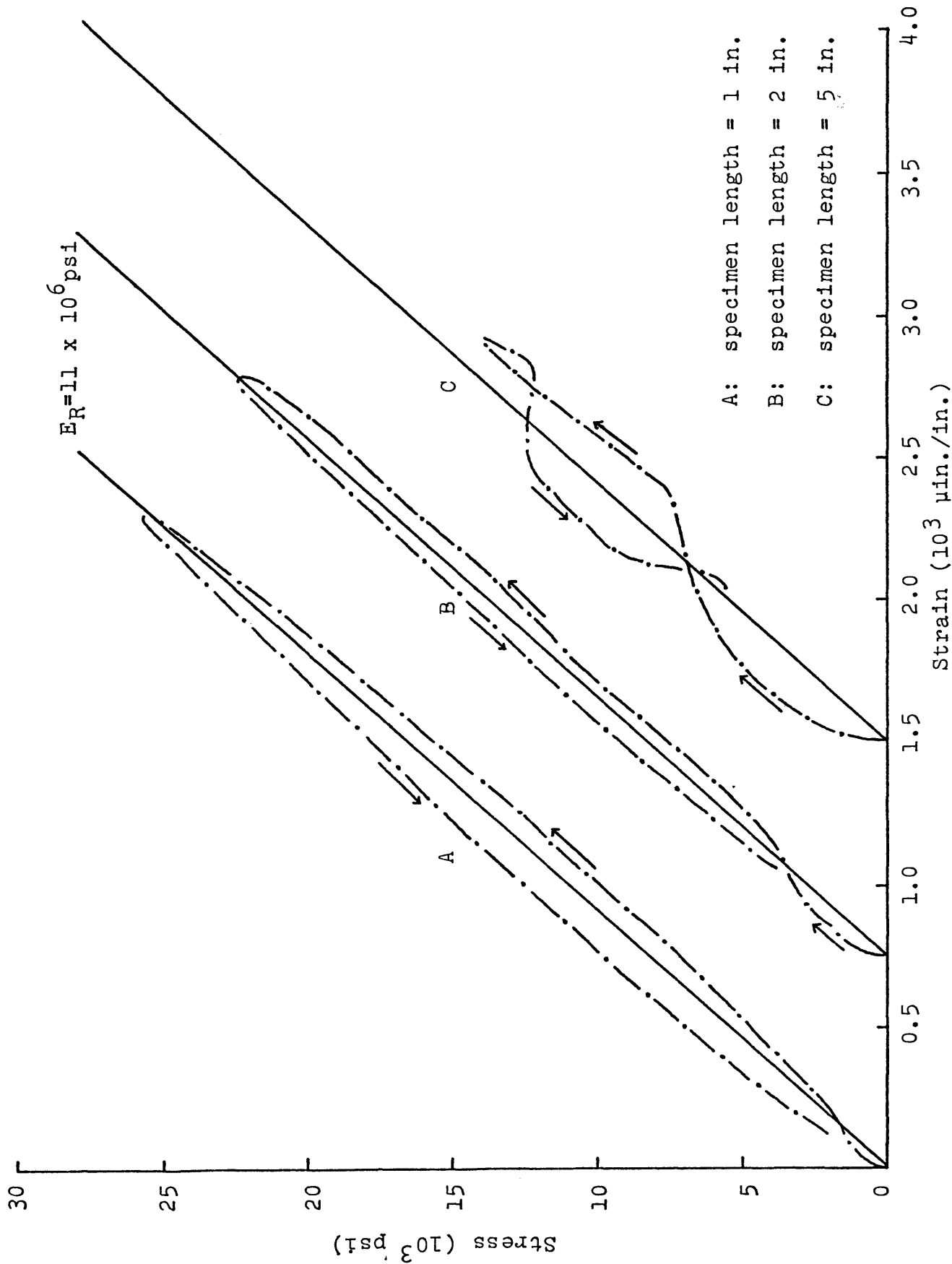


Figure 5. Comparison of Stress-Strain Curves Derived From the Strain Waves of Figure 4 With the Given Value (E_R). The Incident Strain Wave Amplitude $A_0 = 995$ in./in. Data Points Were Taken at 2 μ sec Intervals.

incident, reflected, and transmitted waves are recorded at equal distances from the specimen ends so that direct scaling methods can aid in determining corresponding times, errors can be easily introduced. To simulate this condition, the transmitted wave was shifted along the time axis by an amount of 0.48 sec (this is equivalent to neglecting the time (Δt) necessary for a wave to travel through a 0.1-in. long specimen with a longitudinal wave velocity of 208,000 in./sec). The resulting stress-strain curve (shown together with the correctly derived one in figure 6) has an apparent elastic constant 68 percent higher than the actual. On the basis of this result one would conclude that a rate of loading effect exists. In actual fact, it is a result of how the analysis was done and not rock behavior at all.

In the actual evaluation of experimental strain waves a decision must be made on the time intervals at which the strain amplitudes are read. Since the integration of the strain-time curves is also carried out using this interval. If the time interval chosen is large compared with the duration of the incident wave, errors introduced by integration can be very significant. This is illustrated in figures 7 and 8 which apply to identical experiments except that the integration interval in the case of figure 7 is 2 microseconds whereas in figure 8 it is 1 microsecond. It is not practical to choose a time interval small compared with the time necessary for the wave front to travel from

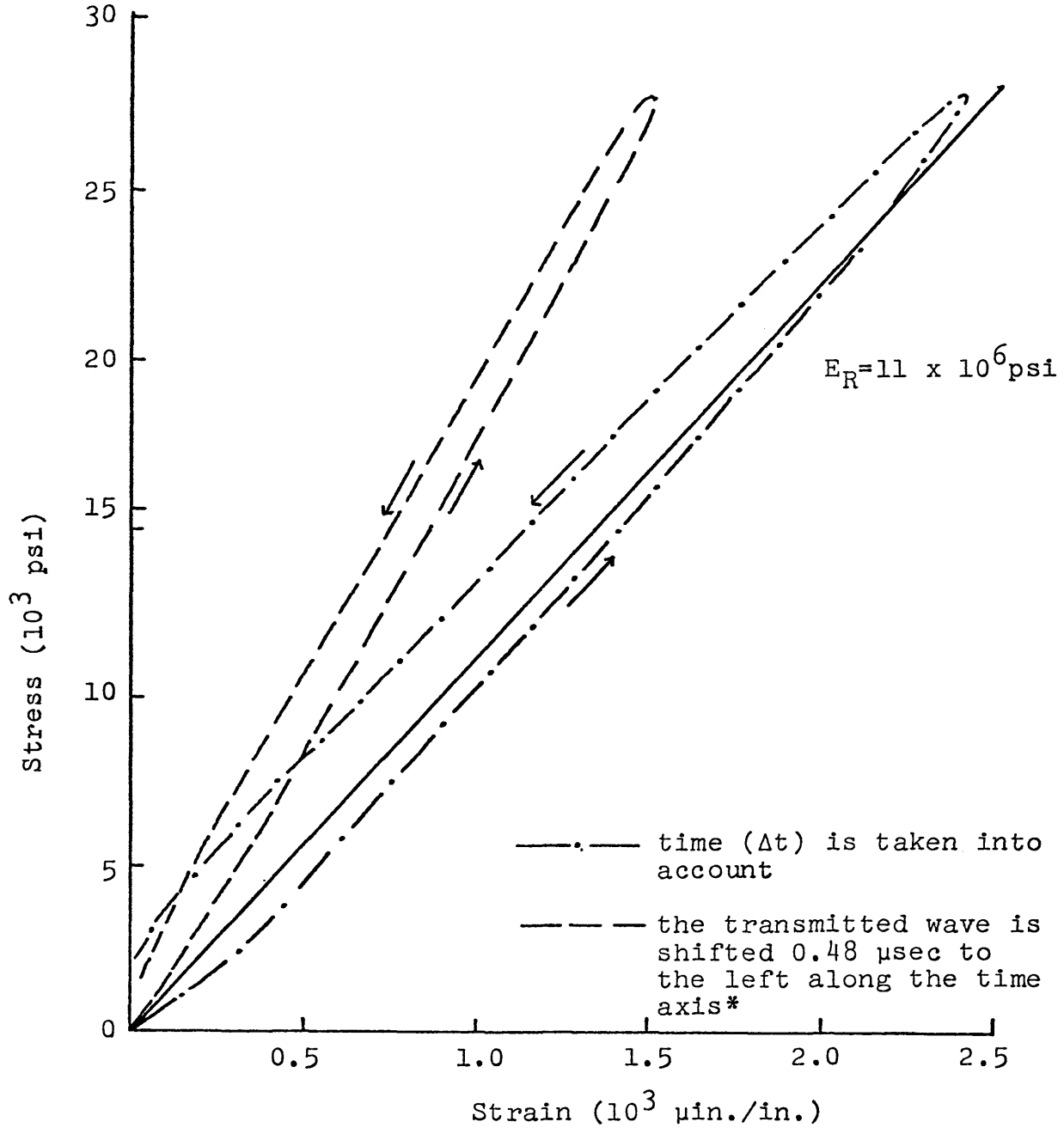


Figure 6. The Effect of Neglecting the Time (Δt) Required for a Wave to Traverse the Sample on the Derived Stress-Strain Curves. Data Taken from Figure 4 for a Specimen Length of 0.1 in.

*Neglecting the effect of specimen length.

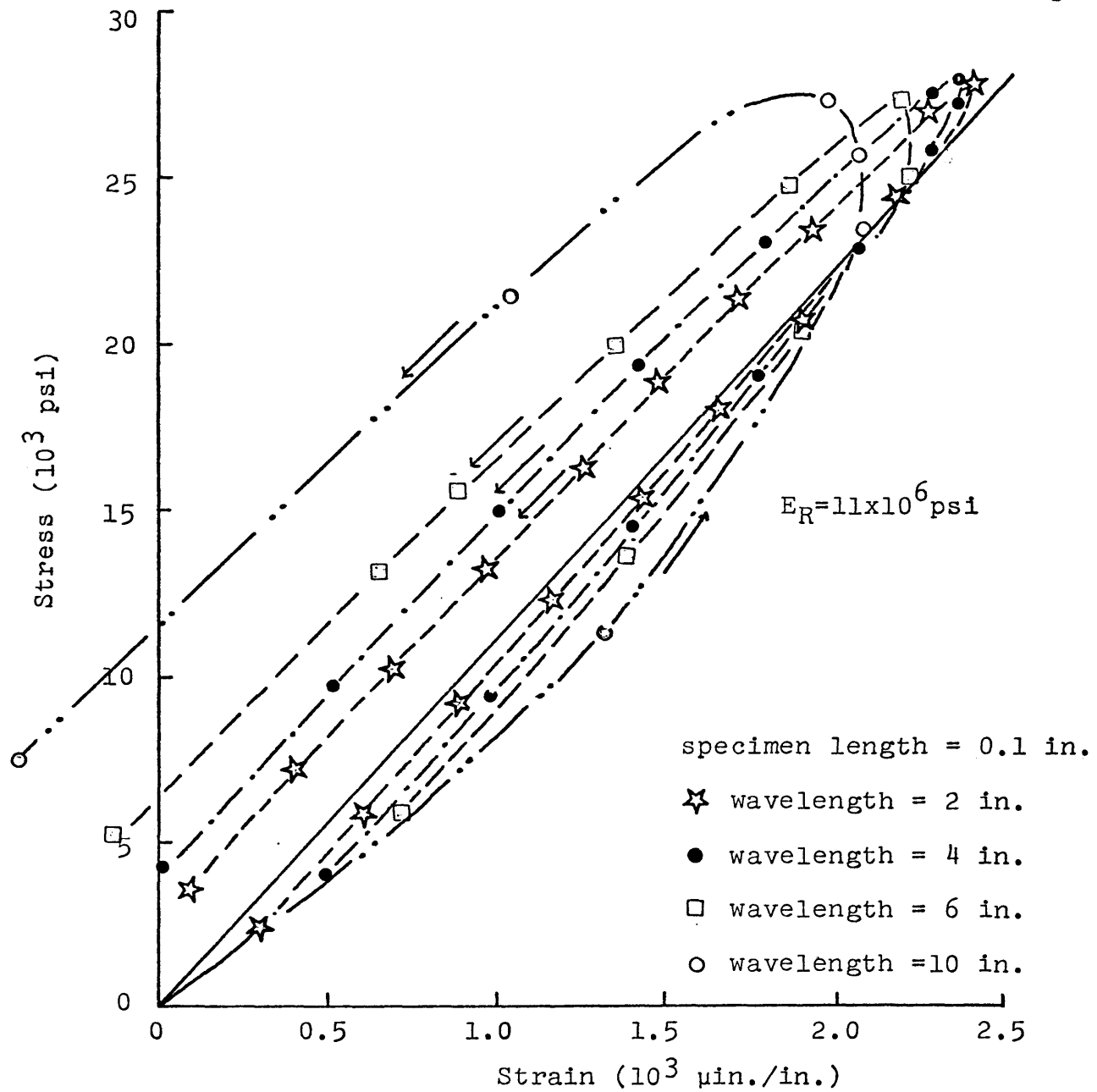


Figure 7. Comparison of Derived Stress-Strain Curves for a Given Specimen Length and Various Incident Wave Lengths. The Curves Were Calculated Using a 2 μ sec Integration Interval. The Incident Wave Amplitude (A_0) is Equal to 995 μ in./in. and Rock Properties are the Same as in Figure 4.

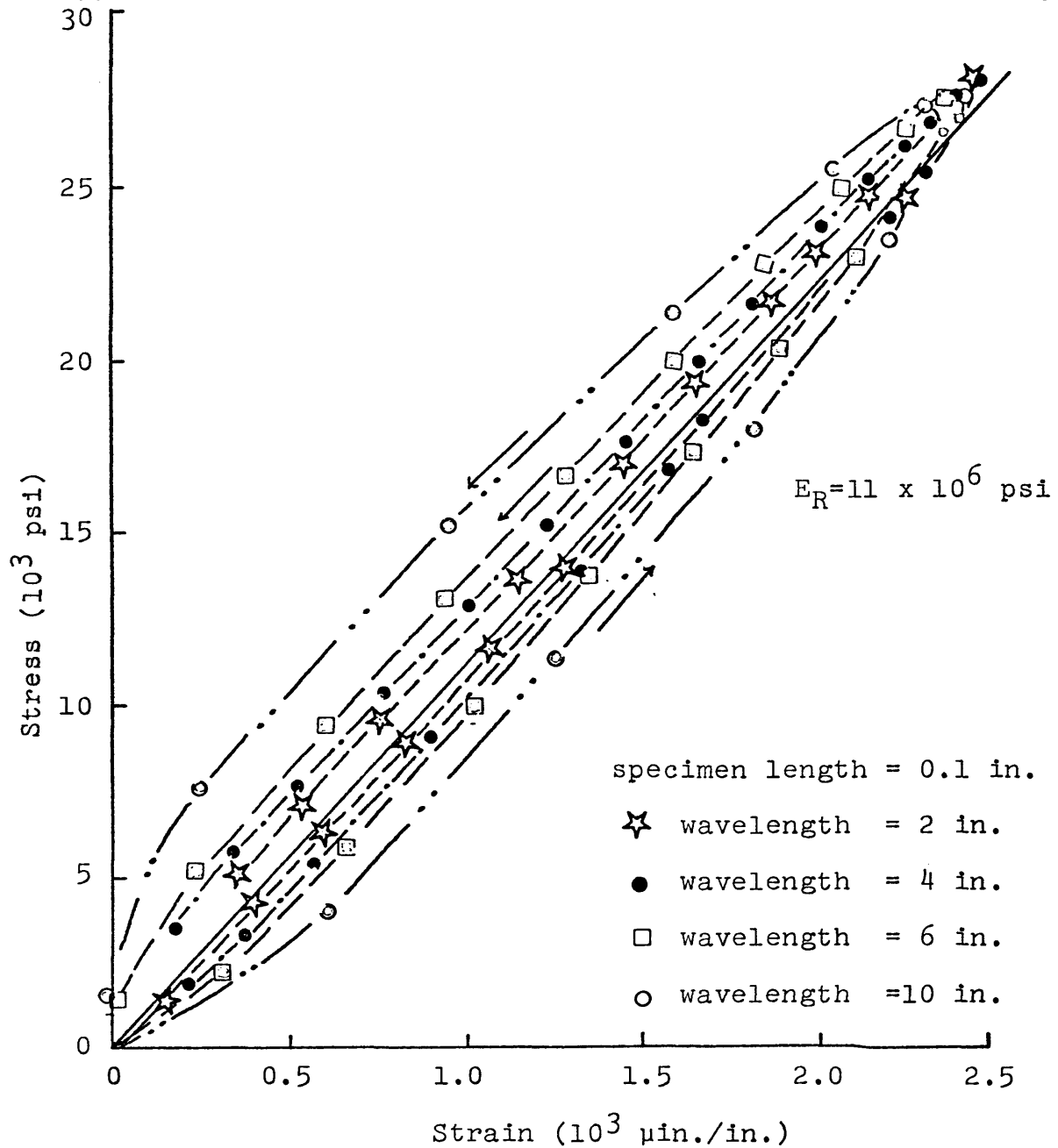


Figure 8. Comparison of Derived Stress-Strain Curves for a Given Specimen Length and Various Incident Wave Lengths. The Curves Were Calculated Using a 1 μ Sec Integration Interval. The Data Used is the Same as in Figure 7.

the first face of the rock specimen to the second. The first few points obtained will be meaningless since for the first few microseconds the stresses at the two specimen faces will not be uniform.

An important feature of split bar test is that the strain wave attenuation or the energy loss in the specimen can be readily obtained by due consideration of the energy content of the various parts of the waves. Table 1 shows the energy breakdown after the assumed strain wave passes through the ideal specimen having an impedance (the product of the density and the wave velocity, $\rho_R c_R$) different from that of the steel bars ($\rho_S c_S$). For a given wave form, the percent energy contained in the incident wave which will be transmitted into the second steel bar, or reflected back into the first steel bar depends on the impedance ratio of the specimen and steel bars ($\rho_S c_S / \rho_R c_R$) and also on the specimen length. For a given incident pulse length as seen in Table 1, the amount of energy reflected back into the first steel bar increases with increasing specimen lengths until certain constant ratio is reached. The other noticeable result apparent in the table is that for a very long specimen a certain amount of energy contained in the long tail of reflecter and transmitted waves would not be able to calculate, because only a finite point may be taken along the time axis, thus it will appear as apparent energy loss in the specimen.

Table 1. The Energy Consideration of an Incident Sinusoidal Stress Pulse Related to Specimen Length and Stress Pulse Length.

Pulse Length λ (in.)	Specimen Length & (in.)	Energy Content E_i (in.-lbs)	Reflected Part E_r (in.-lbs)	Transmitted Part E_t (in.-lbs)	Apparent Percent Energy Loss E_l/E_i (%)
	0.10		0.5	21.2	0.00
	0.50		5.3	16.4	0.00
2	1.00	21.7	7.5	14.2	0.00
	2.00		7.5	14.2	0.00
	5.00		7.4	14.1	0.73
	0.10		0.3	43.2	0.00
	0.50		4.8	38.7	0.00
4	1.00	43.5	10.6	32.9	0.00
	2.00		15.1	28.5	0.00
	5.00		14.9	28.3	0.73
	0.10		0.2	65.1	0.00
	0.50		3.9	61.4	0.00
6	1.00	65.3	10.4	54.8	0.00
	2.00		19.9	45.4	0.00
	5.00		22.3	42.5	0.73
	0.10		0.1	108.7	0.00
	0.50		2.7	106.1	0.00
10	1.00	108.8	8.6	100.2	0.00
	2.00		21.3	87.4	0.10
	5.00		33.8	70.2	4.40

EXPERIMENTATION

The computer simulation study of the split Hopkinson bar has suggested the method of data analysis which must be used to obtain representative stress-strain curves for the rock specimens. With this work as a guide an experimental program was carried out to investigate the effect of rate of loading on rock properties, the strain wave transmission and energy loss, and the dynamic fracturing mechanism of the specimen. A detailed description of the split Hopkinson bar equipment, testing procedures, and the data reduction process are given in the following sections.

Description of the Split Hopkinson Bar

The split Hopkinson bar presently being used by the author in the Department of Mining is shown in figure 9. A diagrammatic representation of the apparatus is shown in figure 10. The incident and transmitter bars are made from 1-in. diameter high strength stainless steel rod. Each is 3-ft long to avoid any overlapping of the incident and reflected pulses. The plane circular faces of the bars between which a specimen is sandwiched were finished to a high degree of flatness. *How much? ± 0.1 in.? or ± 0.0000000*

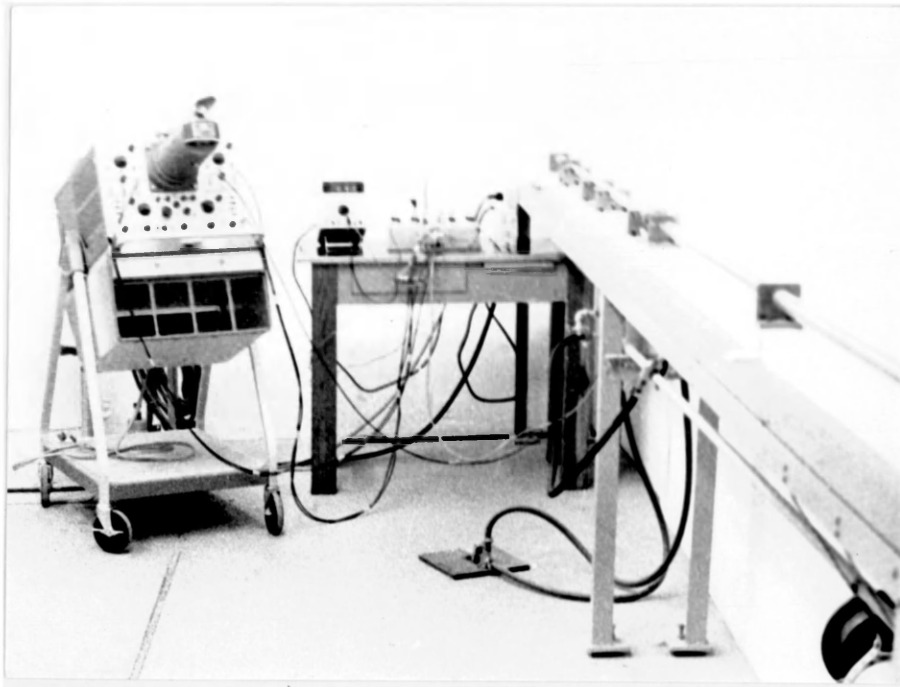
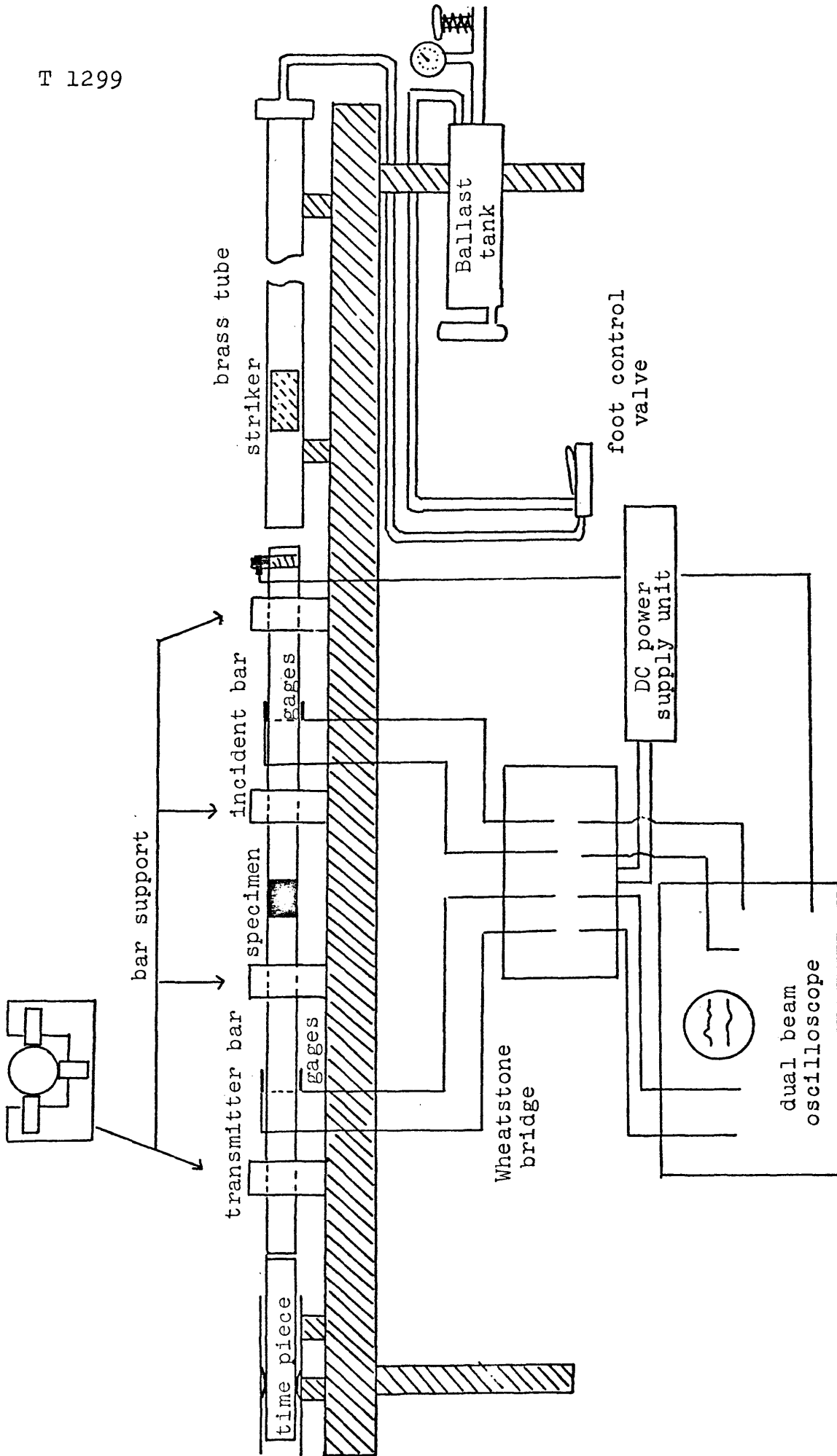


Figure 9. Split Hopkinson Bar Apparatus.



The system is set on a long bench, each bar being supported by two "U" shaped steel holders. Each holder consists of three roller bearings which allow the bars to move freely in a horizontal direction only. The specimen is held in place between the aligned bars by transparent tape.

A steel striker (made from the same material as the bars) is accelerated by compressed air down a 9-ft long brass tube with 1-in. inner diameter. Admission of the compressed air to the tube is controlled by a foot valve. Holes several inches before the open end of the brass tube allow the driving air to escape ensuring that the striker delivers one blow only to the end of the bar. A 12-in. long stainless steel bar (1" diameter) placed in contact with the transmitter bar serves as a momentum trap.

A pair of strain gages (SR-4, type FAE 12-12S6L, G.F. = 2.01) glued to the middle of each bar using EPY-150 epoxy cement and covered with gage-kote were used to detect the various strain waves. The gages are placed on opposite sides of the bar and connected in series so as to be insensitive to bending. Each of the two pairs of strain gages is connected to a Wheatstone Bridge, the output of which is fed into a Tektronix type 565 Dual Beam Oscilloscope. The bridge voltage is supplied by Harrison Lab (model 801C) power supplies.

The signal from the strain gages on the incident bar is fed into the upper beam, and signal from the gages on

the transmitter bar to the lower beam of the oscilloscope. Triggering of the oscilloscope is accomplished by a signal from an accelerometer attached to the incident bar one inch from the end impacted by the striker. The strain waves were recorded on TRI-X film using a 35 mm oscilloscope camera. A 75 mm polaroid camera (Hewlett Packard model 196A) was also used.

Testing Procedure

Four rock types including Colorado Red Granite, Yule Marble, Indiana Limestone and Gray Sandstone were used in the experiment. A geological description of the rocks are given in Appendix III. For a given rock type, 1-in. diameter cores were drilled from the same block and in the same direction with a thin walled diamond bit. The cores were cut into several lengths and the ends were then ground flat and parallel to within ± 0.001 in. The specimens were sandwiched between the incident and transmitter bars and held in place by transparent tape at two specimen ends. In all tests great care is taken to assure that the loading bars are in intimate contact with the specimens. The time piece (momentum trap) was also carefully positioned in contact with the transmitter bar.

The D.C. power supply, oscilloscope, and amplifier were given sufficient warm-up time before any tests were run. The

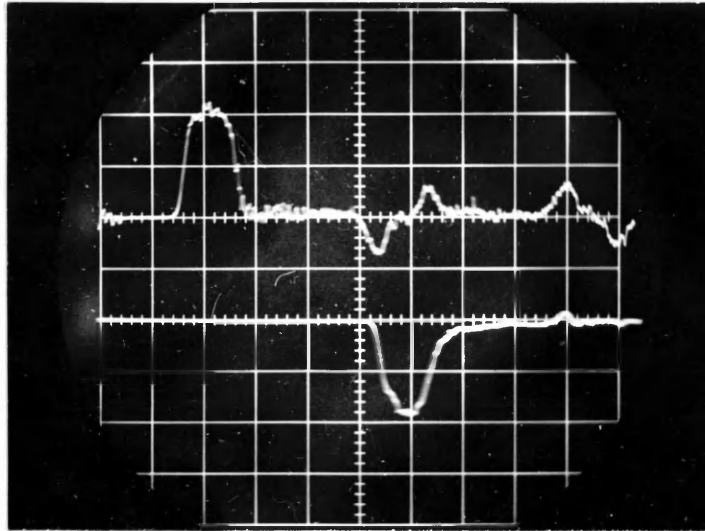
strain gages were balanced by adjusting the potentiometers of the Wheatstone bridge. Voltage input to the bridge was set at 10.00 volts throughout the experiment. For calibration purposes, the current through the gages was measured using a Honeywell Model 333R digital meter. A diagram of the Wheatstone bridge circuit used and calculations of the strain sensitivity of the system are presented in Appendix IV. The sensitivity of the system is 199 $\mu\text{in./in./mv}$. The vertical deflection and the horizontal time scale of the oscilloscope were calibrated using the built-in calibration unit.

Before testing, the striker bar was sent to the back end of the brass tube using a compressed air blast. The proper air pressure was set for the ballast tank, then the oscilloscope was switched to external trigger and the foot control valve was depressed.

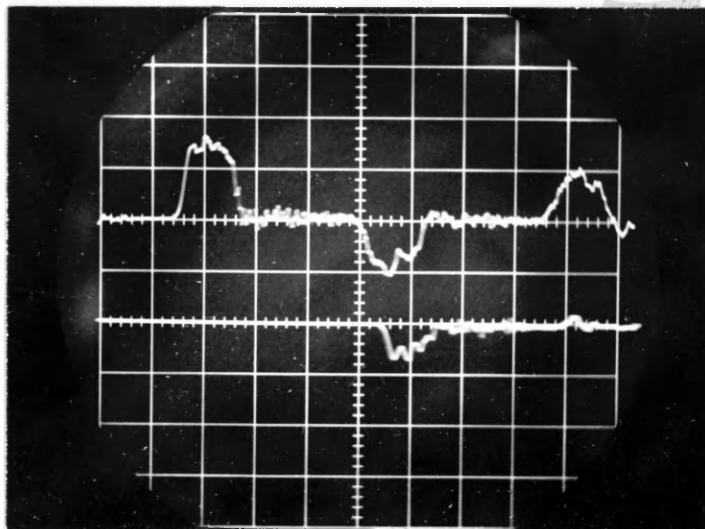
A picture of the waves displayed on the oscilloscope screen was taken for each test. Some typical pictures for different rock types are shown in figures 11 and 12. The transmitted waves in the pictures were reversed to avoid overlap of the waves.

Data Reduction

The stress-strain curves and energy loss in the specimens were studied using various strain pulses. In theory,

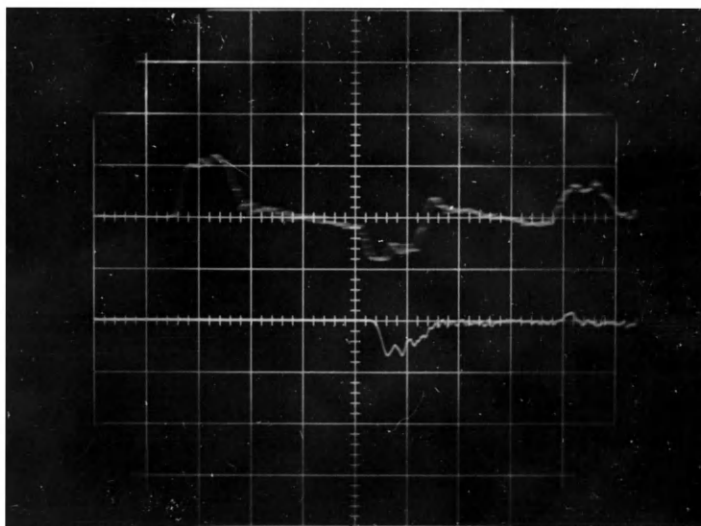


A. Colorado Red Granite.

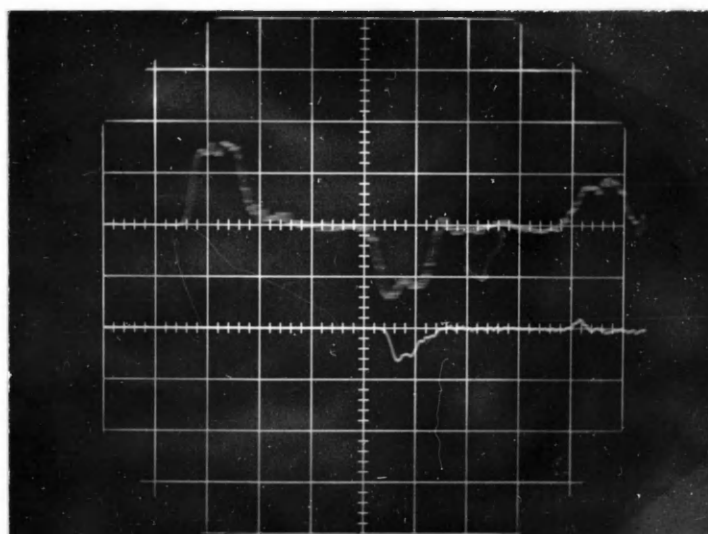


B. Yule Marble.

Figure 11. Oscilloscope Traces of Incident, Reflected (Upper Beam), and Transmitted (Lower Beam) Waves. (Horizontal Sweep 50 μ sec/cm)



A. Indiana Limestone.



B. Gray Sandstone.

Figure 12. Oscilloscope Traces of Incident, Reflected (Upper Beam) and Transmitted (Lower Beam) Waves. (Horizontal Sweep 50 μ sec/cm)

the wave length of the incident strain pulse is equal to twice the striker length. Thus changing the striker length gives different impact wave lengths. In these experiments striker bars having lengths of 1-, 2-, 3-, and 5-inches were prepared. Changing the air pressure in the shooting system gives different striker impact velocities and consequently different strain amplitudes.

The computer simulation study of the split Hopkinson bar has suggested the optimum specimen length and wave lengths to be used in the experiment. A 5-in. striker and nominal specimen length of 1-in. were generally used in the study, although a limited number of experiments were also conducted using different specimen lengths and striker lengths.

The oscilloscope picture taken for each test was enlarged to a particular size using a slide projector and the strain-time waves traced on tracing paper. The proper starting time for each wave is determined carefully from the wave velocity (C_s) in the steel bar,* together with the distances between the accelerometer and strain gage stations.

The properly superimposed incident, reflected, and transmitted strain waves for analyzing a typical test are

*The value of C_s (194,600 in./sec) was calculated using equation (4-7). The density $\rho_s = 0.288$ lb/in. was determined by direct measurement and the Young's modulus $E_s = 27.9$ psi was determined by static loading tests as given in Appendix V.

presented in figure 13A. The schematic diagram shows that the incident and reflected waves start at exactly the same moment, but transmitted waves are delayed for a short time interval (Δt), which depends on the wave velocity in the specimen.

The vertical sensitivity of the strain amplitude shown on the right side of the graph represents the actual elastic strain amplitude in the steel bar.

The average stresses and average strains were calculated using equations (3-16) and (3-18). For the numerical integration of the wave, the strain amplitude must be read at certain time intervals. A 2-microsecond interval was chosen, and found to be satisfactory. A computer program was prepared (Appendix II) to do the calculations. The strain amplitudes are read using a digitizer (Oskar Model K) at 2-microsecond intervals and directly punched onto data cards.

The derived average stress-time and average strain-time curves for this typical test are shown in figure 13B and 13C. The slope of these curves, which depends somewhat on the rise time of the incident wave, the wave length in the specimen, and the maximum strain amplitude represent the average stress rate and average strain rate of the test. Therefore, even for the same system conditions, the rates will not be the same when testing different materials. For this special case, they are approximately 1.5×10^9 psi/sec and 2×10^2 per second, respectively.

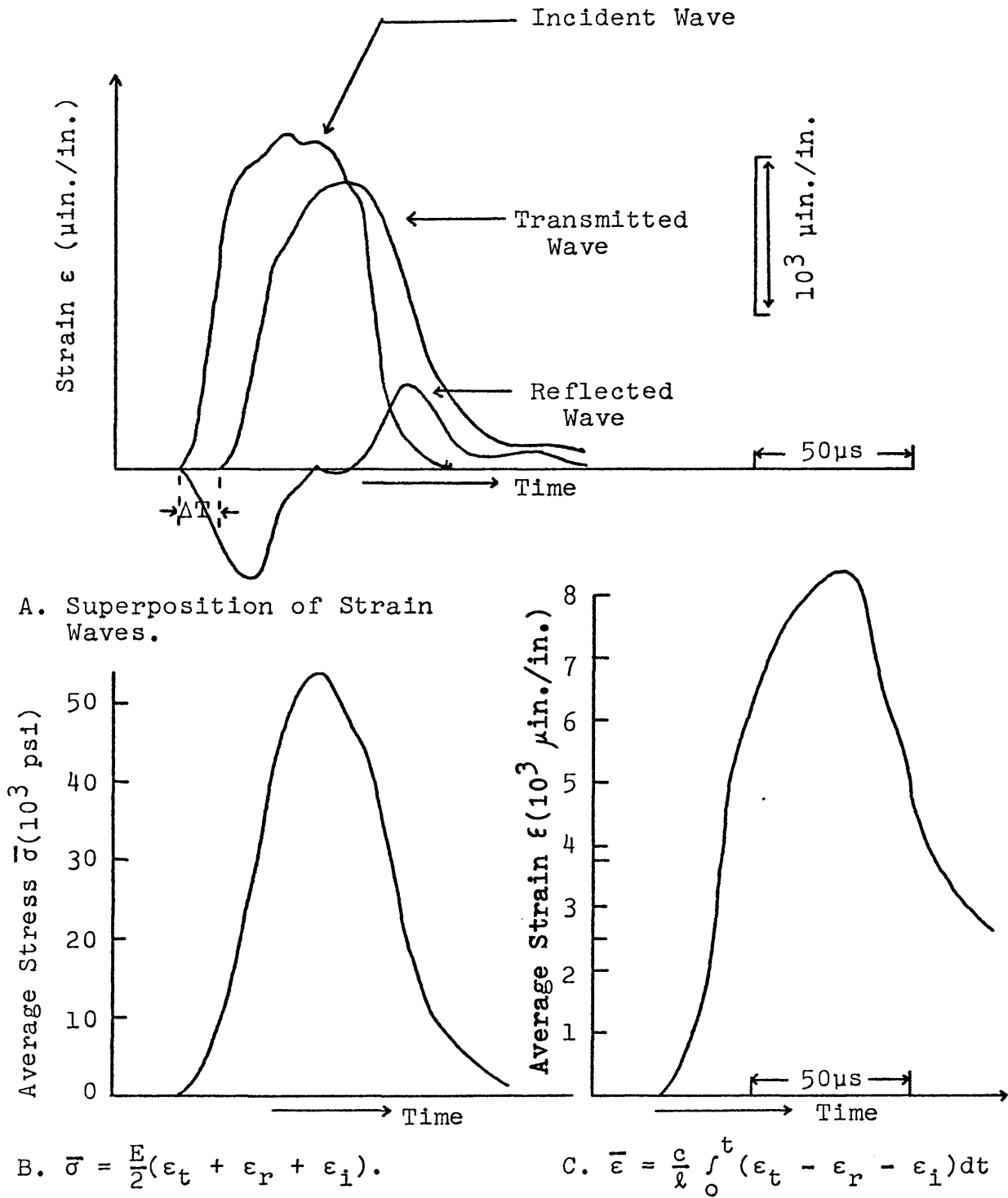


Figure 13. Analysis of Strain Waves for a Typical Experiment (for Colorado Red Granite, G-104, 5-in. Striker, Specimen Length = 1.056 in.).

The final plot of the stress versus strain is also shown on figure 14.

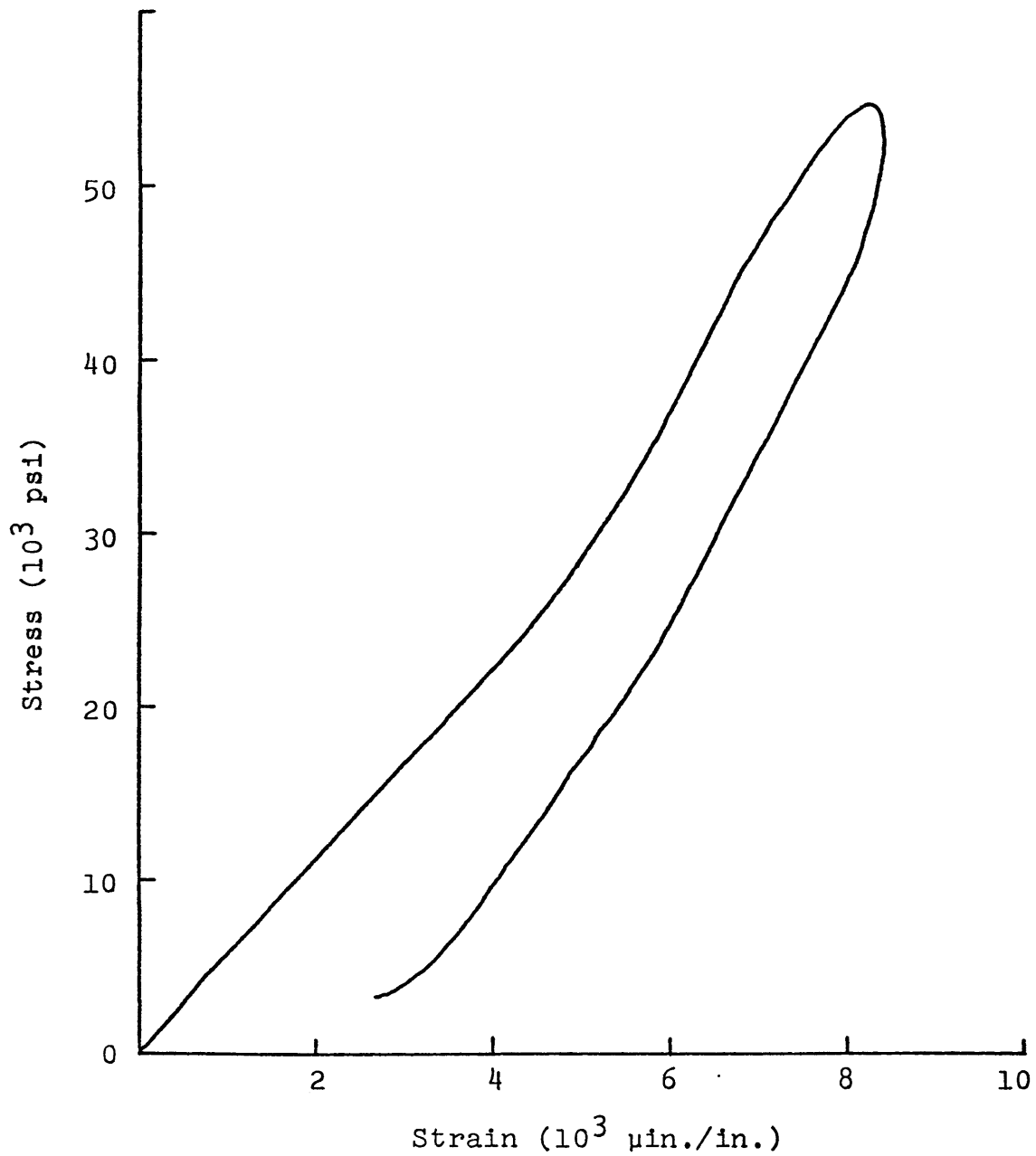


Figure 14. Derived Average Stress-Strain Curve for Colorado Red Granite (Specimen G-104).

TESTS AND RESULTS

Stress-Strain Behavior

In the initial series of tests, incident waves of several different lengths were used. Figure 15 shows some typical stress-strain curves for Gray Sandstone subjected to multiple impacts of a 1-in. striker (the data points are at 2- μ s intervals). The three curves in figure 16 are for an Indiana Limestone specimen subjected to consecutive strikes using three different wave lengths (produced by 1-, 2-, and 3-in. strikers). In figure 17 are shown curves for Colorado Red Granite impacted by a 5-in. striker. The specimen failed at the second impact.

The results, as expected, reveal that the dynamic stress-strain behavior of rock depends very much on the impact history of the rock. The specimen is expected to be weakened by a former strike, provided that the impulse amplitude is high enough. This effect is shown by a general decrease in the slope of the stress-strain curves as the number of strikes is increased.

The effect of the incident wave length on the stress-strain behavior of rock is harder to assess. A number of uncertainties (change in wave length changes the loading rate, the accuracy of the reading and the error of integration)

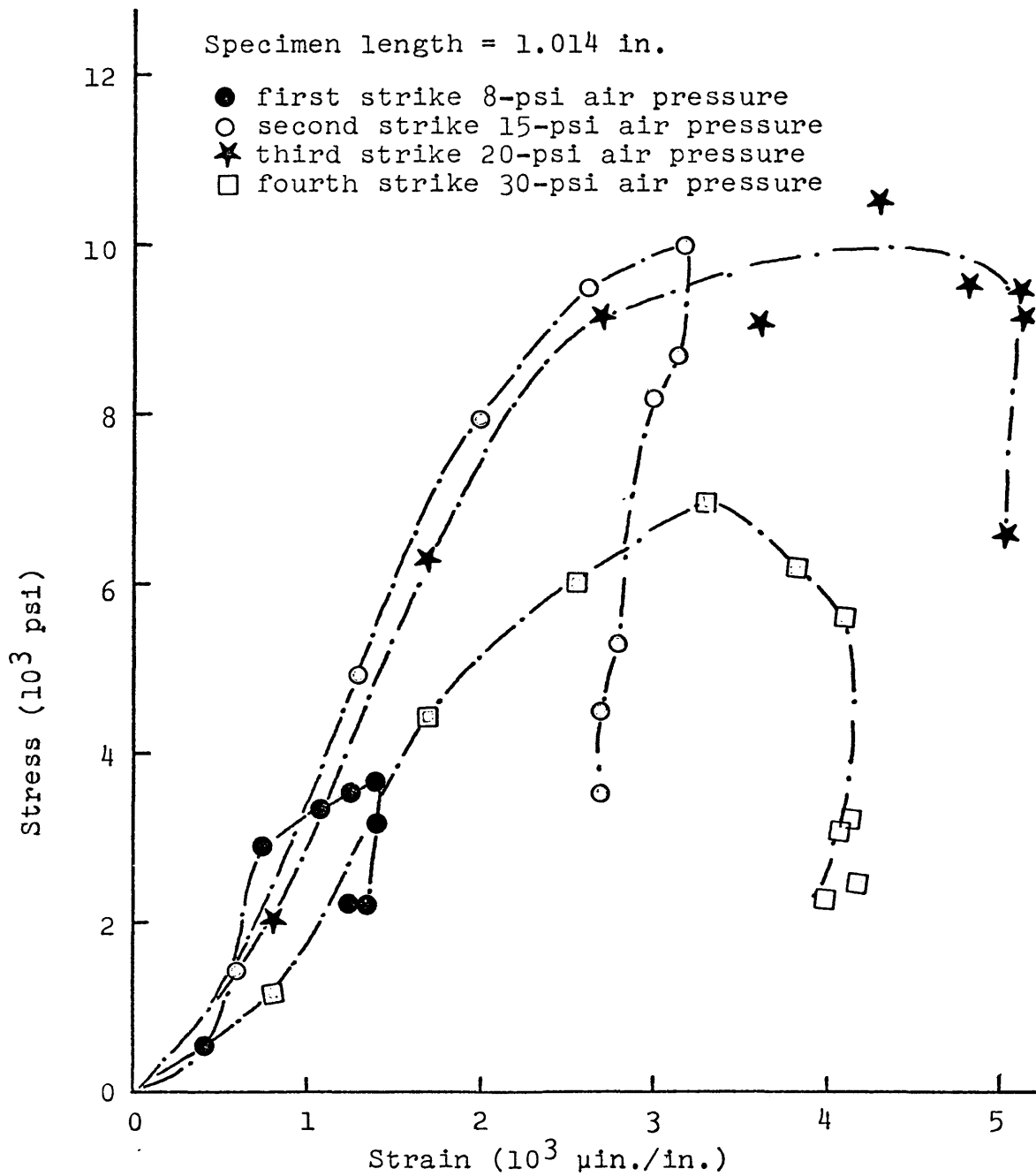


Figure 15. Dynamic Stress-strain Curves for Gray Sandstone using a 1-in. Striker at Increasing Striking Velocities.

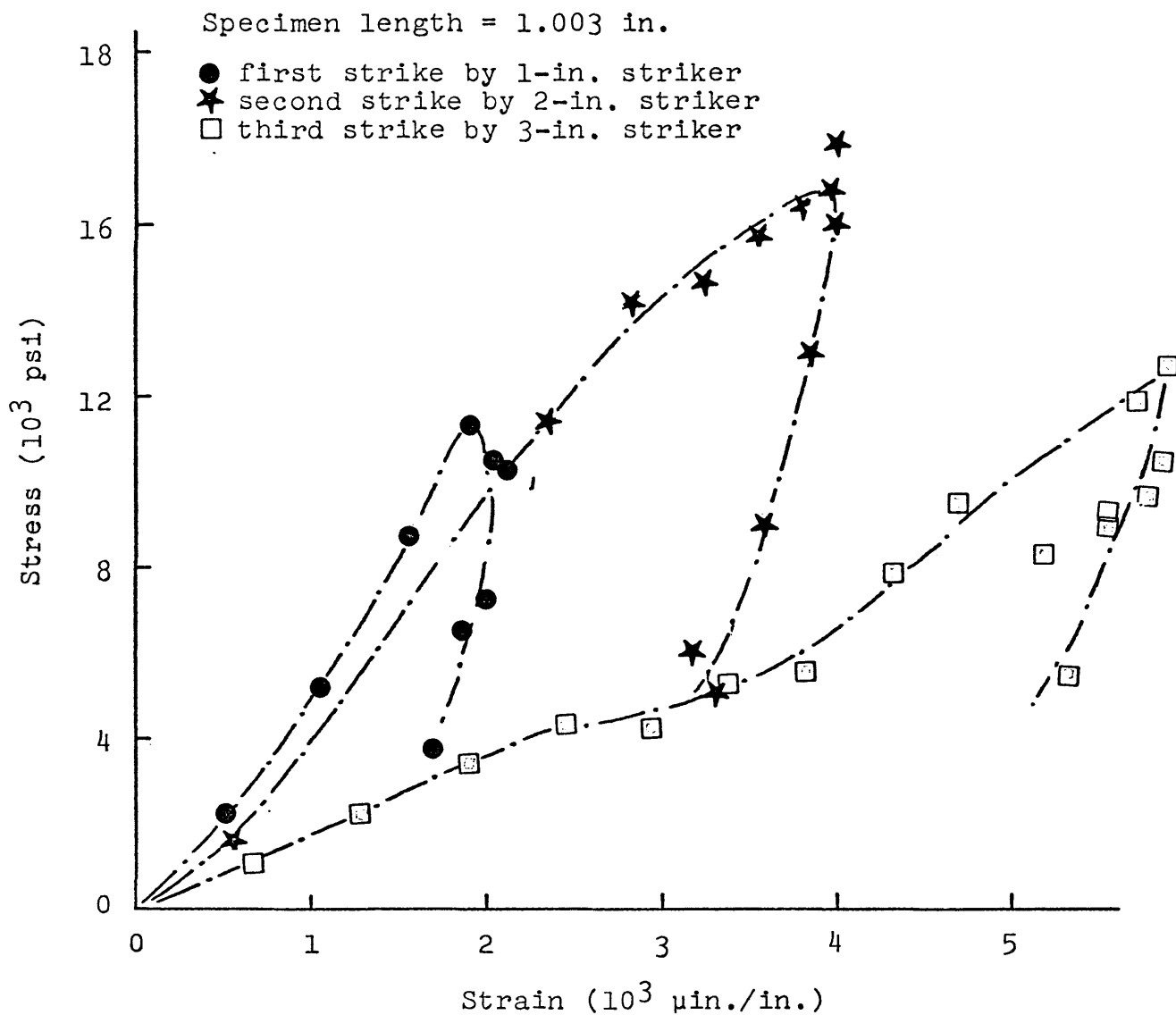


Figure 16. Dynamic Stress-strain Curves for Indiana Limestone for Successive Impacts using Several Striker Lengths.

involved in this analysis made it difficult to make definite conclusions. However, it is believed that the effect of wave length on the stress-strain behavior is not more than the inherent variation between the specimens themselves.

From the early tests it was realized that if the experimental results were to be meaningful, certain testing standards had to be established and used throughout the experiments. These are:

(1) At least five specimens were tested for each rock type and testing arrangement.

(2) A 5-in. striker was used exclusively in the experiments to provide the loading.

(3) The impact velocities were adjusted so that the amplitude of the incident wave was well above the maximum dynamic failure strength of the specimen (i.e., all the specimens fail at the first strike).

(4) The strain-time waves obtained were analyzed according to the process outlined in the previous section.

Because of the large number of curves involved only the typical curves for each type of rocks are shown here (figures 18 to 21). The results are very reproducible. To prevent confusion, the data points were not shown on the graphs.

The related static* tests using the same specimen end

*A detailed description of the equipment and procedures used is given on Appendix VI. The loading rates were kept at approximately 100 psi/sec. Normally two specimens having dimensions 1-in. in length by 1-in. in diameter were tested for each of the rock types to obtain the stress-strain relations. The static stress-strain curves were recorded directly using an X-Y recorder.

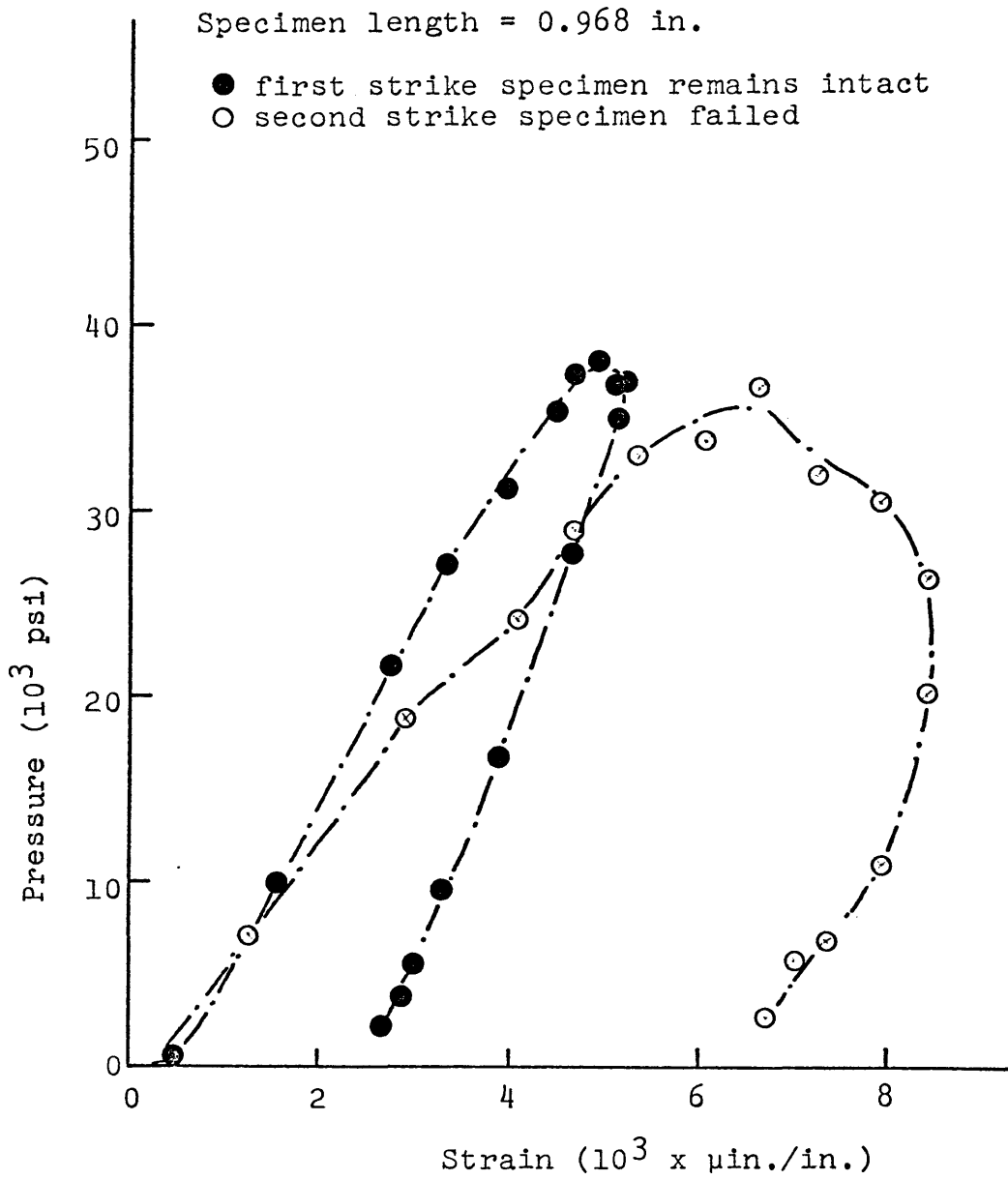


Figure 17. Dynamic Stress-strain Curves for Colorado Red Granite for Successive Impacts using a 5-in. Striker.

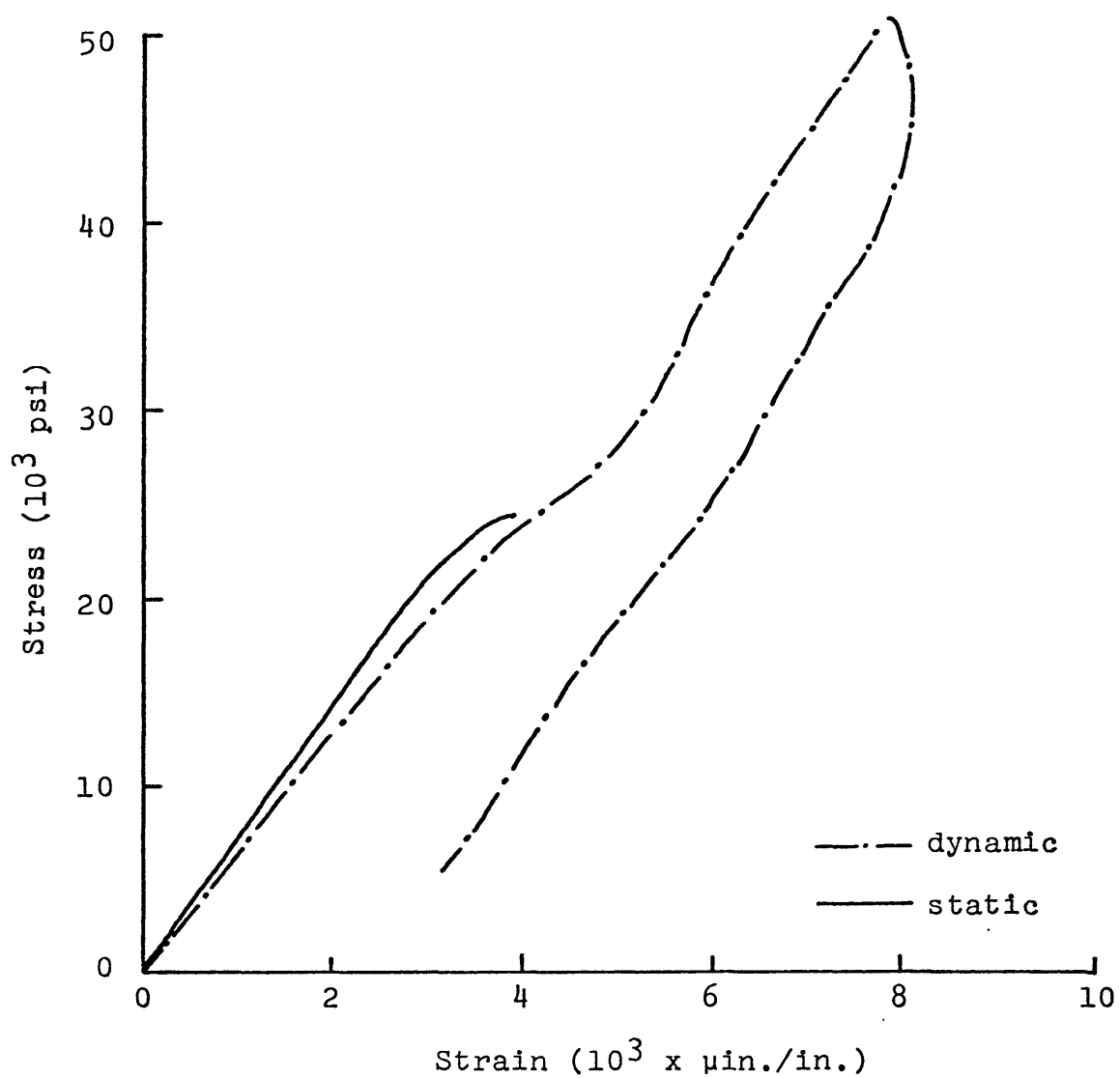


Figure 18. Experimental Static and Dynamic Stress-Strain Curves for Colorado Red Granite.

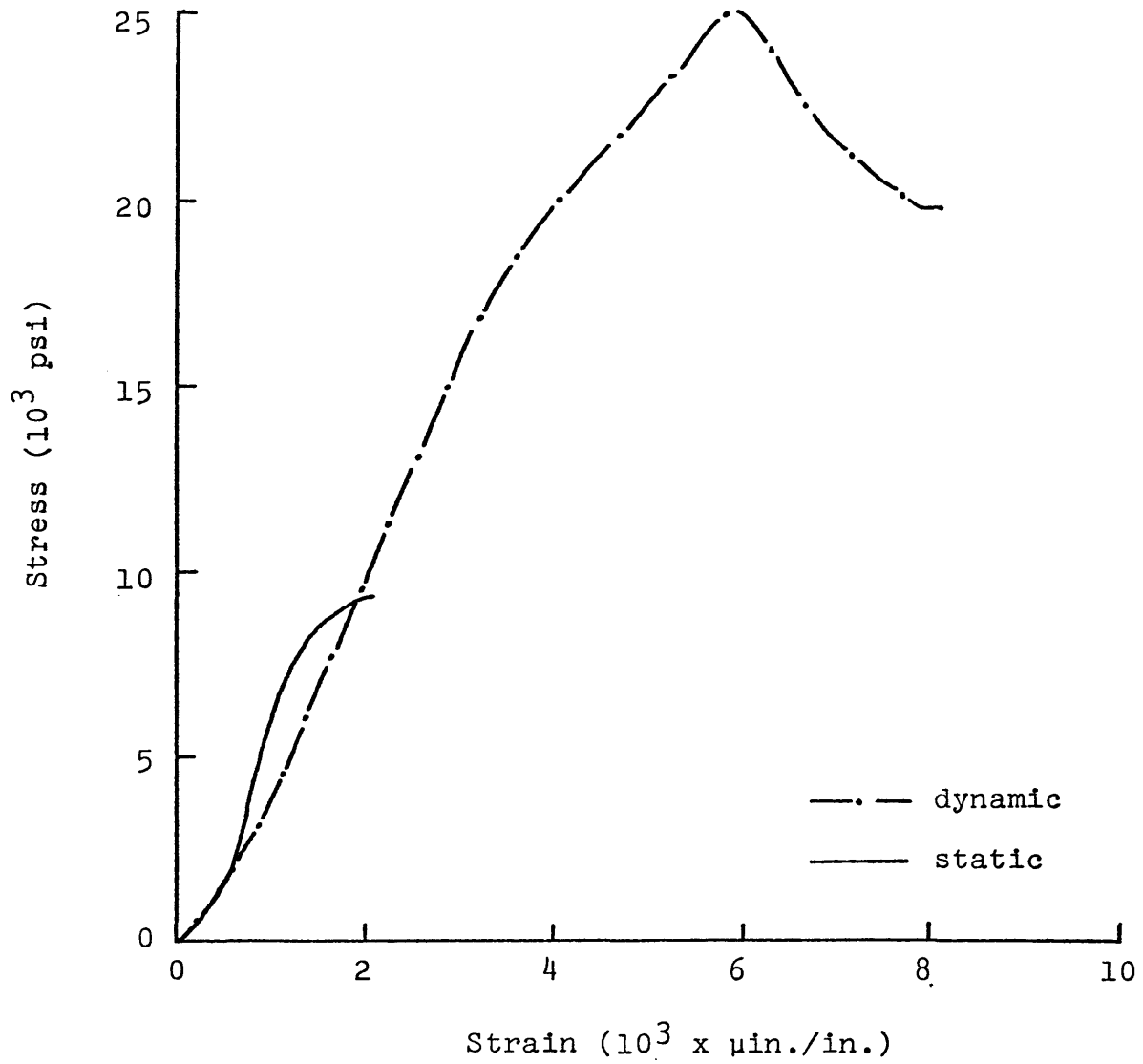


Figure 19. Experimental Static and Dynamic Stress-Strain Curves for Yule Marble.

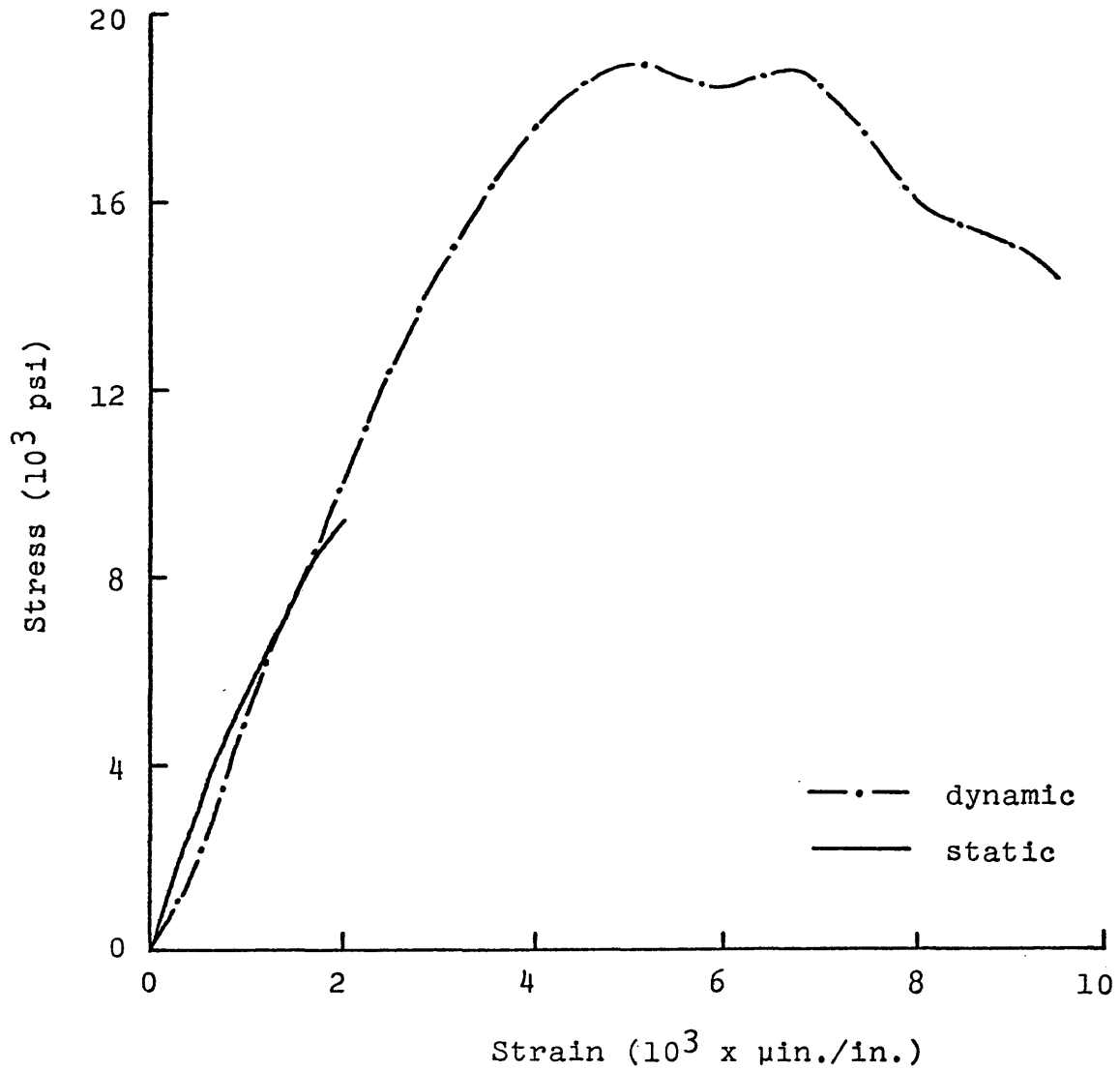


Figure 20. Experimental Static and Dynamic Stress-Strain Curves for Indiana Limestone.

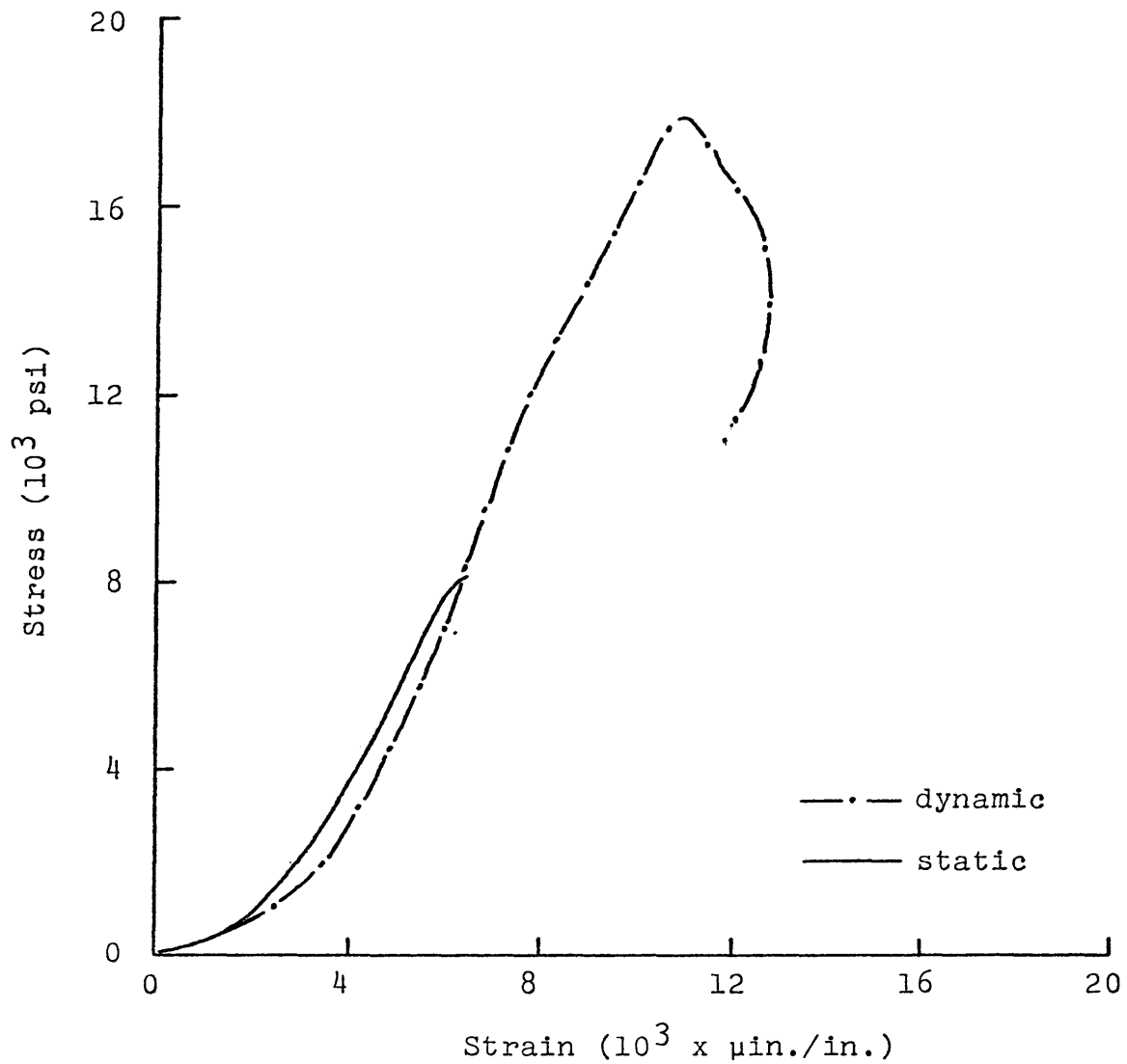


Figure 21. Experimental Static and Dynamic Stress-Strain Curves for Gray Sandstone.

conditions were performed on each rock type. The results are also presented in figures 18 to 21.

The shape of static curves agree well with the average dynamic stress-strain curves for all four rock types. However, the maximum stress levels that can be tolerated dynamically by the specimens appear to be more than double the static values.

The dynamic and static Young's moduli given as the tangent values of their respective stress-strain curves at 50% of maximum stress for each specimen tested are listed in Table 2. Also listed are the dynamic Young's moduli obtained by the resonant frequency method.* Excellent agreement (considering the variation of the rock properties within rock masses) was found between the dynamic Young's moduli from the split bar tests and the static Young's moduli. Some investigators (Friedman et. al., 1968; Perkins, 1969), using the split Hopkinson bar method to test rocks, have found in some cases that the apparent dynamic Young's moduli were higher than those obtained by low-loading rate or static testing machines. Because of incomplete descriptions of the methods used to superimpose the strain waves, it is not

*Five 2-in. long specimens of each rock type cut from the same block of rock mass were tested using this method. The dynamic Young's moduli were calculated using the measured longitudinal natural frequencies of the rock specimens. A detailed description of the equipment and the procedures used, and the calculations is given in Appendix VII.

Table 2. Dynamic and Static Young's Modulus for Four Rock Types.

Dynamic Young's Modulus			Static Young's Modulus					
Split Hopkinson Bar Test			Resonant Frequency Method			Static Loading Test		
Specimen	Length	Young's Modulus (10 ⁶ psi)	Specimen	Young's Modulus (10 ⁶ psi)	Specimen	Young's Modulus (10 ⁶ psi)	Specimen	Young's Modulus (10 ⁶ psi)
*G-101	1.060	6.7	G-201	7.2	G-111	6.9		
G-102	1.046	7.2	G-202	8.2	G-112	7.0		
G-103	1.056	8.2	G-203	8.1				
G-104	1.020	7.1	G-204	10.2				
G-105	1.056	7.2	G-205	9.2				
*M-101	1.043	5.8	M-201	2.8	M-111	4.6		
M-102	1.043	5.9	M-202	3.2	M-112	5.0		
M-103	1.044	5.7	M-203	3.8				
M-104	1.001	4.4	M-204	3.7				
M-105	1.005	4.2	M-205	3.9				
*L-101	1.003	5.3	L-201	7.7	L-111	5.0		
L-102	0.985	4.2	L-202	7.6	L-112	4.3		
L-103	1.048	4.5	L-203	6.0				
L-104	1.025	5.5	L-204	4.6				
L-105	0.968	5.1	L-205	7.0				
*S-101	1.020	3.5	S-201	2.6	S-111	2.2		
S-102	1.038	2.8	S-202	2.2	S-112	2.3		
S-103	1.031	2.9	S-203	1.9				
S-104	1.060	3.3	S-204	2.1				
S-105	1.055	3.2	S-205	2.4				

*G - Colorado Red Granite, M - Yule Marble, L - Indiana Limestone,
 S - Gray Sandstone.

known whether these effects were produced by the method of analysis or represent true rock behavior, i.e., existence of rate of loading effects. In Hakalehto's (1967) work, an error was found in the equation used to calculate the average stress and thus his curves are also in error. No rate of loading effect on the Young's modulus was found in the present tests for all four types of rock. Discrepancies between the results obtained by the resonant frequency method and that of the split bar test or static loading test are considered to be due to the character of the testing system, instead of rate of loading effects.

In Table 3 the uniaxial compressive strengths of the specimens under dynamic split Hopkinson bar and static loading are presented. The ratios of dynamic to static compressive strength are also shown in the table. In all the cases, the dynamic strengths are more than double the static strengths with the ratios being highest for Yule Marble and lowest for Colorado Red Granite. Possible reasons for the strain rate or stress rate strength dependency will be discussed later.

Strain Wave Transmission and Energy

Loss in the Specimen

The portion of the total energy going into rock fracturing can be readily analyzed through calculation of the

Table 3. Dynamic and Static Uniaxial Compressive Strength Values.

<u>Dynamic 5-in. Striker</u>		<u>Static Test</u>		
<u>Specimen</u>	<u>Compressive Strength (D) (10³ psi)</u>	<u>Specimen</u>	<u>Compressive Strength (S) (10³ psi)</u>	<u>Ratio</u>
*G-101	49.0	G-111	24.5	
G-102	51.1	G-112	31.8	
G-103	54.6	G-113	35.4	
G-104	52.3	G-114	22.0	
G-105	<u>54.7</u>	G-115	<u>28.0</u>	
	Avg. <u>52.3</u>		Avg. <u>26.3</u>	2.0
*M-101	31.3	M-111	9.2	
M-102	23.0	M-112	10.2	
M-103	20.9	M-113	9.4	
M-104	30.1	M-114	8.4	
M-105	<u>20.0</u>	M-115	<u>9.9</u>	
	Avg. <u>25.1</u>		Avg. <u>9.4</u>	2.7
*L-101	20.5	L-111	9.0	
L-102	16.9	L-112	7.2	
L-103	20.1	L-113	7.7	
L-104	17.0	L-114	8.3	
L-105	<u>16.9</u>	L-115	<u>9.6</u>	
	Avg. <u>18.3</u>		Avg. <u>8.4</u>	2.2
*S-101	13.1	S-111	8.0	
S-102	20.9	S-112	8.7	
S-103	17.5	S-113	5.1	
S-104	17.6	S-114	8.0	
S-105	<u>16.7</u>	S-115	<u>8.6</u>	
	Avg. <u>17.2</u>		Avg. <u>7.7</u>	2.2

*G - Colorado Red Granite, M - Yule Marble, L - Indiana Limestone, S - Gray Sandstone.

energy content of the various recorded elastic strain-time waves. In Table 4 values of the strain energy (in. in.-lbs) contained in the incident, reflected, and transmitted parts of a number of strain waves are given. Also listed are the maximum average stresses transmitted by the specimens, the sum of the transmitted and reflected strain energy (denoted as the total recovered energy), the energy loss in the specimen, the percent energy loss in terms of the incident energy in the specimens and the specific fracture energy. All specimens were approximately 1-in. long, were impacted by a 5-in. long striker and failed in the first strike.

For a given incident wave length, the amount of incident strain energy reflected back into the incident bar or transmitted through the transmitter bar depends on the "impedance match" of the specimens and steel bars, and also on the specimen length. This energy balance is described by equation (3-26).

If the amplitude of the wave entering the specimen is higher than the critical fracture strength of the solid, energy will be dissipated in the specimen to create new fracture surfaces and go into kinetic energy of the fragments. This can be expressed as

$$E_l = E_{sf} + E_{mv} + E_o$$

Table 4. Analysis of the Energy Content in Strain Waves.

Specimen	Maximum Stress (10 ³ psi)	Incident Energy (in.-lbs)		Reflected Energy (in.-lbs)		Transmitted Energy (in.-lbs)		Total Recovered Energy (in.-lbs)		Specific Fracture Energy (lbs/in ²)		Percent Energy Loss %
		E _i	E _r	E _r	E _t	E _r +E _t	E _l	E _s	E _s			
*G-101	49.0	713	81	406	487	226	288	32				
G-102	51.1	677	46	450	496	181	230	27				
G-103	54.6	775	47	534	581	194	247	25				
G-104	52.4	763	56	580	536	228	290	30				
G-105	54.7	781	57	503	560	201	281	28				
*M-101	31.3	688	131	132	263	425	541	62				
M-102	23.0	405	118	65	183	222	283	55				
M-103	20.9	435	145	52	197	238	303	55				
M-104	30.1	428	68	127	195	233	297	54				
M-105	20.1	390	129	49	178	212	270	54				
*L-101	13.7	410	323	39	362	49	62	12				
L-102	20.9	313	181	65	246	67	85	22				
L-103	17.5	290	171	48	219	71	90	24				
L-104	17.6	312	172	48	220	92	117	29				
L-105	16.7	228	148	50	198	30	38	13				
*S-101	20.5	440	148	72	220	221	281	50				
S-102	16.9	-	-	-	-	-	-	-				
S-103	20.1	335	107	75	182	152	192	45				
S-104	15.2	235	108	50	158	77	98	33				
S-105	16.9	237	105	49	154	84	69	35				

*G - Colorado Red Granite, M - Yule Marble, L - Indiana Limestone, S - Gray Sandstone.

where:

E_{sf} = creation of new fracture surfaces

E_{mv} = energy used in the motion of the fragments

E_o = all other energy losses

Other forms of energy loss include: frictional loss between the bar and specimen interfaces, sliding between the fracture surfaces, scattering of the waves at the grain boundaries, and possible inelastic deformations.

For a brittle solid, the greatest part of energy loss can probably be contributed to that needed to create new fracture surfaces. Since all the specimens failed at a single strike, the energy loss in the specimen divided by the volume of the specimen gives the amount of energy necessary to break a unit volume of rock under existing test conditions. These values are called the specific fracture energy of the rock (E_{sp}). The specific fracture energy is observed to increase as the incident energy increases. This is because when the specimen fails violently, the excess energy goes into producing motion of the rock fragments (pieces of rock fly away).

Although the specific fracture energy was also found to depend on the mode of failure of the specimens, a limiting value of the specific fracture energy or the minimum specific fracture energy for a given type of rock may be of value as a rock breaking index.

A series of experiments was conducted to examine the strain wave transmission and energy loss in partially failed specimens. Multiple impacts were performed on specimens of Colorado Red Granite having lengths of 1-, 1.5-, and 2-inches. The results including the number of consecutive strikes given to the specimens, the maximum loading stress, incident, reflected, and transmitted strain energies, the energy loss, and the percent energy loss in terms of the incident strain energy are summarized in Tables 5 to 7.

The incident strain energy, maximum stress, and the percent energy loss as a function of the number of the consecutive strikes are plotted in figures 22 to 24.

Initial loading of the specimens was done with a stress amplitude lower than their static compressive strength. The stress amplitudes were gradually increased until the specimen finally failed. The strike numbers where the specimens partially failed are indicated by a star. Additional strikes were given at the same or at a lower striking velocity after the specimens showed signs of partial failure or some visible fault at the specimen surfaces. It can be concluded that:

- (1) At low stress levels the rock behaves elastically with only minor and irregular energy losses in the specimens.

A number of multiple impact tests performed at low impact amplitudes (stress amplitudes lower than the static failure strength of the rock) revealed that specimens could be impacted over 20 strikes at these

Table 5. Energy Loss in Specimens Subjected to Multiple Impact - Specimen G-121,
Length = 1.045 in.

No. of Strikes	Maximum Stress (10 ³ psi)	Incident Energy E _i (in.-lbs)	Reflected Energy E _r (in.-lbs)	Transmitted Energy E _t (in.-lbs)	Total		Percent Energy Loss %
					Recovered Energy E _r +E _t (in.-lbs)	Energy Loss E _l (in.-lbs)	
1	15.1	56	18	31	49	37	12
2	21.8	109	29	64	93	15	14
3	25.7	159	52	82	134	24	15
4	34.3	258	51	155	206	52	20
5	33.4	283	41	173	214	49	17
6	27.9	162	29	117	146	16	10
7	36.9	403	63	188	251	152	38
*8	30.1	213	46	148	194	19	9
9	8.3	36	22	6	28	8	22

Table 6. Energy Loss in Specimens Subjected to Multiple Impact - Specimen G-221, Length = 1.568 in.

No. of Strikes	Maximum Stress (10 ³ psi)	Incident Energy E _i (in.-lbs)	Reflected Energy E _r (in.-lbs)	Transmitted Energy E _t (in.-lbs)	Total Recovered Energy E _r +E _t (in.-lbs)	Energy Loss E _l (in.-lbs)	Percent Energy Loss %
1	9.4	23	7	13	20	3	11
2	21.4	108	23	81	104	5	4
3	24.2	164	34	100	134	30	18
4	34.9	416	68	225	293	123	29
5	36.6	363	55	228	283	81	22
*6	36.2	395	89	214	303	92	23
7	34.5	413	66	230	296	116	28
8	29.2	416	92	130	222	194	47

Table 7. Energy Loss in Specimens Subjected to Multiple Impact - Specimen G-321, Length = 2.011 in.)

No. of Strikes	Maximum Stress (10 ³ psi)	Incident Energy E_i (in.-lbs)	Reflected Energy E_r (in.-lbs)	Transmitted Energy E_t (in.-lbs)	Total Recovered Energy $E_r + E_t$ (in.-lbs)	Energy Loss E_l (in.-lbs)	Percent Energy Loss %
1	16.6	79	23	44	67	12	16
2	15.9	98	52	27	79	19	20
3	20.1	149	47	73	120	29	19
4	27.6	233	54	118	162	62	27
5	30.2	289	63	154	217	72	25
6	34.8	364	87	187	274	91	25
7	31.6	400	108	156	264	135	34
*8	39.9	565	93	240	333	232	41
9	31.0	533	107	153	260	273	51

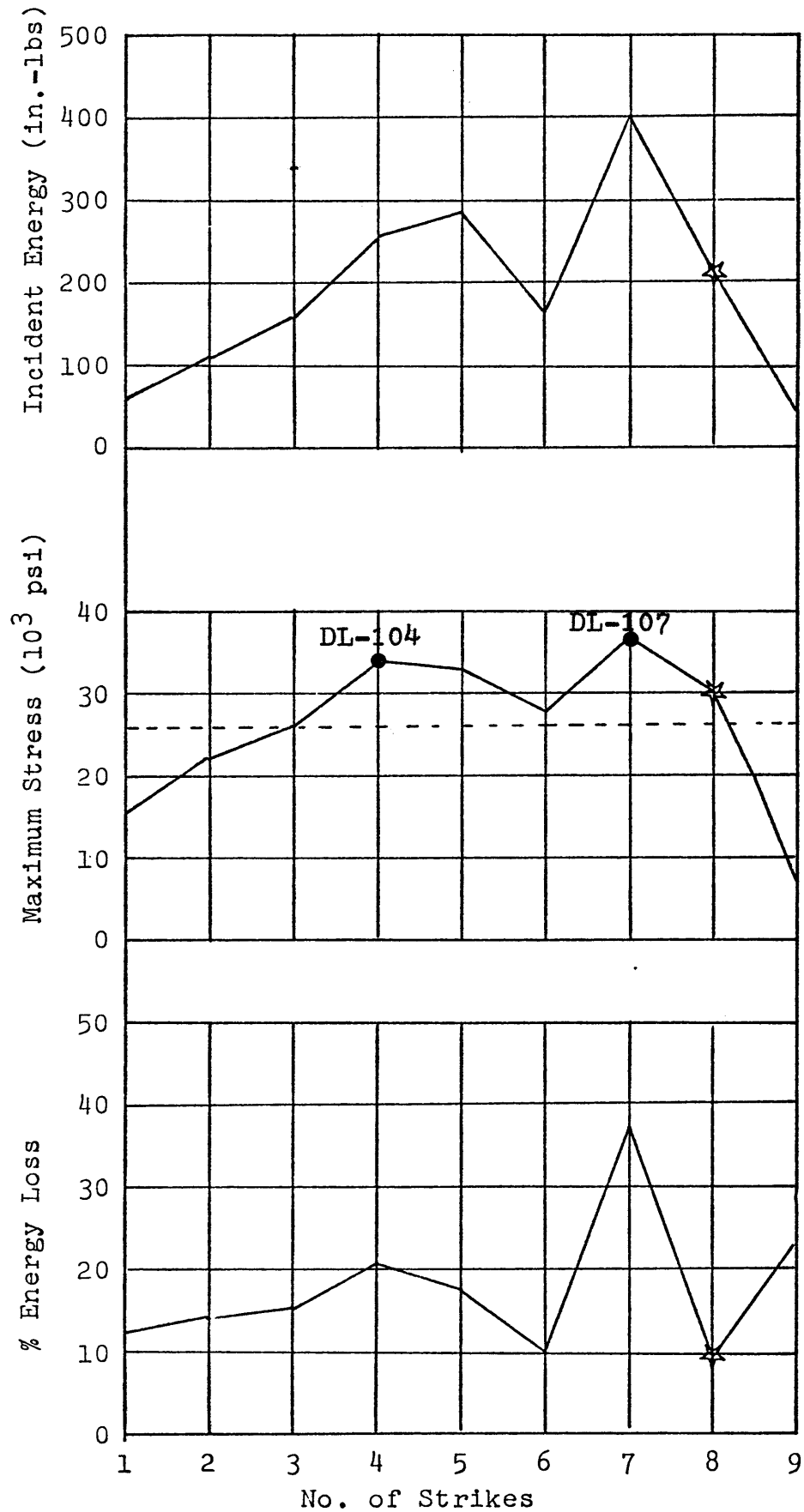


Figure 22. Correlation of the Incident Energy, Maximum Stress and Percent Energy Loss with the Number of Consecutive Strikes - Specimen G-121, Length = 1.045 in.

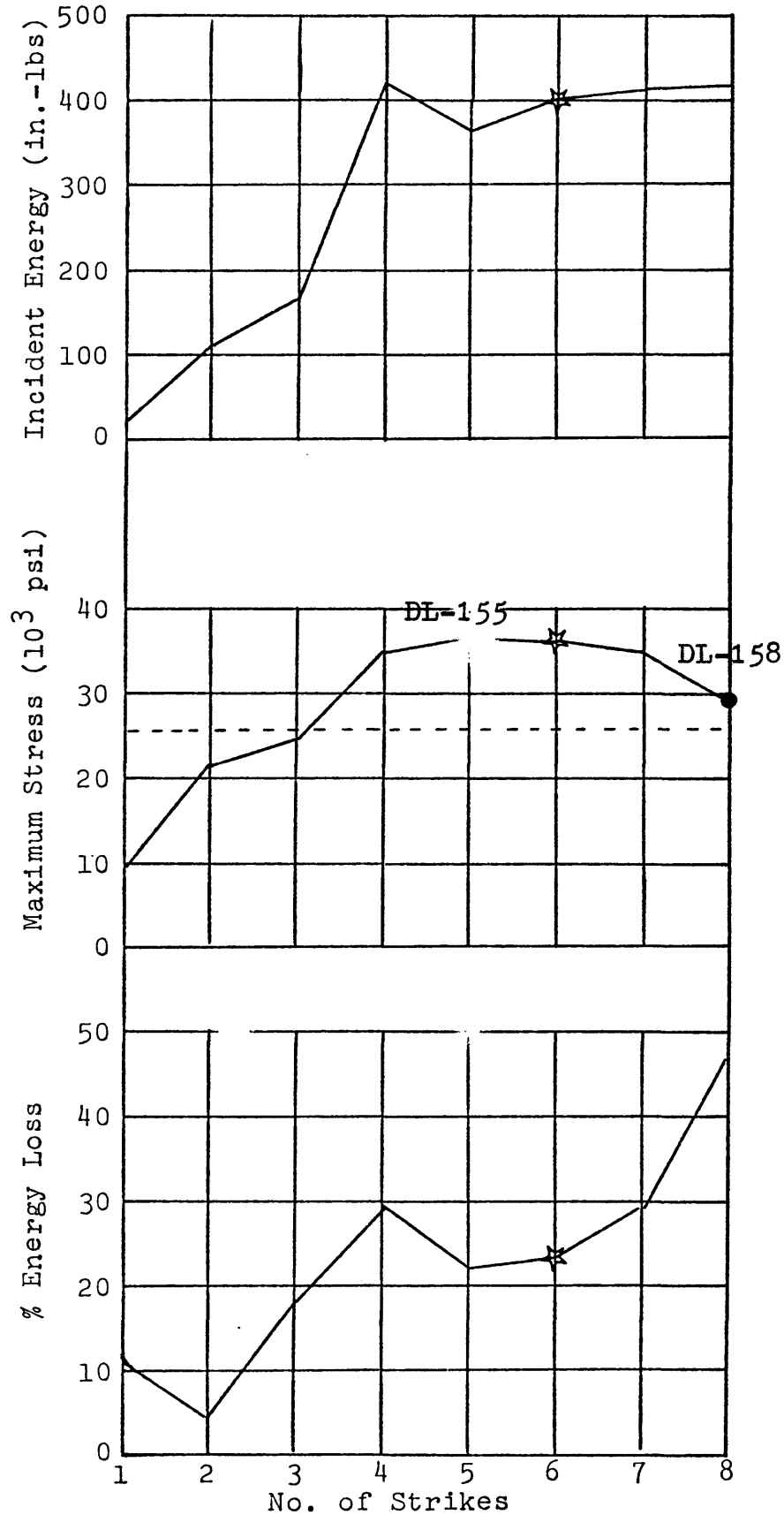


Figure 23. Correlation of the Incident Energy, Maximum Stress, and Percent Energy Loss with the Number of Consecutive Strikes - Specimen G-221, Length = 1.568 in.

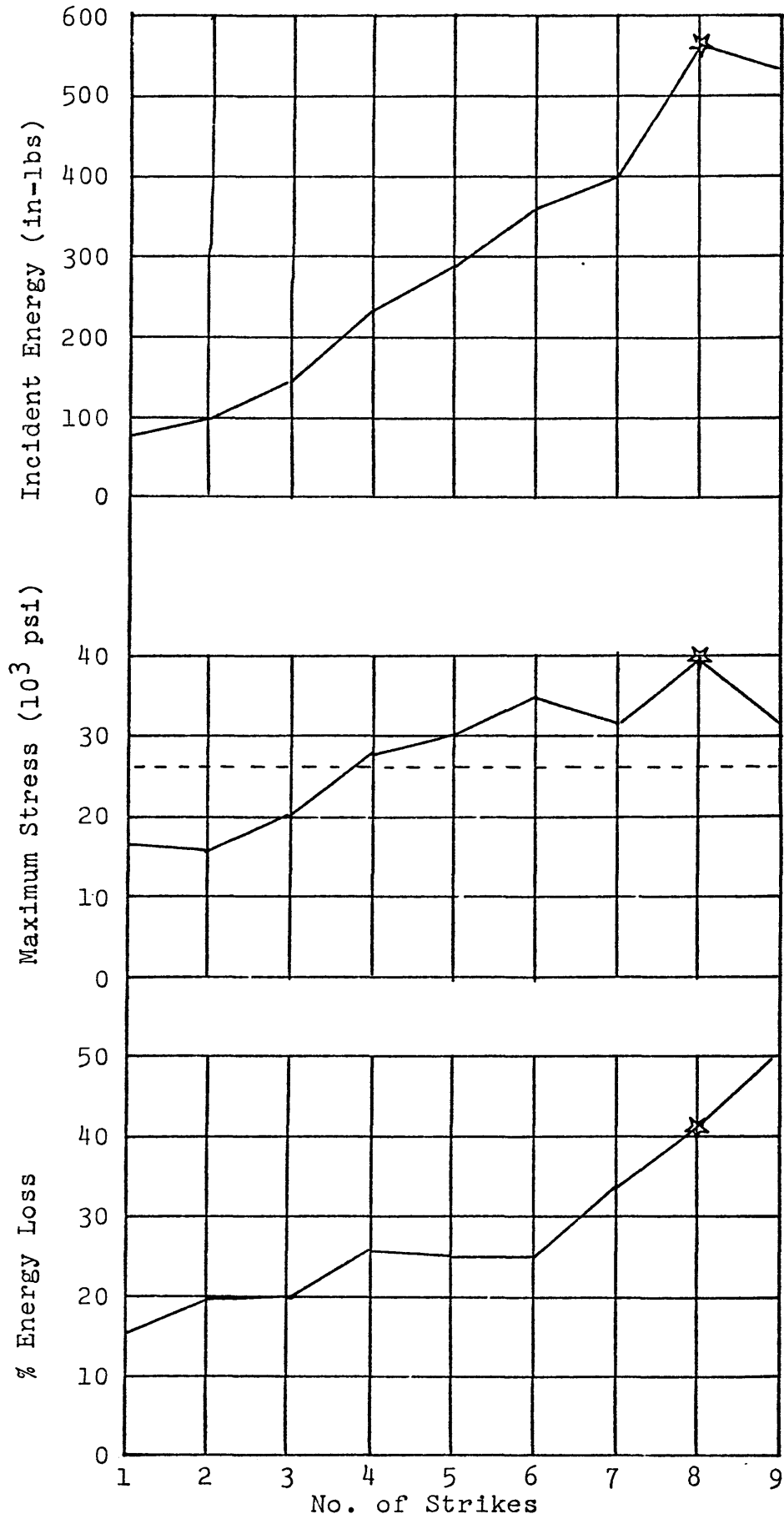


Figure 24. Correlation of the Incident Energy, Maximum Stress and Percent Energy Loss with the Number of Consecutive Strikes - Specimen G-321, Length = 2.011 in.

stress levels and remain intact.

- (2) Before the specimens appeared to partially fail, the energy loss in the specimen increased gradually as the incident energy increased. The percent energy loss in general follows the same trend. However, after the specimens reached partial failure, the percentage energy loss greatly increased.
- (3) The maximum stress in the specimen (as determined from the stress-strain curves) and the total recovered energy decreases after the specimen has partially failed even if the amplitude of the strain waves are kept at the same level.
- (4) A comparison of the results in Tables 4 and 5 shows that the maximum stresses which can be tolerated by specimens subjected to multiple impact is considerably lower than that of the specimens subjected to a single strike. The strike where the maximum stress is reached by the specimen does not necessarily correspond to the strike where partial failure of the specimen was observed (see the test for Specimen G-121 for example).

Fracture of Rock Under the
Split Hopkinson Bar Test

A careful examination of polished sections of Colorado Red Granite specimens was conducted to compare rock failure

mechanisms under impact and static loading. The observations were limited to Colorado Red Granite specimens, since substantial amounts of the partially fractured parts of the other rock types could not be successfully recovered. For Yule Marble and Gray Sandstone under impact loading, it was observed that general failure of these rocks was not accompanied by the formation of a single shear zone (as is common for some other rock types), but rather by a general loosening of the grains. After testing, the specimens resemble a rather loosely packed sand.

After testing, the granite specimens were placed in a steel mold, cast in hydrostone and sectioned. They were then polished, treated with a fluorescent dye (type Zyglo ZL-22), and the surfaces examined under a microscope. The fluorescent sections were photographed under combined ultraviolet light and white light using 35 mm plus-X film. Some representative pictures are included in figures 25 to 32. Figures 25, 26, and 27 show the longitudinal cross sections of 1-in. specimens under static uniaxial compressive load. Specimen SL-101 was loaded to 80% of its average compressive strength. No signs of additional fracturing can be observed by comparison with undeformed specimens. Specimen SL-102 was loaded to 97% of its average compressive strength. Extensive intra-granular fracturing and loosening of grain boundaries within the specimens is evident. Specimen SL-103 was loaded to its full strength. Some major axially oriented

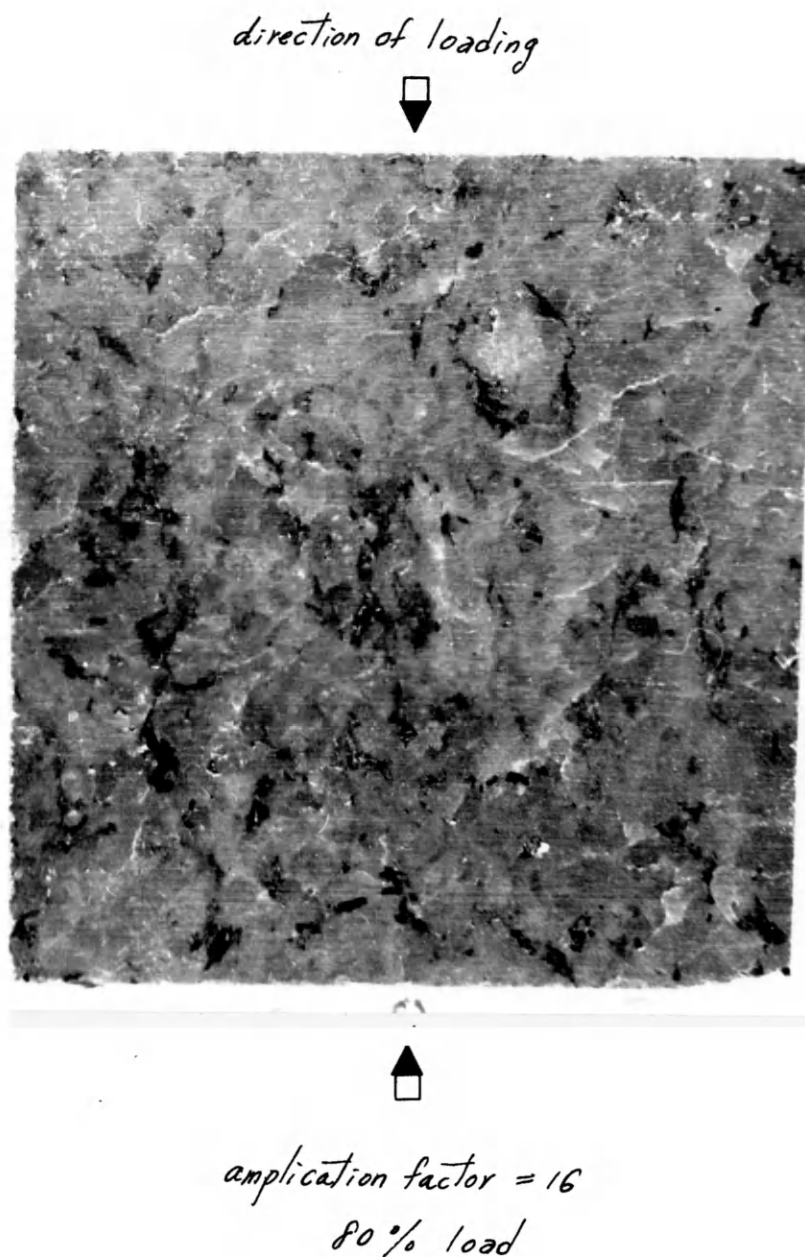


Figure 25. Longitudinal Cross Section of Colorado Red Granite Specimen Loaded in the Static Testing Machine (SL-101, 1-in. long).

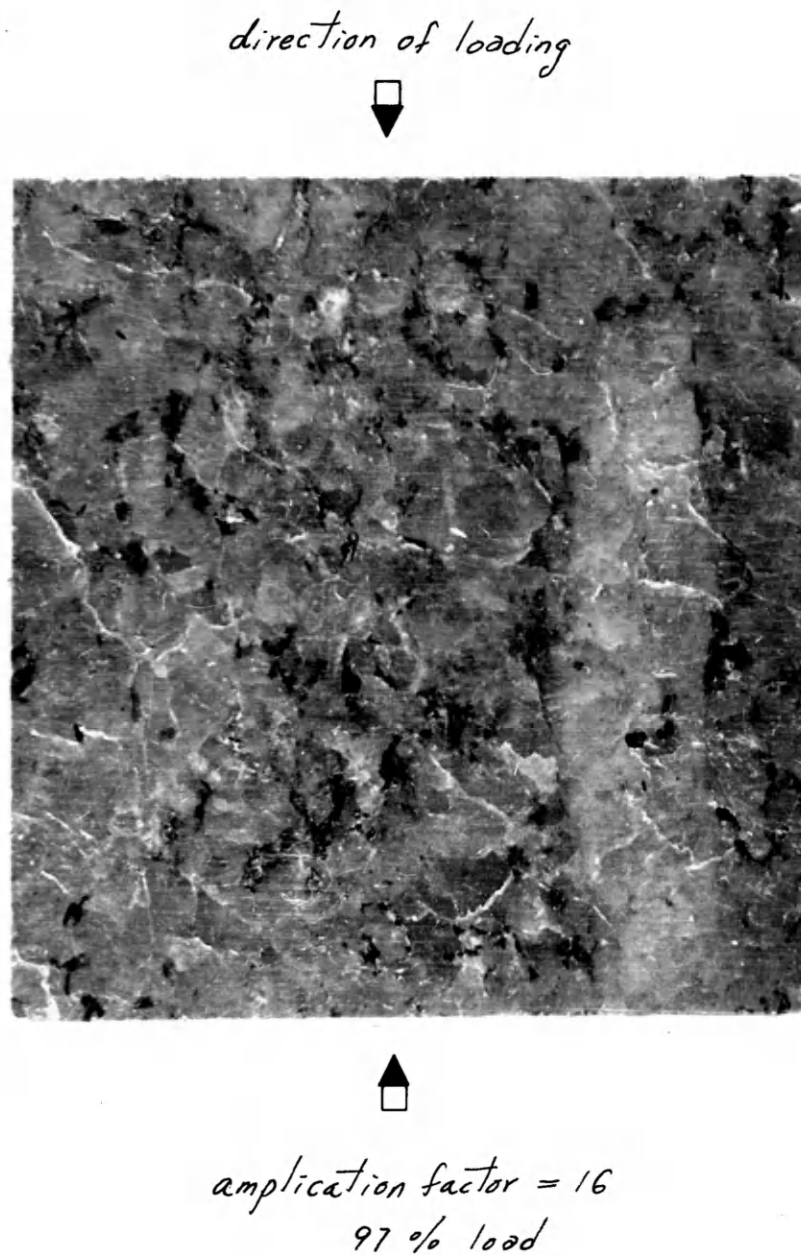


Figure 26. Longitudinal Cross Section of Colorado Red Granite Specimen Loaded in the Static Testing Machine (SL-102, 1-in. long).

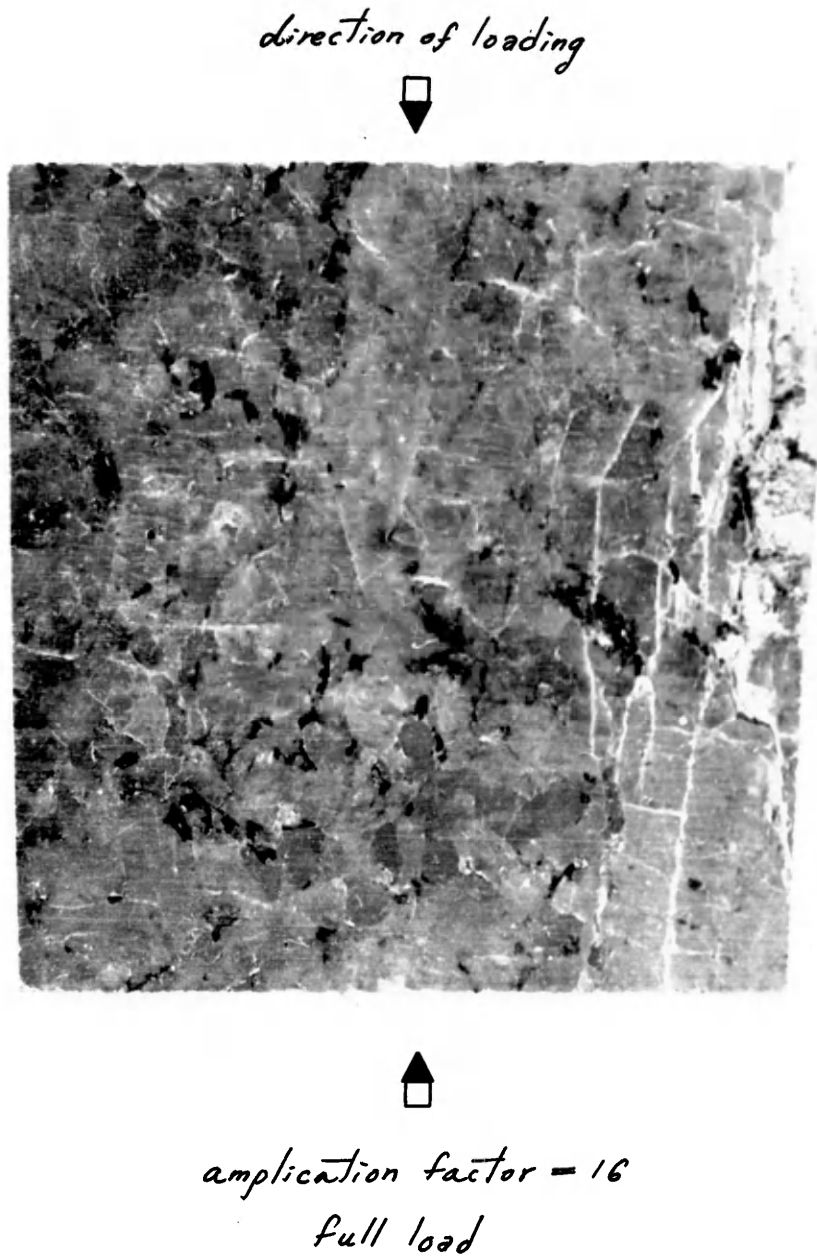


Figure 27. Longitudinal Cross Section of Colorado Red Granite Specimen Loaded in the Static Testing Machine (SL-103, 1-in. long).

cracks which lead to general failure of the specimens were observed in all specimens.

Figures 28-31 show the longitudinal cross sections of specimens under impact loading. Specimens DL-104 and DL-107 correspond to the loading history indicated on figure 22. Similarly, specimens DL-155 and DL-158 correspond to the loading history indicated on figure 23.

Fracture appears to be initiated quite similarly under both static and dynamic loading conditions. Extensive fracture growth was observed long before the specimen reaches its "dynamic compressive strength" as given by the single strike tests. As a matter of fact, fractures were observed at about the same critical stress level. Through multiple loading of the specimens, the degree of fracturing has been gradually increased as the total number of impacts is increased.

Under impact loading, fractures were observed to be initiated within the specimens along the grain boundaries in a random fashion, however they tend to extend parallel to the stress wave directions.

A microscopic examination of the cracks show that the crack surfaces are much more irregular than under static loading conditions. Apparently sliding along the crack surfaces was not evident at this stage in the sequence of events leading to general failure of the specimens. Major

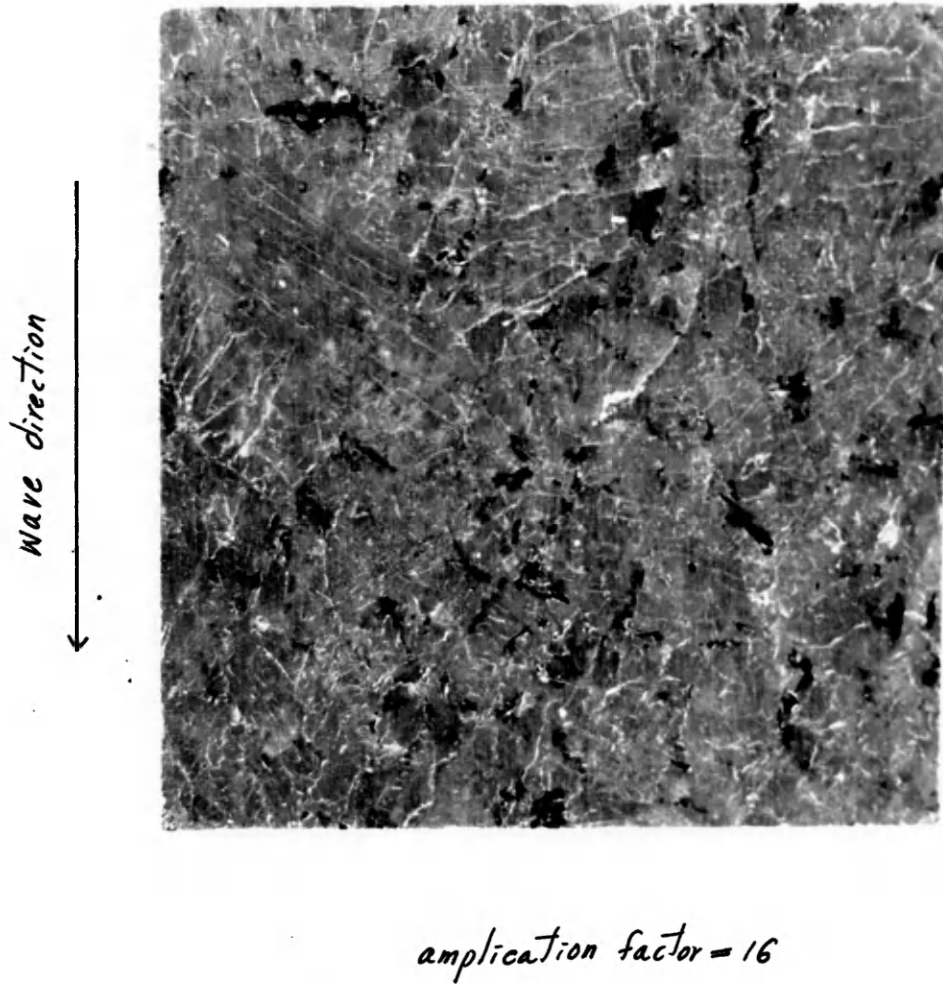
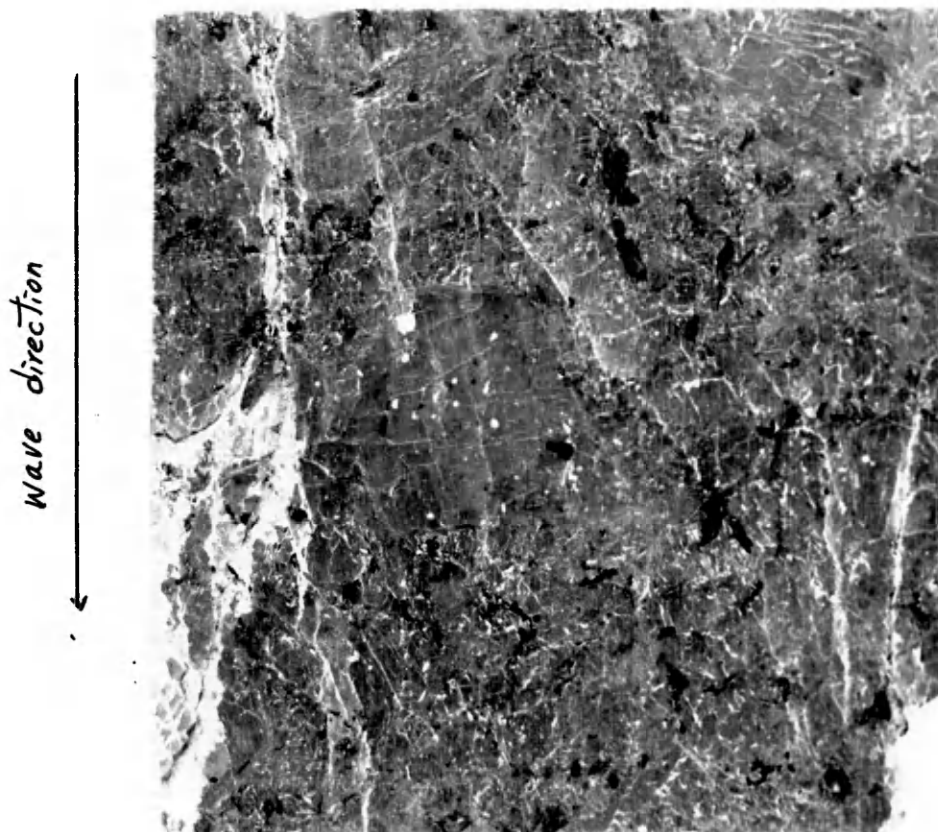
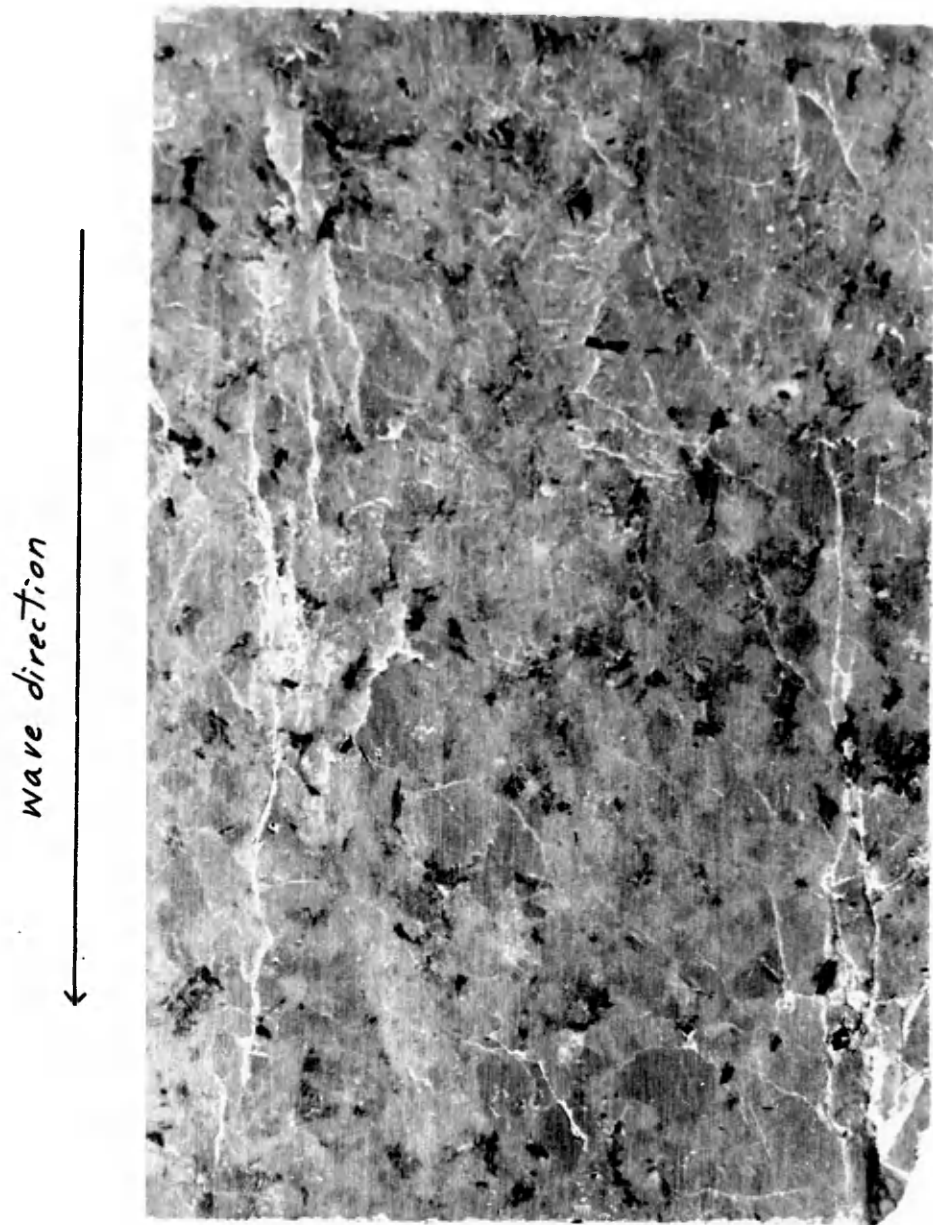


Figure 28. Longitudinal Cross Section of Colorado Red Granite Specimen Loaded in the Split Hopkinson Bar (DL-104, 1-in. long).



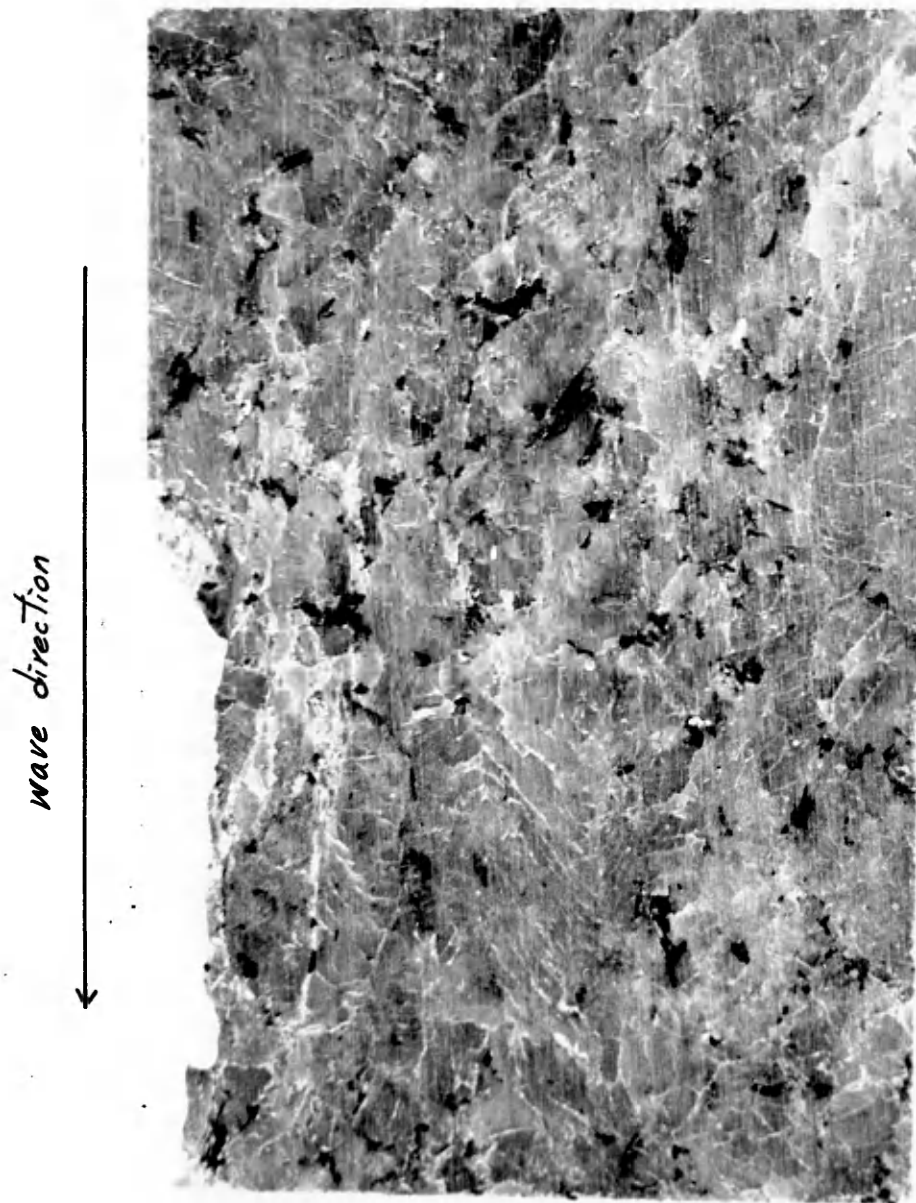
amplification factor = 16

Figure 29. Longitudinal Cross Section of Colorado Red Granite Specimen Loaded in the Split Hopkinson Bar (DL-107, 1-in. long).



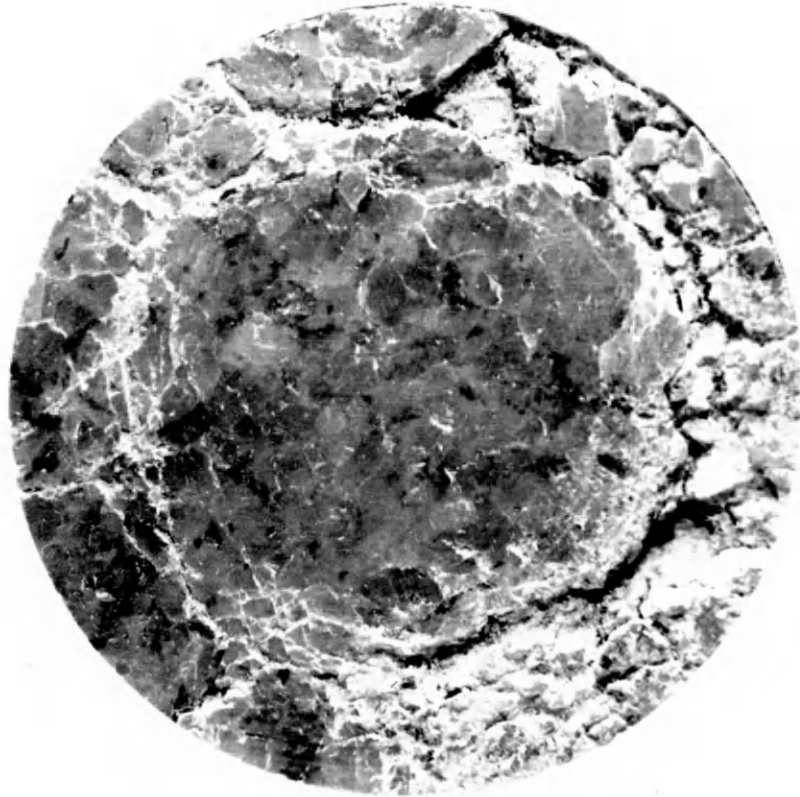
amplification factor = 16

Figure 30. Longitudinal Cross Section of Colorado Red Granite Specimen Loaded in the Split Hopkinson Bar (DL-155, 1.5-in. long).



amplification factor = 16

Figure 31. Longitudinal Cross Section of Colorado Red Granite Specimen Loaded in the Split Hopkinson Bar (DL-158, 1.5-in. long).



amplification factor = 16

Figure 32. Transverse Cross Section of Colorado Red Granite Specimen Loaded in the Split Hopkinson Bar (G-103, 0.25-in. from the Impacted End).

faults developed only after a great number of cracks have already initiated and extended. This is quite different from that observed in static loading in which one or more major faults develop and lead to general failure of the specimen long before any great extent of crack initiation is possible.

A higher intensity of cracks throughout the specimens was found in the split Hopkinson bar loading. The initiation or extension of the microcracks were thought of as the locations where local stresses (due to stress concentration at the tip of the microcracks or due to the irregularities in the specimens) exceed the critical strength of the rock. In static loading the applied stress increases slowly, microcracks will first be initiated at the location with highest stress concentration, then the location with the second highest stress concentration. After a finite number of microcracks have been extended, they will join together and cause final failure of the specimen. However, in dynamic loading, it is felt that the instantaneous maximum stresses carried by the strain wave may be well above the critical fracturing stress level. The propagation speed of the longer cracks may be slower than the increase in stress amplitude. The crack initiation will thus at the same time go to locations with a much lower stress concentration; i.e., the existing microcracks which in the static cases were not critical become critical. The probability of crack initiation

increases and the number of cracks increase accordingly.

In most cases, the cracks were distributed more uniformly across the cross section of the specimens than in static loading. This agrees with the observation of Hakalehto (1967). Figure 32 shows a transverse cross section of a specimen subjected to a single blow. The specimen was cut 0.25-in. from its impacted end. Extension fractures developed concentric to its longitudinal axis; the effect of end confinement is significant and leads to a well defined failure cone.

DISCUSSION

Dynamic Loading and Unloading Processes

Although rock is often characterized as a linearly elastic material it contains randomly oriented micro-cracks and pore spaces which lead to a nonlinear behavior. A representative uniaxial stress-strain curve for rock during static loading and unloading cycles is shown as the solid line of figure 33. The loading portion of the curve can be divided into the following three regions. The nonlinear behavior at low stress level arising from the closing up of the microcracks and pores is shown as region I. Region II represents the linearly elastic behavior of the bulk material, and region III represents the stage of nucleation of micro-cracks which leads to final general failure of the specimen. The slope of the curve depends both on the magnitude of the uniaxial stress and whether the stress is increasing (loading) or decreasing (unloading). Thus, for many rocks, the Young's modulus is not a constant but depends on the stress conditions and history of stress application. In addition to non-linear elastic behavior many rocks also exhibit an inelastic behavior indicated by the area included in the loading and unloading cycle at point A.

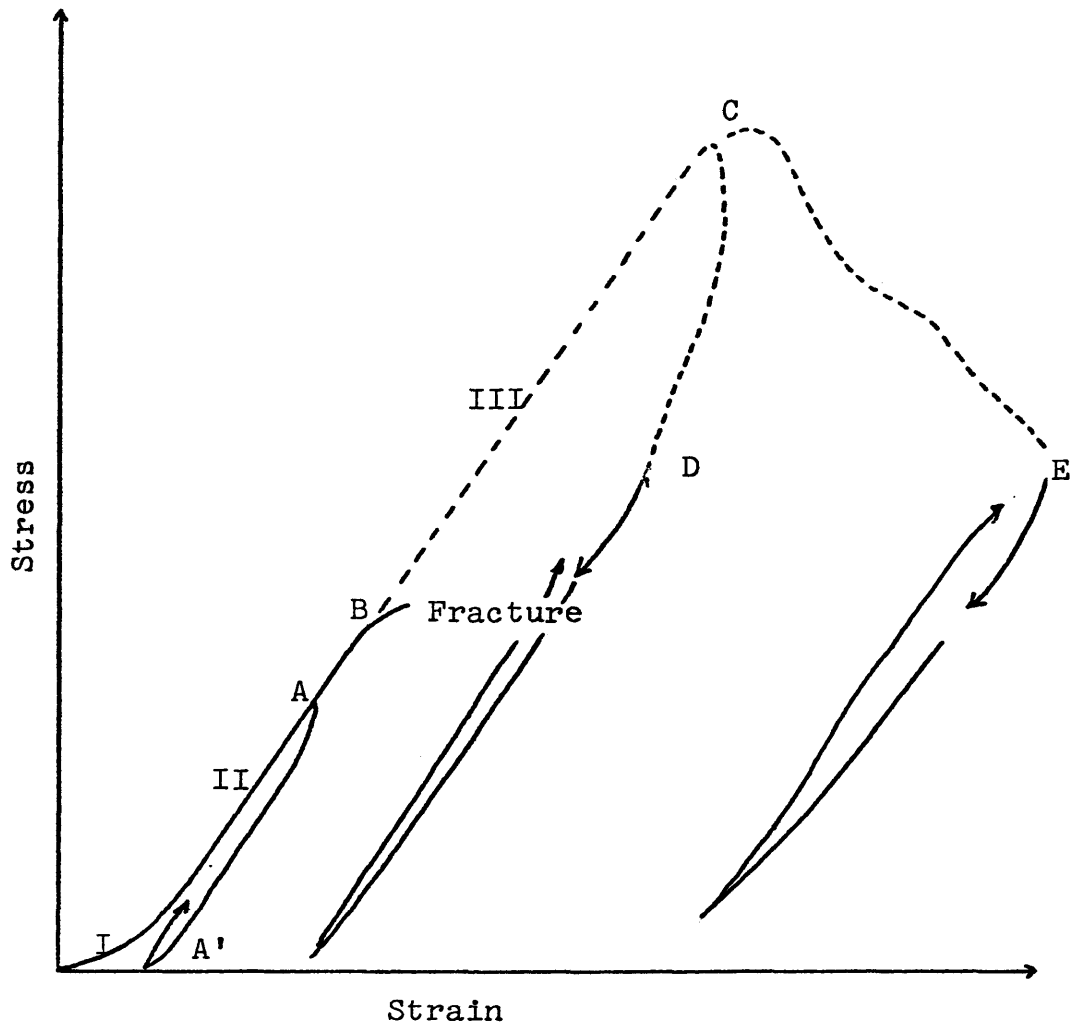


Figure 33. Standard Stress-strain Curves for Static and Dynamic Loading.

An examination of the static stress-strain curves of Gray Sandstone and Yule Marble reveals that both rocks follow all three stages of the loading process of the standard curve depicted in figure 33. For Colorado Red Granite and Indiana Limestone the first stage of the non-linear portion at low stress level (closing of cracks and pores) is not very significant. The dynamic curves closely follow the static curves up to the final stages of crack nucleation. It appears that crack initiation takes place at a similar stress level for both dynamic and static loading. It is suggested that crack growth begins at point B (where the behavior of the rock once again begins to be non-linear).

A standard dynamic stress-strain curve according to the experimental observations is drawn as a dotted line above the standard static stress-strain curves. The loading part of the curve is also divided into three regions. Regions I and II are part of the standard curve for static loading. Region III is similar to the final region of the static curve (where the rock reaches its critical extension stress at point B), but extends beyond that to the much higher stress level C, denoted as the "dynamic compressive strength" of the specimen.

In region III, the stress-strain relationship is unchanged; however, a great number of cracks have already

initiated and extended. As the stress level increases along this path, more crack nucleation is observed.

Curves D and E designate the post-failure or unloading portions of the dynamic curves. These curves are incomplete, since they are usually terminated by an excessive amount of "noise" in the tail portion of the strain-waves. A considerable hysteresis loop representing a large amount of dissipative energy loss in the specimen characterizes this unloading curve. The hysteresis loop, commonly found in the static uniaxial stress-strain curve of rock as shown in the loop A-A'-A is small. It has been explained as being due to frictional effects along the crack surfaces.

Similarities appear to exist between the post-failure characteristic under impact loading and that for rock in the fractured region under low loading rates (determined from "complete stress-strain curve").

A complete stress-strain curve for rock can only be obtained by using a high modulus or "stiff" testing system as shown by Wawersik (1968). The relationship between the load carrying ability and the displacement of a specimen once its strength has been exceeded depends strongly on the character of the testing system. Figure 34 shows that if the slope of the unloading characteristic K of the machine is steeper than that of the specimen K_p , the energy (proportional to the area AEFB) released by the machine during an

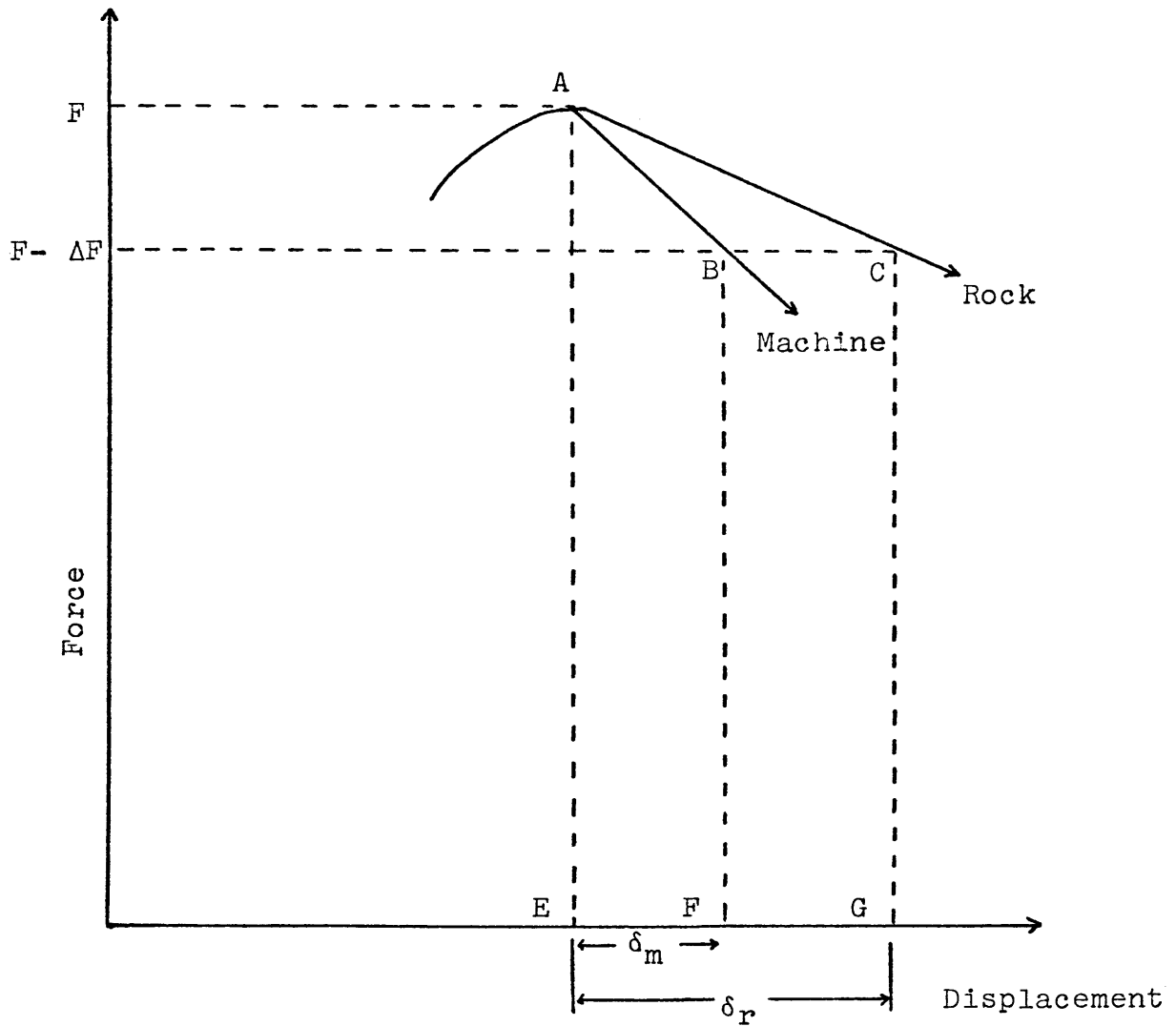


Figure 34. Idealized Force-Displacement Curves for Components of Testing System.

incremental increase in deformation (beyond the deformation corresponding to the maximum load at point B) is less than the energy AEGC which the specimen can absorb. Thus, point A. represents a stable equilibrium configuration of the rock-machine system and the specimen will not fail violently.

The split Hopkinson bar can be, in a certain sense, considered as a "stiff" testing machine. The specimen is loaded by a "travelling" strain wave and the energy carried by the strain wave is limited. In other words a "controlled amount of energy" is given to the specimen during both loading and unloading processes. For an ordinary testing machine (or a "soft" machine), the loading platens gradually store a large amount of energy during the loading cycle. The energy is released to the specimen at an accelerated rate as the specimen loses its strength. A high unloading strain rate is caused by a high velocity rebound of the platens (the strain rate can be thought of as the relative velocities between the loading platens divided by the distance between the platens). For a loading strain wave, the strain rate is almost constant during both loading and unloading cycles (see figure 13c).

A complete force-displacement curve for Tennessee Marble by Wawersik (1968) is reproduced in figure 35. A series of unloading and loading cycles during stable failure of the rock specimen are given. A decrease in the slope for consecutive unloading and loading cycles indicate that rock

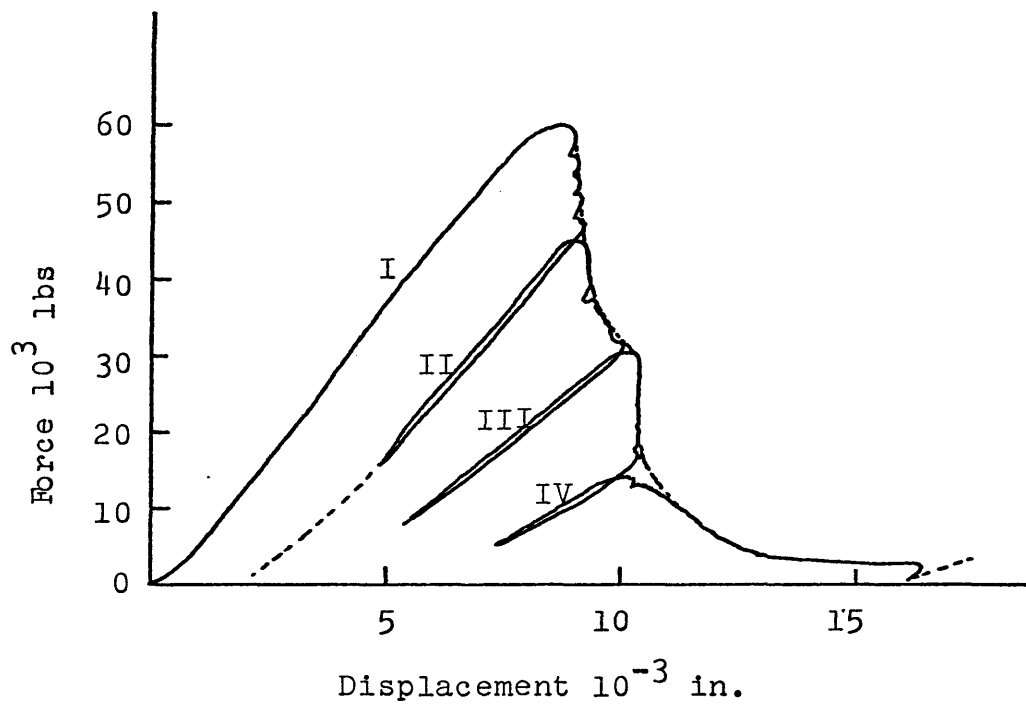


Figure 35. A Complete Force-Displacement Curve for Tennessee Marble (by Wawersik).

specimen has been permanently damaged along the stable failure passes. The dotted line shows the failure envelope of the specimen.

The post-failure curves for rocks under dynamic loading are very similar to that shown in figure 35. It is, however, complicated by the fact that additional energy must be supplied to the specimen to cause a positive deformation even if the maximum load carrying ability already exceeded. If the energy is not available, an unloading curve in the fracture region shown as curve D in figure 33 is obtained instead of one following the failure envelope of the rock (curve E). In most cases, the energy carried by the strain wave is not sufficient to obtain a complete failure envelope from a single strike (except for some weaker rocks such as Yule Marble and Indiana Limestone). Under multiple impacts additional energy is supplied to the rock specimen to cause stable failure of the specimens. The loading and unloading curves for a number of consecutive strikes (as given in figures 15, 16, and 17) are similar to that of the unloading and loading cycles in the failure region shown in figure 35.

Elastic Moduli for a Major and Minor Stress Cycle

The lack of agreement between values of Young's modulus obtained using the resonant frequency method and the other dynamic methods can be explained by considering the conditions

under which the values are measured. As seen in figure 36 (reproduced from Cook and Hodgson, 1965), the vibration of the specimen in the resonant technique corresponds to the superposition of a small alternating stress on the existing applied stress (in this case the existing stress is equal to zero). Such a stress cycle might be shown schematically as the loop a-a'-a in the figure. The Young's modulus of the split Hopkinson bar test and static test are taken as the slope of the stress-strain curve at a certain defined stress value. The moduli calculated from the resonant frequency correspond to some average slope of the loop representing the vibration. Thus, the value would be expected to be different from the other tests as was found to be the case.

Usually the average slope of a small stress cycle (loading and unloading) is greater than the tangent value at the same stress level (the greater moduli of a minor stress cycle are attributed to the frictional resistance to sliding across crack surfaces). Thus, higher values are usually found for the dynamic Young's moduli measured using the frequency method than the initial tangent moduli (the slope of a major stress-strain curve at zero stress level). In table 2, values of the dynamic and static Young's modulus from the split bar and static tests for all four rock types are given (tangent values measured at 50% of its maximum stress level). The initial tangent modulus, in general, is different from these values. For Colorado Red Granite and

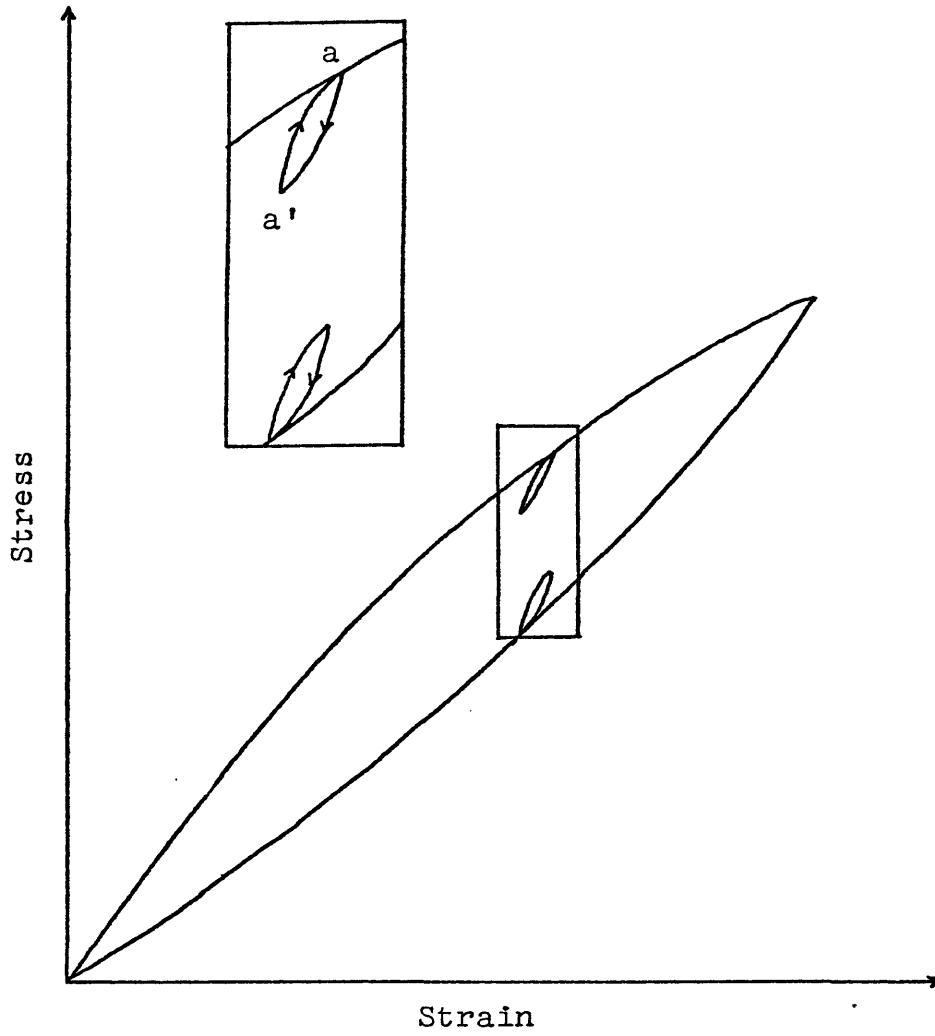


Figure 36. Directions of Movement Around Major and Minor Stress Cycles (by Cook and Hodgson).

Indiana Limestone, the slope of the major stress-strain curves is near constant at all stress levels (see figures 18 and 20), i.e. the initial tangent moduli are nearly the same as Young's moduli at 50% of its maximum stress level. By this reasoning, the dynamic Young's moduli from resonant frequency method are greater than that at 50% of its maximum stress level. However, for Yule Marble and Gray Sandstone, the initial tangent moduli are much smaller than that at 50% of its maximum stress level (see figures 19 and 21). The Young's moduli from resonant frequency method for these two rock types are found smaller than that at 50% of its maximum stress level.

Strain Rate Sensitivity of the Compressive Strength

The compressive strengths of certain rocks have been found to be strain rate sensitive. To obtain an insight into the effect of strain rate on the strength of rock, the basic rock fracturing process is reviewed.

Fracturing of rock occurs by the separation of the material into parts. It is a well known fact that the forces necessary to break atomic bonds in a solid are much greater than the observed strength. Griffith (1924) assumed that defects in the form of narrow cracks produced stress concentrations which weakened brittle materials. He proposed that

fracture occurs when the stress at or near the crack tip exceeds the strength of the atomic bonds in this region. Using expressions for the stress field around an isolated crack in an elastic homogeneous body, Griffith developed a fracture initiation criterion.

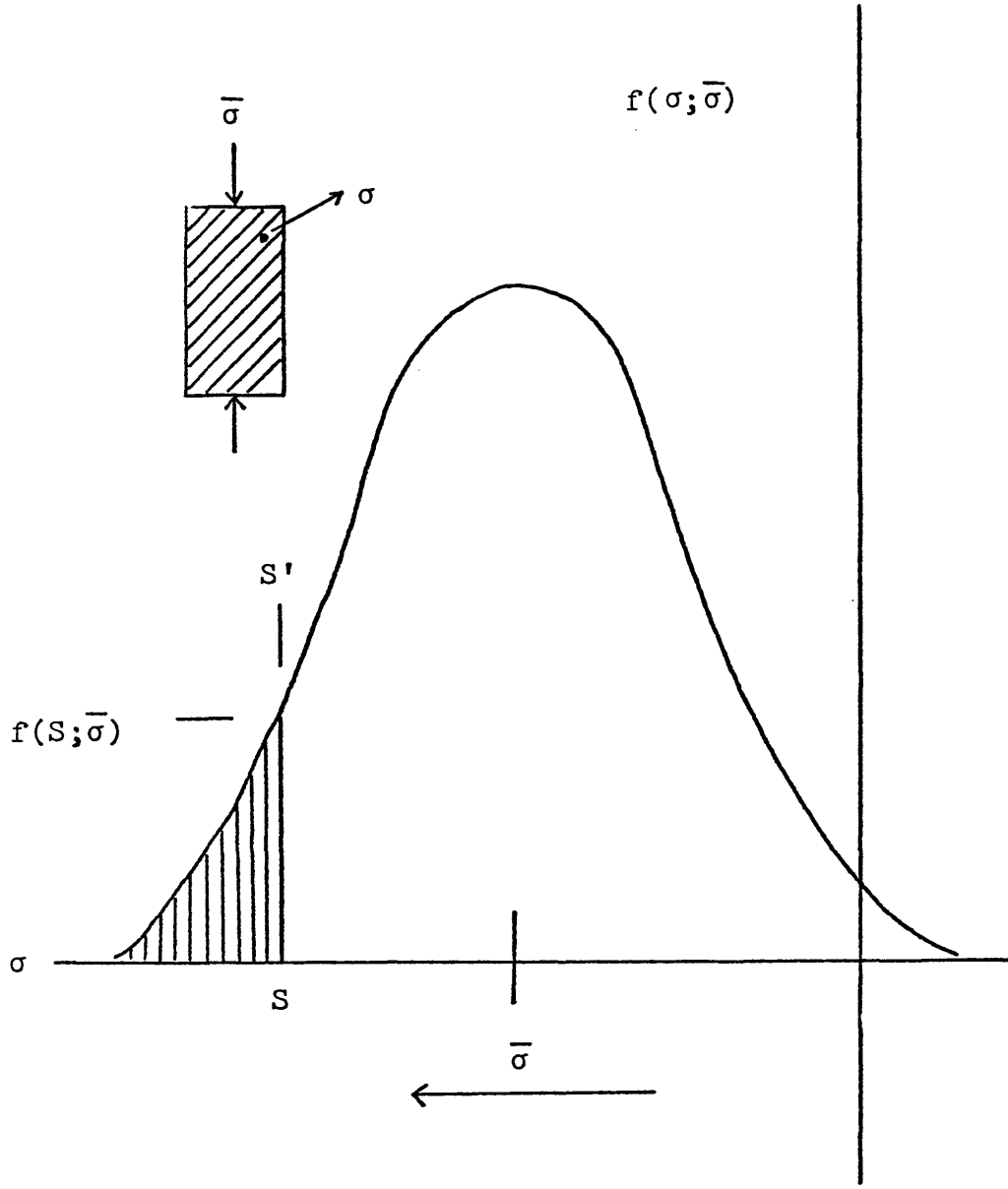
According to Griffith's model, in a tensile field once initiated the crack propagates unstably and the specimen fractures. The problem becomes more difficult in a compressive field. Various investigators; Brace and Bombilakis (1963), Hoek and Bieniawski (1965) studied crack growth photoelastically in glass plates stressed in compression. They found that the initiation of crack growth under such conditions did not lead to failure but the cracks became stable after propagating some fraction of their initial length. The cracks tended to grow in the direction of the maximum principal stress.

If a uniform stress field is applied to an inhomogeneous material such as rock, local stresses can be very different from the applied value. The stress concentrations along the grain boundaries, pores and cracks will further complicate the matter.

As an inhomogeneous rock specimen is subjected to an increasing applied stress, there will be a certain point in the rock where the stress will exceed the strength. A crack which may be an inherent microcrack or a grain boundary will then propagate. The crack will be arrested by the adjacent

region in which the stress is lower. As the applied stress is increased still higher, the region with the next highest stress concentration will fail, and so on, until some sort of instability produces fracture of the entire body.

The variation of stress within an inhomogeneous rock specimen can be best described by a statistical model such as illustrated schematically in figure 37. Assuming an inhomogeneous brittle material under a uniform applied stress $\bar{\sigma}$, the local stress at a point in the specimen due to stress concentration (designated by σ) varies in a random fashion throughout the body. With such a model, σ can be considered to be a random variable. Therefore, the probability that the stress at a point is some value σ is given by a probability density function $f(\sigma; \bar{\sigma})$. The form of this function depends on the specimen being tested. One such function is represented in figure 37. The horizontal axis on the graph is the stress axis σ . The variable σ represents the applied uniform stress in the specimen (it is also the statistical average stress in the specimen), and S is the local strength of the rock. The vertical axis is the relative frequency of occurrence (or the probability density) for a certain specific stress level. For example $f(S; \bar{\sigma})$ represent the relative frequency of occurrence where the local stress σ is equal to S . If the local stress σ exceeds the local strength S , fracture will then occur within the region. The local strength S will, in general, vary since



σ = local stresses in the specimen
 $\bar{\sigma}$ = statistical average stress
 S = applied uniform stress

Figure 37. A Schematic Diagram of the Statistical Stress Distribution in the Specimen.

it depends on the size and orientation of the cracks present. From the simple Griffith model the stress required to initiate crack growth is given by

$$S = \sqrt{\frac{4\gamma E}{\pi C}} \quad (7-1)$$

where:

γ = specific surface energy of the rock

C = crack length.

This value (S) will be assumed to represent the local strength.

The shaded area on the graph to the left of SS' (denoted by $F(S; \bar{\sigma})$) is the probability that the local stress in the specimen will exceed the local strength S . As $\bar{\sigma}$ is increased the probability density function will move to the left and eventually there will be a finite probability that the stress in a region will exceed S , and microfracturing will begin.

Observations of the fracture patterns in the partially failed statically and dynamically loaded specimens showed no difference in the basic mode of fracturing. The only difference was that region III of the static stress-strain curves was extended to larger strains and stresses. Consequently the "apparent" fracture strength is increased.

The statistical model applies only to a uniformly applied stress field, so that the probability distribution of σ will not be a function of position. However, in dynamic loading, the applied stress is not uniform along the

axial direction of the specimen unless the specimen is short compared with the duration of the wave. This was the case in the experiments performed in this project.

Using the concept of the probability density function, it is seen that the microfracturing activity will increase as the applied uniform stress increases. The number of microcracks in the specimen is proportional to the probability that local stress will exceed the local strength S . The dependence of the number of microcracks on the stress can be expressed as

$$N \propto F(S; \bar{\sigma}) \quad (7-2)$$

The number of microcracks is shown to be an increasing function of the applied uniform stress $\bar{\sigma}$. This has been verified by experimental observations.

In static testing, the longest, most critically oriented crack will propagate first. When the stress existing at the crack tip is reduced to a value less than S it will stop. The presence of this crack essentially distresses the region in the near vicinity. The crack having the next longest length and most favorable orientation will then propagate. This crack, however, will be somewhat removed from the first crack because of the reduction in the local stress field due to the presence of the freeface. This process continues as the stress is increased. It is characterized by the formation of a relatively few, major cracks. The cracks in the material between these long cracks cannot propagate because

of the low local stresses. Eventually the cracks join up causing major failure of the specimen.

In the split Hopkinson bar tests the stress is distributed more uniformly across the entire section. The stress at a particular section depends on the pointwise wave velocity and the density of the material. The stress can be determined using the velocity and force continuity at this section using equations similar to the equations given in (4-2) and (4-3). However, for cracks oriented in the direction of the wave motion, these pointwise values will (until very close to complete failure) be very similar. The redistribution of loading that is evident in static testing will not occur in the dynamic case. Essentially all the material will be rather uniformly stressed. This gives rise to the formation of many short cracks.

The stress (denoted as the compressive strength) required for the joining of the few, long cracks formed in the static case into a shear failure plane (producing total failure of the specimen) appears to be about half that needed for the many short cracks formed in the dynamic case.

A Statistical Model of Strain Wave Transmission in the Specimen

Hakalehto (1967) has done a substantial amount of work on the energy transmission in a split Hopkinson bar test. The results for different lengths of Tennessee Marble

impacted by a 5-in. striker at various incident energy levels were plotted as the transmitted energy (E_t) versus the input energy ($E_i - E_r$). The curves are reproduced in figure 38.

He found that a limiting amount of strain energy can be transmitted through the specimen independent of the input energy; the amount depending upon the specimen length and the strength of the material.

The "input energy" defined by Hakalehto (1967) as the difference between incident and reflected strain energy is considered incorrect, since both the reflected and transmitted energy are functions of the material (rock and steel bar) properties.

Curves showing the incident strain energy versus the recovered strain energy (the sum of the transmitted and reflected strain energies) for different specimen lengths are given in figure 39. Similarities were found between the resulting "total recovered energy" (figure 39) curves and "energy transmission" curves (figure 38), but the variation of the "maximum recovered energy" with specimen length is much smaller.

On the basis of the present observations, the energy loss in the specimen is an increasing function of both the number of strikes and the maximum average stress in the specimen. The specimen tested can transmit a much higher

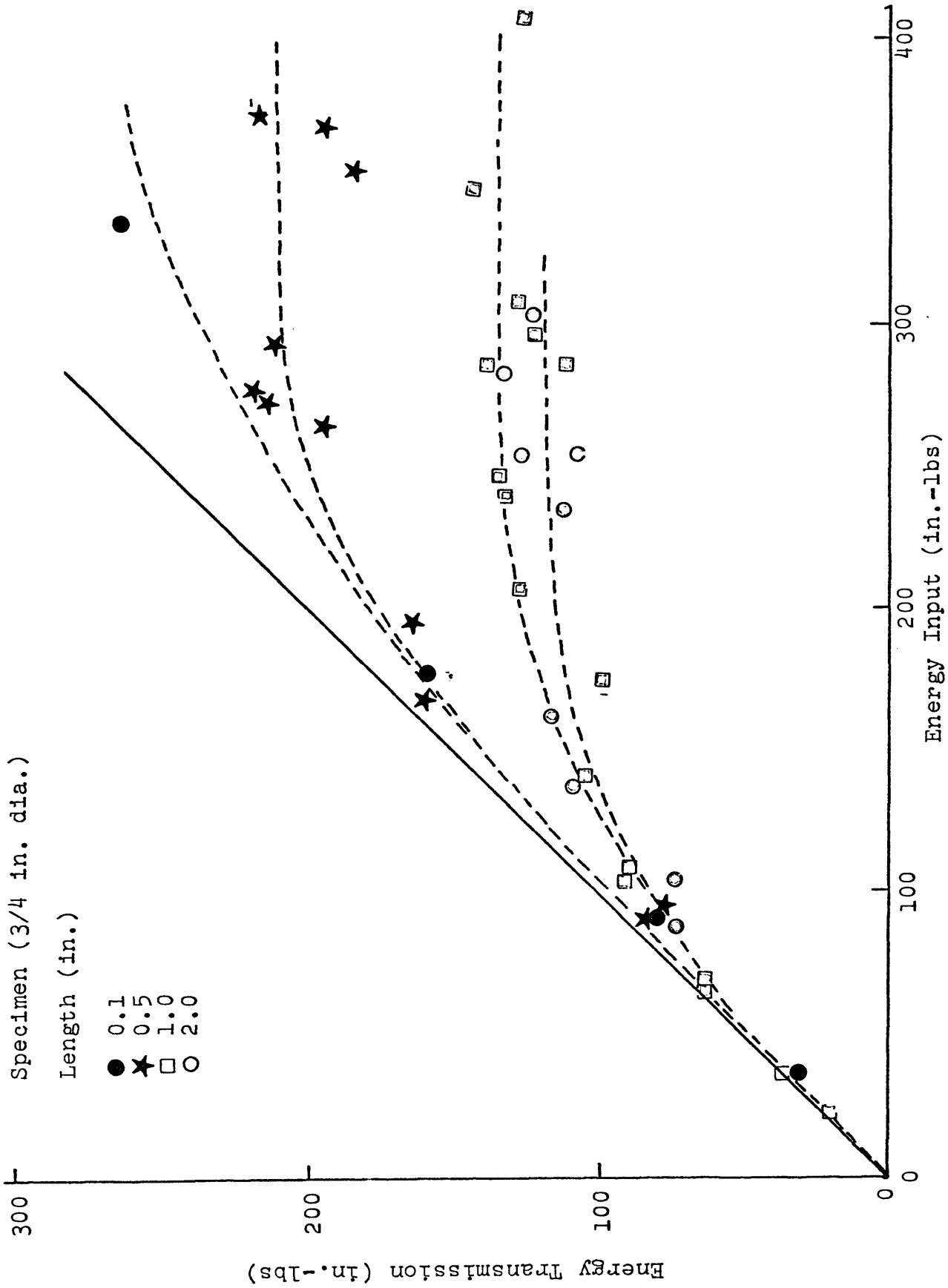


Figure 38. Energy Transmission in Tennessee Marble, 5.0 in. striker (by Hakalehto).

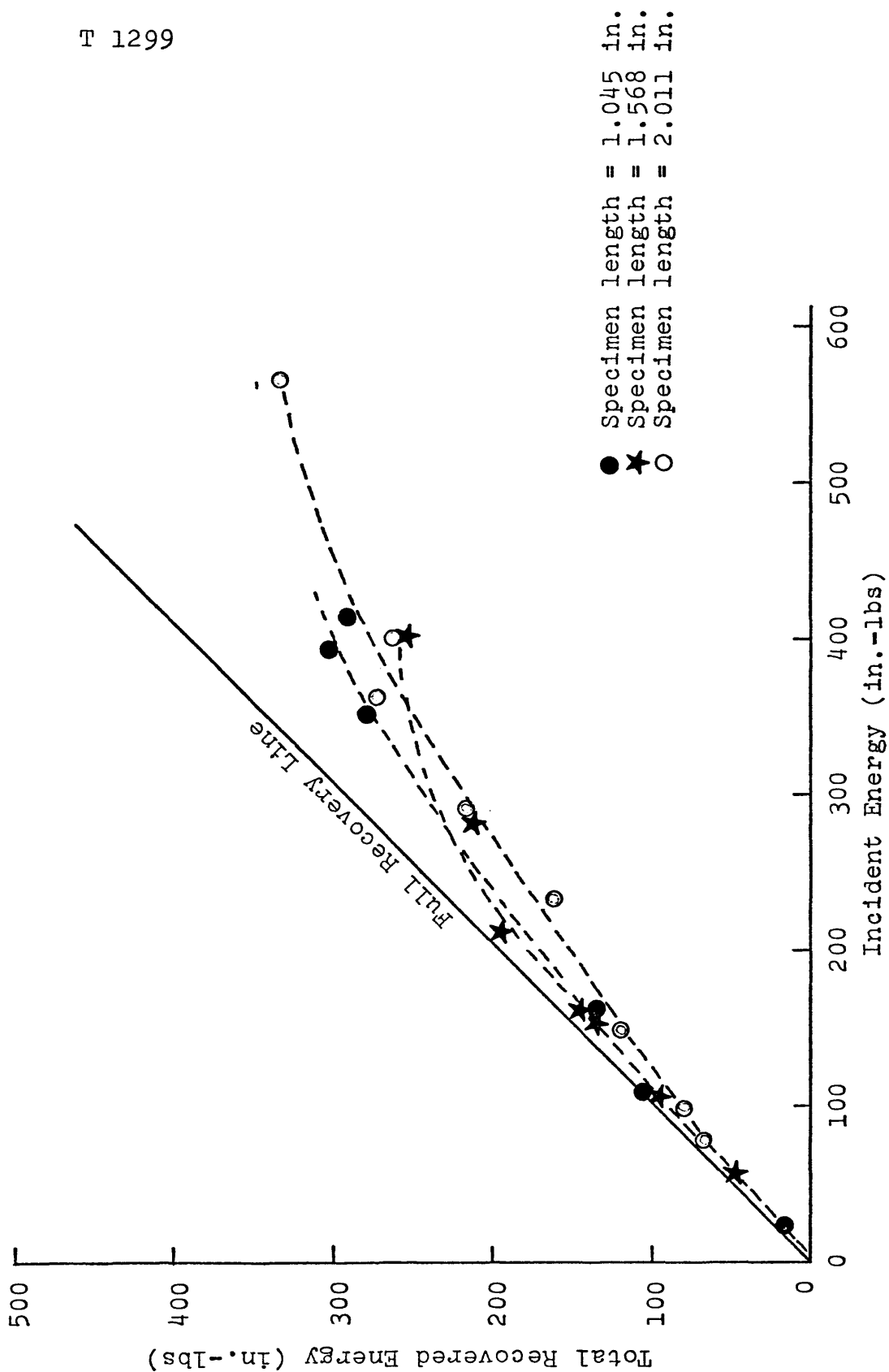


Figure 39. Total Recovered Strain Energy in Colorado Red Granite.

stress level than given by a static test despite that fracture was observed to start at the same stress levels. The wave transmission model introduced by Hakalehto (1967) in which it is assumed that the energy contained in the incident wave above the stress level will be totally dissipated in the specimen is incorrect as a result of an earlier mistake in his analysis.

A stress wave transmission model based on the incident stress wave and the average stress-time wave in the specimen which combines the effects of the reflected and transmitted stress waves with losses in the specimens will serve as a phenomenological explanation of the energy dissipation in the specimens. In this model $\bar{\sigma}(t)$ represents the time function of a uniformly applied stress field in the specimen due to an incident stress wave σ_i . The local stress at a point in the specimen is σ , the variation of the stress σ in the specimen is again given by the probability density function $f(\sigma; \bar{\sigma})$ as in figure 37. At any moment if the local stress σ exceeds the local strength S , as discussed in the previous section, fracture will then occur within the region. Consequently, energy will be dissipated in the specimen. The energy is provided by the part of the stress wave shown by the nonshaded area under the incident stress-time wave as given in figure 40. The shaded area bounded by the average instantaneous stress in the specimen represents the part of the incident wave recovered from the specimen without

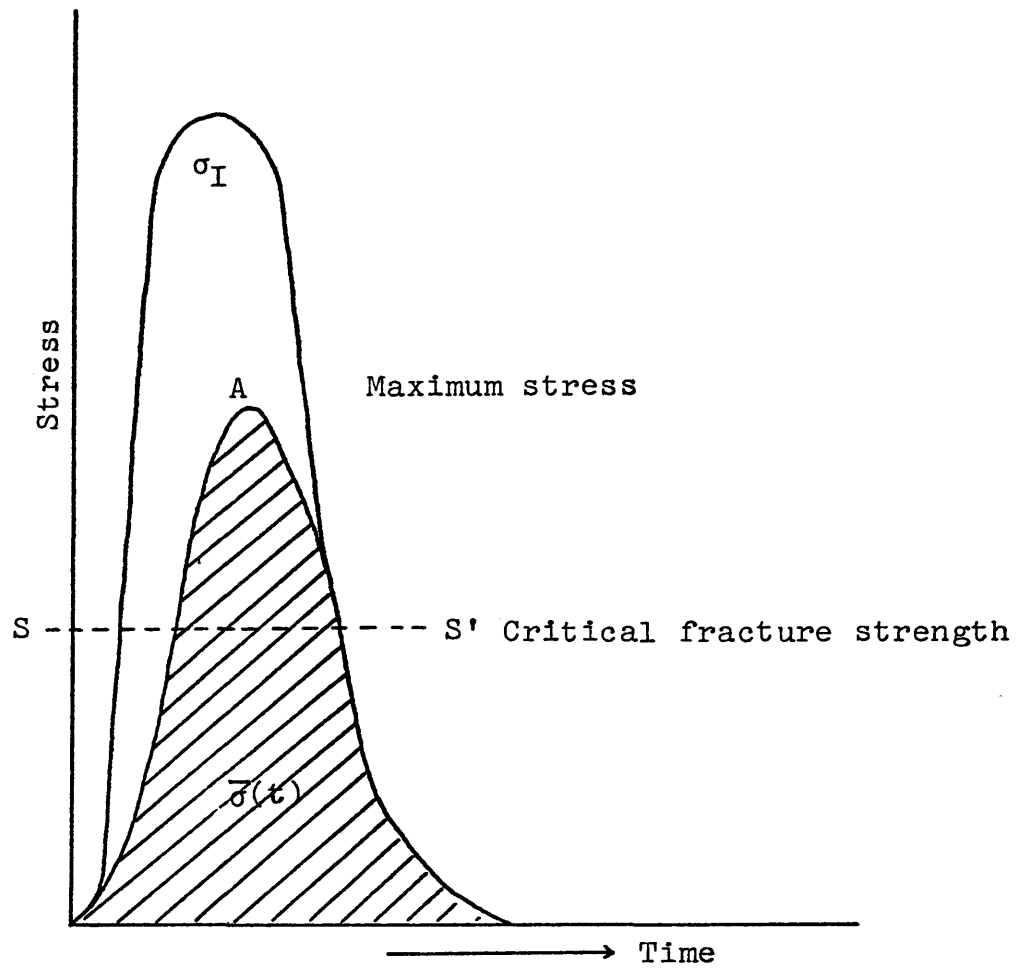


Figure 40. Incident and Average Stress-Time Waves.

dissipation. As the applied uniform stress $\bar{\sigma}$ increases with time the microfracturing activities increase and a larger portion of the incident stress wave will contribute to the energy loss in the specimen. This is shown by an increase in the proportion of the non-shaded area with increase in stress in figure 40. One can write that the energy available for fracturing is

$$E_{\ell} = G(F(S; \bar{\sigma})) \quad (7-4)$$

where G = function of the probability that local stress σ exceeds the local strength S .

Point A in the graph corresponds to the maximum stress transmitted by the specimen, and the shaded area under the average stress-time curve is proportional to the total recovered strain energy. This latter quantity has been observed to be constant for a given incident wave length and a given rock type subjected to a single impact.

In this analysis the local strength S has been considered as constant and the local stress σ varies. In the actual case the local strength is a function of the average crack length C . When a specimen is subjected to multiple impacts and is partially failed, the local strength decreases. According to this model, if the intensity of the incident wave is kept constant, one observes

- (1) a decrease in total recovered energy.
- (2) a decrease in the maximum stress.
- (3) an increase in the energy loss.

Factors Influencing the Results

The derived dynamic properties of rock have been found to depend on the method of wave analysis and the incident wave to specimen length ratio. An evaluation of some other factors influencing the calculated dynamic stress-strain curves, the energy loss in the specimens and observed fracture mechanism are presented below.

Uniformity of Stress Within the Specimen

It is observed that the stresses in general are not uniformly distributed along the specimen axis. When the first wave arrives, the first bar-specimen interface is loaded, but there is no load on the second bar-specimen interface. Constant stress over the whole length of the specimen does not prevail until several reflections inside the specimen have taken place. This condition requires that the specimen length be short compared with the incident wave length. For a specimen of 1-in. length loaded by a 5-in. striker, the stresses at the two interfaces were found nearly equal within 15- μ s for all tests.

A direct observation on the strain-time wave in the specimen was performed on a few specimens to demonstrate the uniformity of stress along the specimen axis. A pair of SR-4 strain gages with a gage length of 1/8 in. were placed at several positions on Colorado Red Granite specimens 1-in. and 2-in. long. The strain-time waves were directly

recorded using an oscilloscope. The incident strain-time wave in the steel bar was also recorded. The shape of the resultant strain waves from the center of 1-in. and 2-in. specimen surfaces, and one-fourth of an inch from the impacted end of a two inch specimen are shown in figure 41. Minor differences were found between the strain waves. The strain waves in a longer specimen exhibit a longer rise and decay time. Comparing the waves at two different locations, B and C on the same specimen, one finds that the wave forms are nearly the same. A slight time lag, as expected, is found for the wave C.

The observed strain-time waves are not smooth, but contain a number of high frequency kinks. A number of unsuccessful tests due to a premature failure of the strain-gages were tried before some waves were recorded. The strain-time curves given were limited to a stress amplitude lower than its critical value. The direct method of obtaining the strain history in the specimen is useful for qualitatively checking the results; however, it is insufficient as a general practice.

A strain-time curve obtained from the theoretical wave analysis (described in the theory section) together with one measured directly are presented in figure 42.

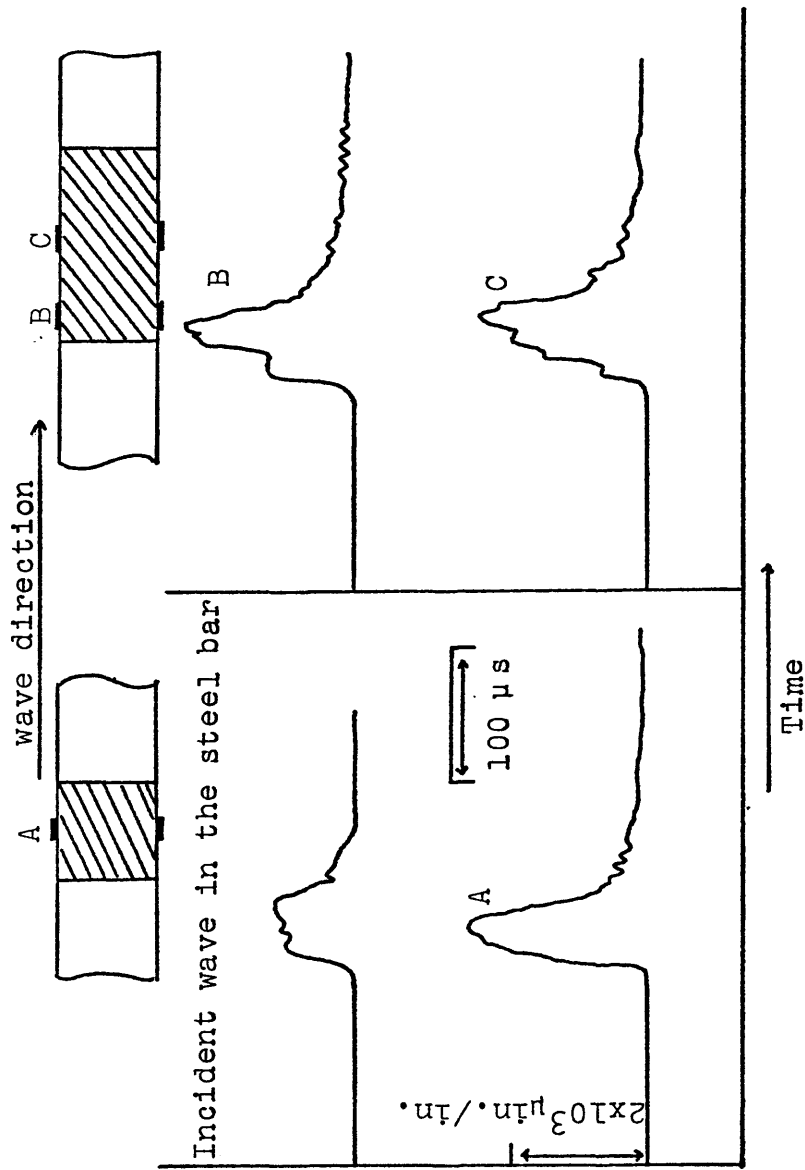


Figure 41. Observed Strain-Time Wave on the Specimen Surface.

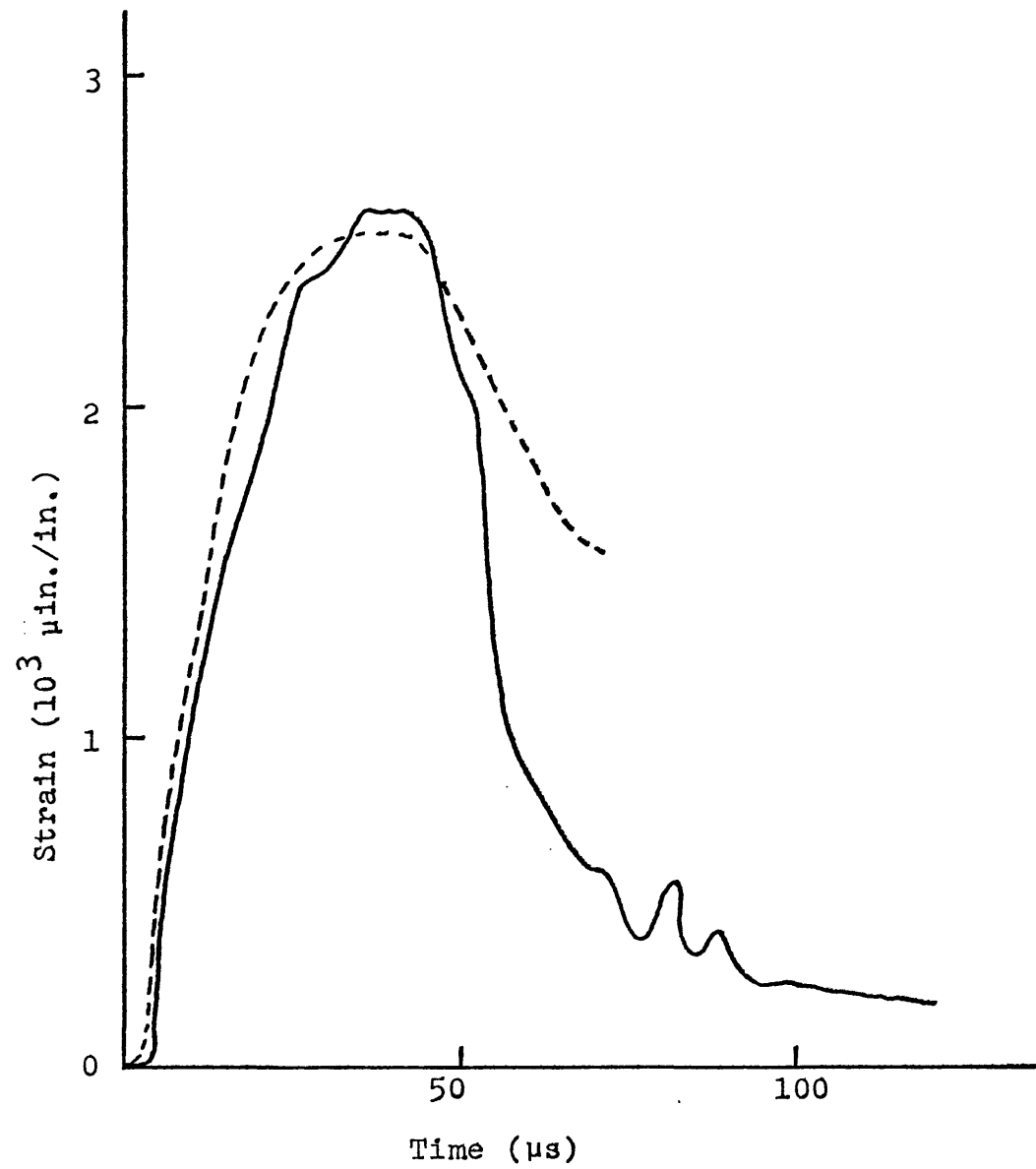
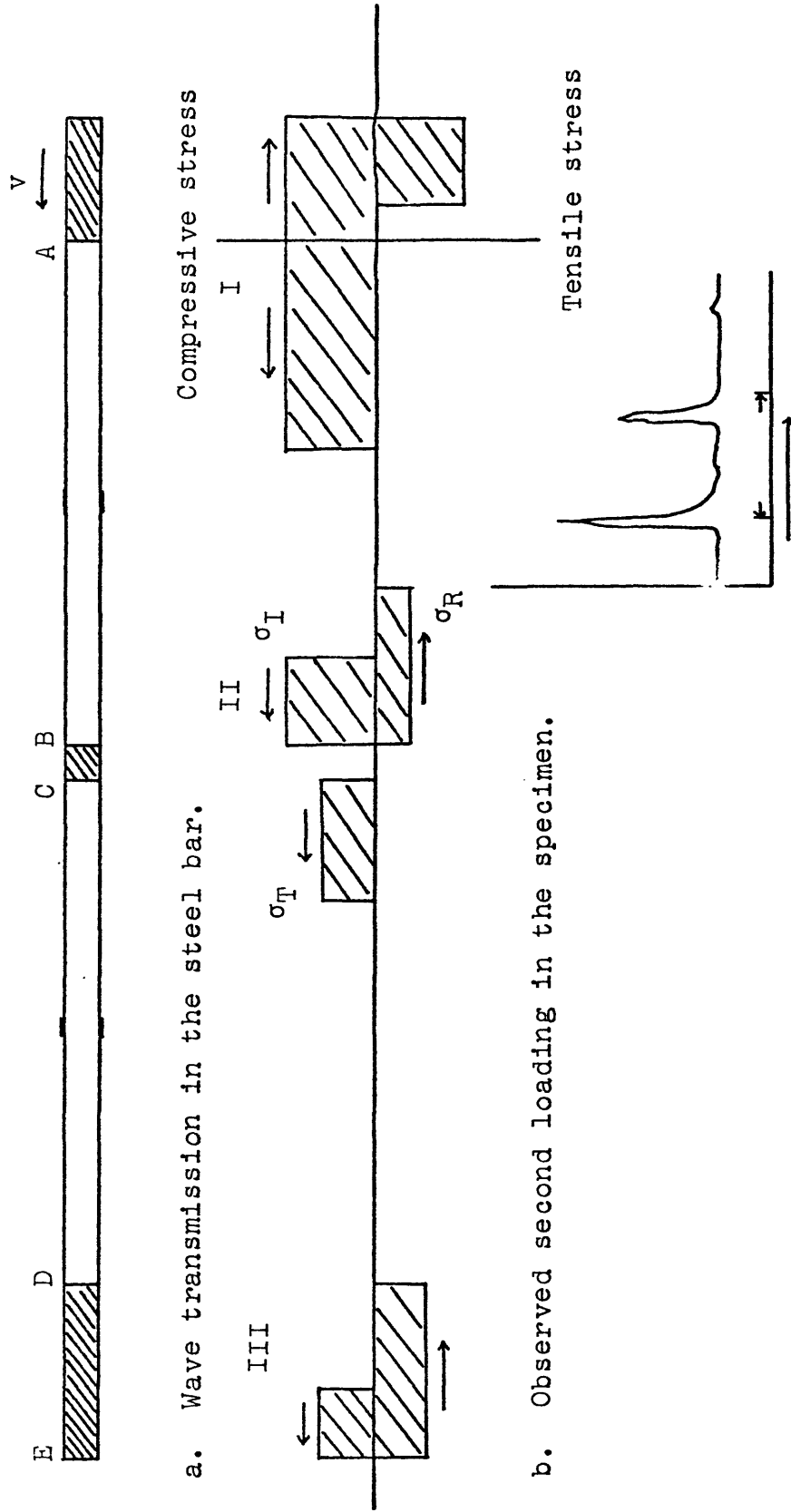


Figure 42. Comparison of an Average Strain-Time Wave With a Measured Strain-Time Wave.

Loading History of the Specimen

The fact that a specimen subjected to impact of a striker bar is sometimes more complicated than just simple loading and unloading has been disregarded by some investigators. This may have some significant effect on the observed rock properties. The sequence of strain wave transmission and reflection in the steel bars when the striker impacts on one end of the steel bar with velocity v , as shown schematically in figure 42a. A compressive wave having a length approximately twice that of the striker bar will travel from the interface A towards the specimen BC. Upon striking, the striker bar will be at rest and in contact with the bar. For simplicity, the compressive wave is assumed to be a square wave with amplitude σ_i . As the wave reaches BC, multiple reflection occurs within the specimen. The resultant reflected wave σ_r generally having a leading tensile portion will travel towards A. The resultant transmitted compressive stress wave σ_t , travelling towards D, passes through the joint between the steel bar and momentum trap and is reflected as a tensile wave at the free end E. This tensile wave cannot be transmitted through joint D and will be trapped inside DE. The reflected wave σ_r will be further reflected at end A. The initial compressive part will enter and again load the specimen. Thus a specimen will be subjected to at least two loading-unloading cycles



a. Wave transmission in the steel bar.

b. Observed second loading in the specimen.

Figure 43. Loading History of the Specimen.

for each strike. A strain-time curve showing the second loading in the specimen is given in figure 43b.

For the experiments described in the previous sections in which the specimen failed in the first loading, the effect of 2nd loading can be neglected. However, for rocks under multiple loading, the effect of the 2nd loading must also be taken into account.

If a gap exists between the specimen and the second of the steel bars at the beginning of the test, part of the transmitted compressive wave will reflect from the "free" end of the specimen as a tensile wave before the gap is closed by the particle displacement. A similar effect exists if there is a gap between the momentum trap and the steel bar. This can produce spalling and tensile cracking of the sample. This effect was observed in the specimens when a small gap (about 0.02-in. long) was purposely left at either C or D. Hakalehto (1967) observed some tensile cracks perpendicular to the direction of wave propagation. It is suggested that these tensile cracks may be a result of misalignment between the specimen and the bars. A small gap between the steel bar and the momentum trap of the order of .02 inch is very easy to be introduced in his device which is suspended by four steel wires, instead of being restrained by roller bearings.

Frictional End Effect

The shorter specimen length increases the frictional restraint between the bar and specimens and raised the stress-strain curves to a higher stress level. With the same dimensions and end conditions, the frictional restraint should be the same for both dynamic and static loading provided that strain rate has no effect on the frictional restraint. Investigators in the field of metal testing (Lindholm, 1964) showed that metals have less end restraint for dynamic testing than under static testing, and one might expect the same for rocks. The observation of fracture distribution in the specimens showed that the differences are quite small.

CONCLUSIONS

1. A computer simulation of the split Hopkinson bar method of rock testing has shown that unless extreme care is taken in the analysis of the experimental data, the stress-strain curves obtained can depend more on the method of analysis than on actual rock behavior. Variations in the apparent Young's modulus by nearly 70% were shown to result in one example where the transit time (Δt) through the specimen was neglected. The incident wave length to specimen length ratio has a large effect on the derived stress-strain curves. It is recommended that this ratio be larger than 5.

2. A comparison of static and dynamic results for four rock types has shown no apparent rate of loading effect on the stress-strain curves. The static compressive strength, however, were approximately one-half those observed in the dynamic tests.

3. The static and dynamic Young's modulus calculated as the tangent values at 50% of the respective stress-strain curves were found similar; however, they are different from that calculated by resonant frequency methods. The discrepancies between these values can be explained by the conditions under which the values are measured.

4. The split Hopkinson bar test can be considered as a "stiff" testing system, since the energy carried by the strain wave is limited and the strain rates are constant for both loading and unloading processes. Complete stress-strain curves were obtained by this method.

5. Creation of new fracture surfaces and motion of the fragments contributed to a major part of the energy loss in the specimen as the strain wave traverses the rock specimen. The unit energy loss in the specimen or the minimum specific fracture energy could be useful as a rock breaking index.

6. Rocks are weakened by multiple impacts with sufficiently high impact amplitude. The weakened rock has a lower elastic modulus. It can withstand a lower stress and absorb a higher amount of strain energy.

7. Fractures^{are} initiated at the same stress level for rocks under both dynamic and static loading conditions. However, it was found that more and shorter microcracks were found under dynamic loading than under static loading conditions.

APPENDIX I

Computer Program for Calculating the Reflected
and Transmitted Waves from a Sine Shaped Incident
Compressive Elastic Wave

```
C   THIS PROGRAM IS WRITTEN IN FORTRAN IV LANGUAGE, AND
C   TO BE RUN BY PDP-10 COMPUTER AT CSM.
C   A SINGLE PULSE OF SINE SHAPED INCIDENT STRAIN WAVE
C   IS CONSIDERED.  THE SINE WAVE HAS A MAXIMUM AMPLITUDE
C   EQUALS UNITY.
C   DIMENSION SI(60), SUMR(60), SUMT(60), ST(50, 60),
C   LSR(50, 60)
C   READ 101, L
C   L IS THE NUMBER OF DATA SETS (DIFFERENT COMBINATIONS
C   OF WAVE LENGTH WL(IN.) AND SPECIMEN LENGTH D(IN.))
C   READ 100, PS,CS,E,PR
C   PS IS THE DENSITY OF ROCK SPECIMEN, PR IS THE DENSITY
C   OF STEEL BAR(7.8),E IS THE DYNAMIC YOUNGS MODULUS OF
C   ROCK, CS IS THE LONGITUDINAL WAVE VELOCITY IN STEEL
C   BAR(194600IN./SEC)
C   READ100, WL, D
C   CR= SQRT (E/DR/62.4*32.2*144.)*12.
C   CR IS THE LONGITUDINAL WAVE VELOCITY IN ROCKS
C   PI=3.14159
C   AK=(PR*CR-PS*CS)/(PR*CR+PS*CS)
C   W=PI*CS/WL
```

```
C      W IS THE ANGULAR VELOCITY OF WAVE
      DT=D/CR
C      ST IS THE TIME NECESSARY FOR THE WAVE TRAVELS THROUGH
C      THE SPECIMEN
      DO 500 I=1, 60
      AI=I
      T=WL/CS/30*AI
      IF (W*T-PI) 110, 110, 120
110 SI(I)=SIN(W*T)
C      SI(I) IS THE STRAIN AMPLITUDE FOR THIN SINE WAVE AT
C      EVERY T SEC INTERVAL
      GO TO 125
120 SI(I)=0.0
125 SUMR(I)=SI(I)*AK
      SUMT(I)=0.0
      DO 500 N=1, 50
      AN=N
      IF(T-2.*AN*DT) 130, 130, 140
130 SR(N,I)=0.0
      GO TO 155
140 IF(W*(T-2.*AN*AT)-PI) 150,150,130
150 SR(N,I)= (1.-AK**2)*(0.0-AK)**(2*N-1)*SIN(W*(T-2.*AN*
      1*DT))
155 SUMR(I)=SUMR(I)+SR(N,I)
      IF(T-(2.*AN-1.)*DT) 160, 160, 170
160 ST(N,I)=0.0
      GO TO 500
```

```
170 IF(W*(T-(2.*AN-1.)*DT)-PI) 180, 180, 160
180 ST(N,I) = (1.-AK**2)*(0.0-AK)**(2*N-2)*SIN(W*(T-
      1(2.*AN-1.)*DT))
500 SUMT(I) = SUMT(I) + ST(N,I)
      PRINT 400, M
      PRINT 202, E, PR
      PRINT 203, WL, D
      PRINT 600
      PRINT 200, (SI(I), SUMR(I), SUMT(I), I = 1, 60)
C      SUMR(I), SUMT(I) ARE THE REFLECTED AND TRANSMITTED WAVES
C      FROM ROCK SURFACES
201 PRINT 300
101 FORMAT (214)
100 FORMAT (4F10.0)
400 FORMAT (50H WAVE REFLECTION AND TRANSMISSION CALCULATIONS
      NO., I5)
600 FORMAT (1H0)
300 FORMAT (1H1)
200 FORMAT (5H I =, F15.8, 5H R =, F15.8, 5H T =, F15.8)
202 FORMAT (6H E=, F10.0, 6H PR=, F5.2)
203 FORMAT (6H WL=, F6.2, 6H D=, F6.2)
      STOP
      END
```

APPENDIX II

Computer Program for Stress, Strain, and
Energy Loss Calculations

C THIS PROGRAM IS WRITTEN IN FORTRAN IV LANGUAGE, AND
TO BE RUN BY PDP-10 COMPUTER AT CSM.
DIMENSION RSTAI (N), RSTAR (N), RSTAT (N), STAX (N),
1 X (N), Y (N), STAWI (N), STAWR (N), STAWT (N), STAW (N)
C THE DATA CARDS OF THE STRAIN WAVES ARE PUNCHED BY OSKAR
C MODEL K DIGITIZER AND TO ELIMINATE THE NEGATIVE READINGS
C SET ZERO EQUALS 250. THE TOTAL AMPLIFICATION IS 250.
C RSTAI (N), RSTAR (N), RSTAT (N), ARE ARRAY NAMES OF THE
C AMPLITUDES OF INCIDENT, REFLECTED, TRANSMITTED WAVES
C RESPECTIVELY.
READ 800, N, M
DO 500 L = 1, M
C M IS THE NUMBER OF DATA SETS SUPPLIED
PRINT 600, L
PRINT 625
READ 110, (RSTAI (I), I=1, N)
READ 110, (RSTAR (I), I=1, N)
READ 110, (RSTAT (I), I=1, N)
READ 120, SL, OS, S, E, A, H, CS
C SL = THE SPECIMEN LENGTH IN IN.
C OS = THE SENSITIVITY OF THE VERTICAL BEAMS OF THE
C OSCILLOSCOPE IN MV/CM

```

C      S = STRAIN SENSITIVITY OF GAGES IN THE SYSTEM (199 MICRO
          IN./IN./MV
C      E = YOUNGS MODULUS OF THE BAR (27.9 E 6 PSI)
C      A = CROSS SECTIONAL AREA OF THE BAR (0.7854 SQUARE IN.)
C      H = THE TIME INTERVAL IN MICRO SEC WHERE READINGS ARE
C      TAKEN
C      CS = THE LONGITUDINAL WAVE VELOCITY OF STEEL BAR (194600
C          IN./SEC.)
SUMX = 0.0
SUMWI = 0.0
SUMWR = 0.0
SUMWT = 0.0
DO 350 I=1, N
STAI = (RSTAI (I) - 250.)/250
STAR = (RSTAR (I) - 250.)/250.
STAT = (RSTAT (I) - 250.)/250.
STAY = STAI + STAR + STAT
Y(I) = E/2. * S * STAY * 1.0E-9
C      Y(I) ARE THE STRESS AMPLITUDES AT EVERY H MICRO SEC
C          INTERVAL IN
C      1.0E3 PSI
STAX (I) = STAI - STAR - STAT
SUMX = SUMX + STAX (I)
X (I) = CS/SL * S * OS * H * SUMX * 1.0E-9
C      X (I) ARE THE STRAIN AMPLITUDES AT EVERY H MICRO SEC
C          INTERVAL IN IN.

```

```
C      1.0E3 MICRO IN./IN.
      STAWI(N) = STAI ** 2
      STAWR(N) = STAR ** 2
      STAWT(N) = STAT ** 2
350 PRINT $)), X(I), Y(I)
      CONST = A * CS * E * H * (S*OS) ** 2 * 1.0E-18
      DO 700 I = 1, N
      SUMWI = SUMWI + STAWI (N)
      SUMWR = SUMWR + STAWR (N)
700 SUMWT = SUMWT + STAWT (N)
      WI = CONST * SUMWI
      WR = CONST * SUMWR
      WT = CONST * SUMWT
      W = WI - WR - WT
      PERW = W/WI * 100.
C      WI, WR, WT ARE ENERGY IN IN.-LBS CONTAINED IN INCIDENT,
C      REFLECTED, TRANSMITTED WAVES RESPECTIVELY. W IS THE
C      ENERGY LOSS IN THE SAMPLE, PERW IS THE PERCENTAGE
C      ENERGY LOSS IN THE SAMPLE.
      PRINT 750, W, WI, WR, WT, PERW
      PRINT 450
500 CONTINUE
800 FORMAT (215)
600 FORMAT (36H STRESS STRAIN CALCULATIONS NUMBER, 15)
625 FORMAT (1H0)
110 FORMAT (20 F 4.0)
```

```
120 FORMAT (7F 10.0)
```

```
400 FORMAT (5H X =, F15.5, 10H      Y =, F15.5)
```

```
450 FORMAT (1H1)
```

```
750 FORMAT (5 F 15.5)
```

```
STOP
```

```
END
```

APPENDIX III

Description of Rocks Tested

The four rock types used in the experiments (Colorado Red Granite, Yule Marble, Indiana Limestone, and Gray Sandstone) are described below.

1. Colorado Red Granite - This rock is quarried near Lyons, Colorado, from a formation Precambrian in age. It is a holocrystalline rock, dark red-brown in color, with the following composition: K-feldspar and plagioclase (50%), quartz (40%), and biotite (10%). Most grains are subhedral, although some feldspar grains are euhedral, medium grained and equigranular. The test specimens were cored with the long axis parallel to the flow layering exhibited by the biotite and the minor amounts of tabular feldspar phenocrysts. Although cracks can be seen in the rock mass, care was taken in choosing coring locations so that these were avoided.

2. Yule Marble - This white marble is obtained from a quarry near Marble, Colorado. The rock consists of fairly pure, interlocking calcium carbonate crystals of equal size. The rock is massive and essentially unfractured. Slight banding is evident. The average grain size is approximately 0.02 in.

3. Indiana Limestone - This rock consists of rounded and subangular grains of fossils (mainly broken fragments of sponge specules and micro-fossils with linear orientation, cemented by calcareous mud and secondary calcite recrystallization). The fossils are well preserved and fossil structures are quite evident. The average grain size is approximately 0.03 in.

4. Gray Sandstone - The location for this rock is unknown. It consists of fine-grained, subrounded to subangular minerals. Quartz is the primary constituent (about 90%), with feldspar (8%) and ferromagnesium minerals (2%) making up the rest. Some of the feldspar and ferromagnesiums have been altered to clay minerals and iron oxides. The rock is light gray in color, massive, moderately compacted with equidimension, well sorted grains and is fairly porous.

APPENDIX IV

Strain Sensitivity Calculation of the System

The strain gages used in the experiment are SR-4, Type FAE-12-12S6L, having a resistance of $120.0 \pm 1\%$ ohms, and gage factor of 2.01.

Letting:

R = total gage arm resistance (240 ohms)

m = ratio between fixed resistors (1)

F = gage factor (2.01)

Eab = input voltage (10×10^3 mv)

Ecd = output voltage (mv)

I = current through the gages (ma)

S = sensitivity of the system ($\mu\text{in./in./mv}$)

ϵ = strain ($\mu\text{in./in.}$)

$$S = \frac{\epsilon}{Ecd} = \frac{m+1}{IRmF} = \frac{(m+1)^2}{EabmF} = 199.0 \mu\text{in./in./mv}$$

The current through the gages was measured by a digital meter, which gives $I = 20.9$ ma.

$$S = \frac{m+1}{IRmF} = 198.6 \mu\text{in./in./mv}$$

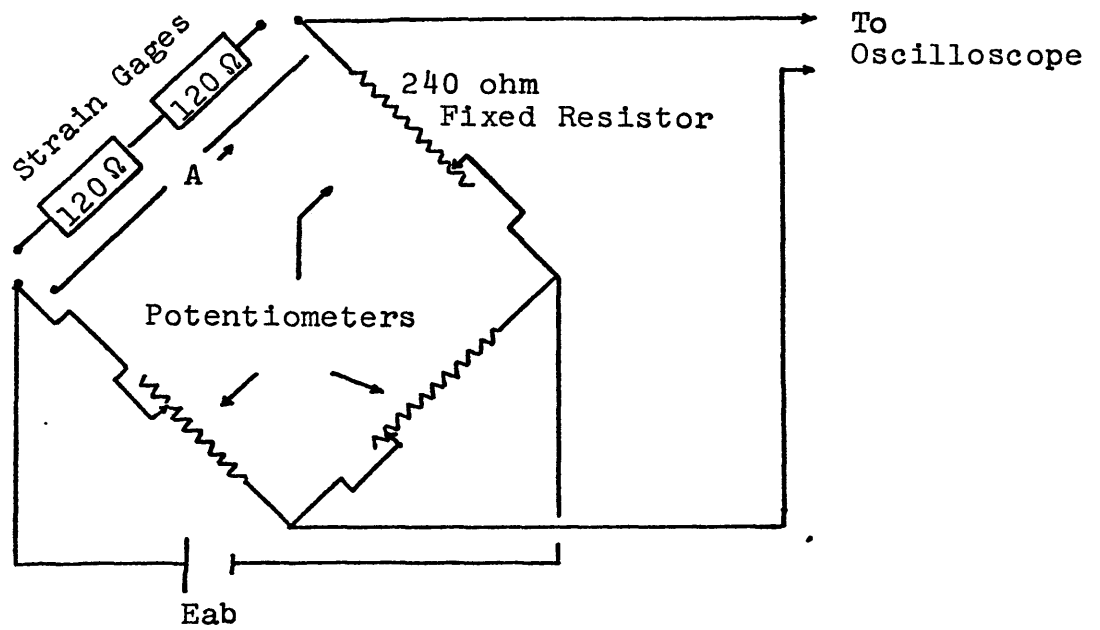


Figure 44. Wheatstone Bridge Circuit.

APPENDIX V

Testing of the Stainless Steel Bar

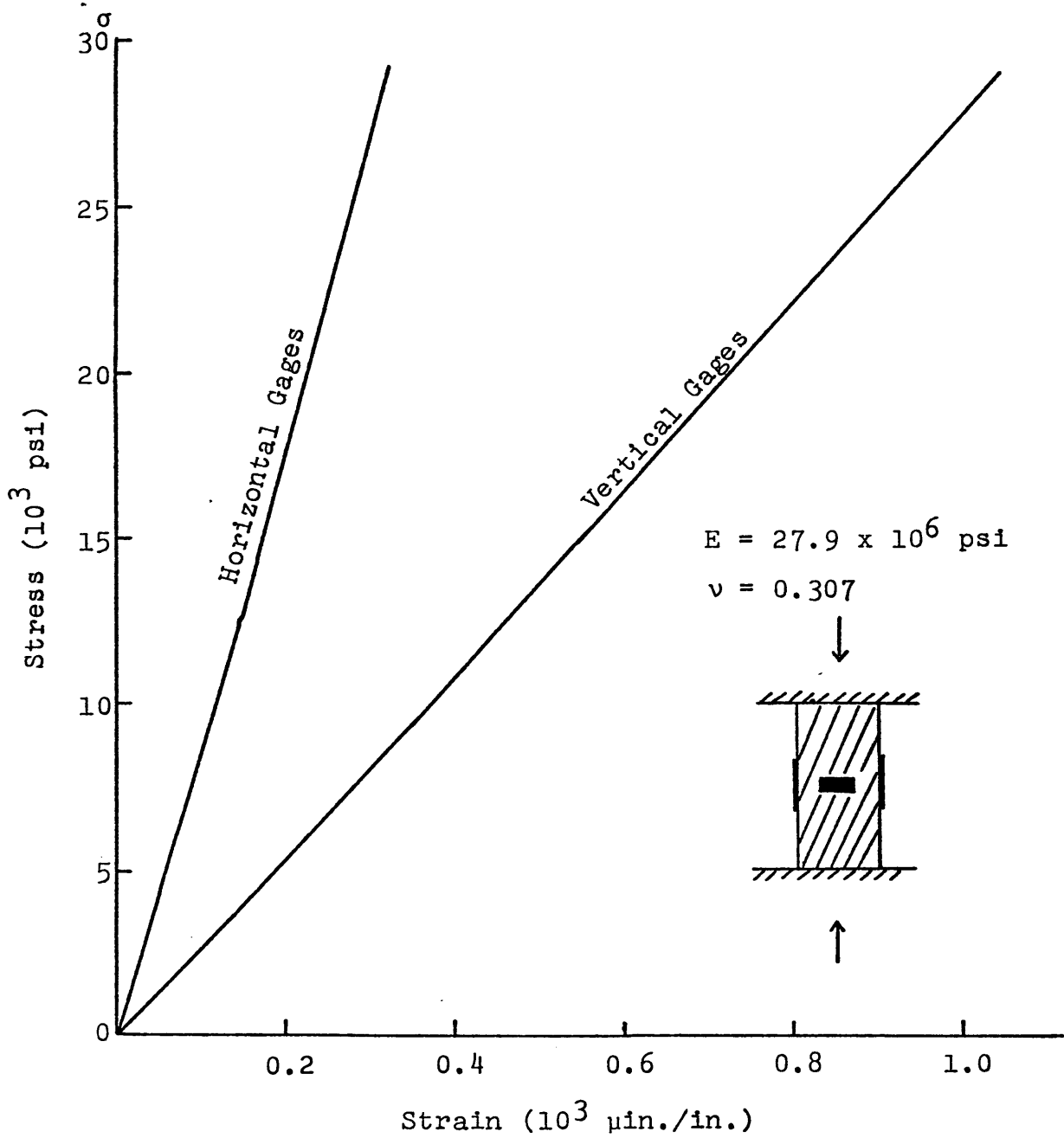


Figure 45. Elastic constants for Bar Material (Stainless Steel Cylinder) Under Static Loading.

APPENDIX VI
Static Testing System

The static tests were performed using a Tinius Olsen testing machine. The experimental setup is shown in figure 43. In order to provide similar end conditions as in the split Hopkinson bar tests, two 1-in. long steel bars (made from the same material as the split bars) were prepared as "caps" for loading the specimen. A pair of SR-4 strain gages wired in series were attached to each cap to act as load cells. Another pair of similar gages were attached to the middle of each specimen to measure the longitudinal strain, thereby compensating for bending across the section. The force measuring gages formed part of a Wheatstone bridge circuit, the output of which was fed into the Y-axis of a Moseley Model 7030A X-Y recorder. Similarly, the gages attached to the specimen formed part of another bridge, the output of which was fed into the X-axis of the same recorder. In this way the static stress-strain curves for the rock cores were obtained directly.

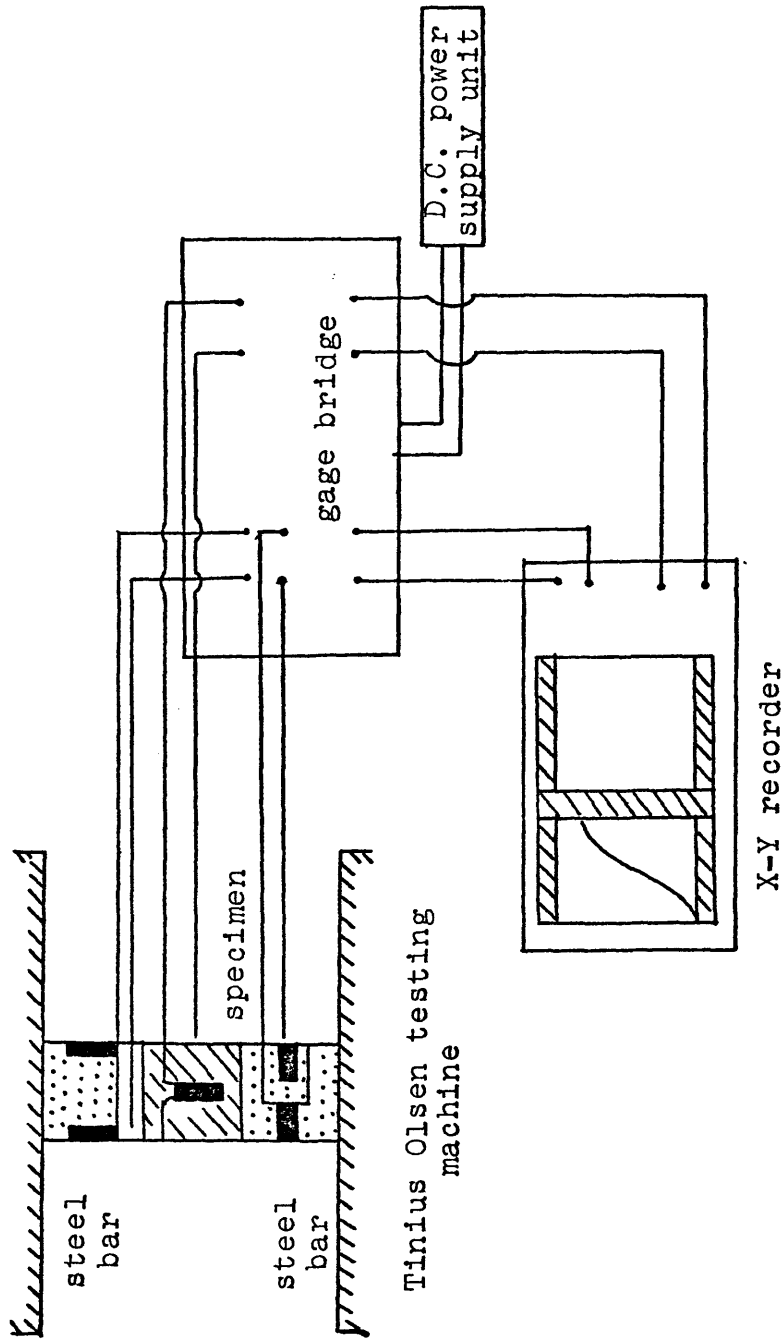


Figure 46. Diagrammatic Representation of the Static Testing Apparatus.

APPENDIX VII

Resonant Frequency Method for Measuring
the Modulus of Elasticity

The natural resonant frequencies of rock specimens were measured using the system shown in figure 44. Five specimens of each rock type having 1-in. diameters and 2-in. nominal lengths were used in the experiment. Vibration of the specimens were produced by cementing to one end of the specimen a crystal pulse driving unit. An identical unit was cemented to the other end of the specimen to sense the vibration amplitude. A continuous train of sine wave pulses with variable frequency were generated by an oscillator and fed into the specimen. To determine the resonant frequency, the oscillator is tuned to give the maximum reading on the oscilloscope.

The modulus of elasticity can be calculated from the measured first order resonant frequency of the specimen with the following corrections:

- | | |
|---|---|
| 1. measured longitudinal frequency | f'_b |
| 2. longitudinal frequency including pole pieces correction | $f_b = f'_b \left(1 + \frac{W'}{W}\right)$ |
| 3. longitudinal bar velocity | $V'_b = 2f'_b L$ |
| 4. true longitudinal bar velocity including lateral inertial correction | $V_b = V'_b \left(1 + \frac{\pi^2 \gamma^2 v^2}{4L^2}\right)$ |

5. modulus of elasticity

$$E = \frac{r}{g} v_b^2$$

where:

W' = weight of both pole pieces = 71.4 gms

W = weight of specimen

r = radius of specimen

v = Poisson's ratio = 0.25

L = specimen length

γ' = specific weight of specimen.

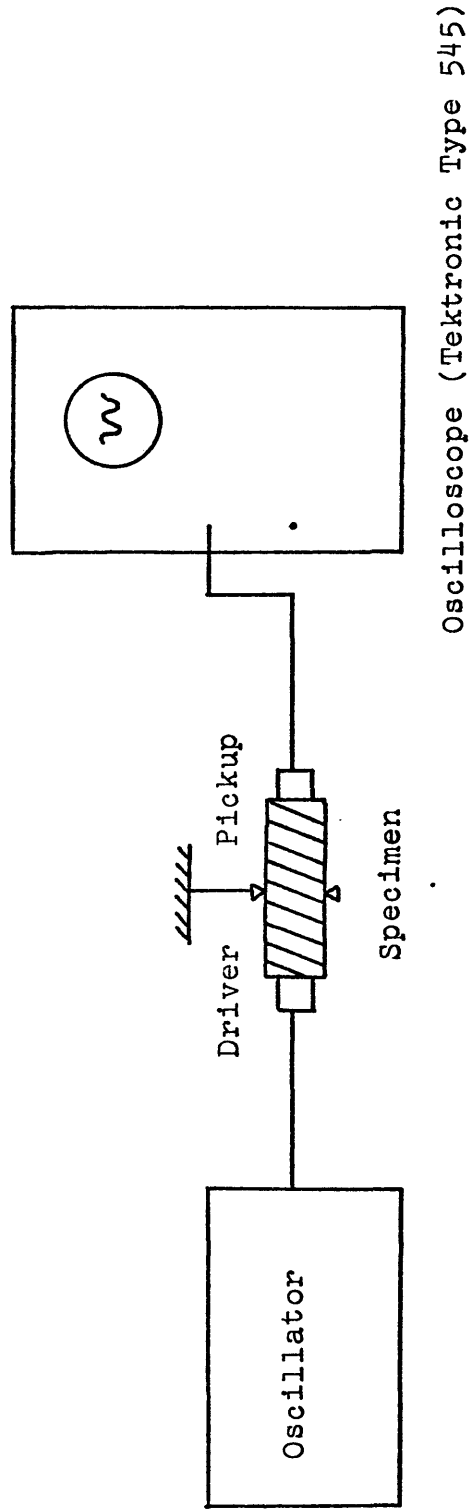


Figure 47. Diagrammatic Representation of the Resonant Frequency Apparatus.

Table 8. Calculations of Dynamic Young's Modulus from Resonant Frequencies.

Specimen	Length (in.)	Weight W(gms)	Measured		Calibrated		Bar Velocity V_b (ft/sec)	Specific Weight γ' (gms/in. ³)	Young's Modulus E(10 ⁶ psi)
			Frequency f_b' (c/sec)	Frequency f_b (c/sec)	Bar Velocity V_b' (ft/sec)	Bar Velocity V_b (ft/sec)			
*G-201	2.068	70.8	20200	40560	13979	14114	43.6	7.2	
G-202	1.979	67.6	22200	45640	15053	15198	43.5	8.2	
G-203	2.009	69.2	21900	44479	14890	15033	43.9	8.1	
G-204	2.048	70.0	24300	49086	16755	16916	43.5	10.2	
G-205	2.060	70.8	23000	46184	15857	16009	43.8	9.2	
*M-201	2.015	70.8	12800	25702	8627	8710	44.7	2.8	
M-202	2.023	71.1	13750	27555	9290	9379	44.7	3.2	
M-203	2.055	72.0	14700	29778	10027	10123	44.6	3.8	
M-204	2.052	71.8	14500	28919	9890	9985	44.6	3.7	
M-205	2.052	72.2	15000	29835	10203	10301	44.8	3.9	
*L-201	2.048	62.5	21100	45196	15423	15571	38.9	7.7	
L-202	2.024	59.9	20900	45813	15454	15603	37.7	7.6	
L-203	2.013	59.6	18700	41103	13790	13923	37.7	6.0	
L-204	1.991	59.0	16400	36244	12027	12142	37.7	4.6	
L-205	1.993	59.4	20300	44700	14849	14992	37.9	7.0	
*S-201	2.052	55.0	12200	28037	9588	9680	34.1	2.6	
S-202	2.052	55.1	11300	25945	8873	8958	34.2	2.2	
S-203	2.055	55.2	10340	23710	8121	8199	34.2	1.9	
S-204	2.068	55.7	10650	24303	8376	8451	34.3	2.1	
S-205	2.054	55.3	11600	26576	9098	9186	34.3	2.4	

*G - Colorado Red Granite, M - Yule Marble, L - Indiana Limestone, S - Gray Sandstone.

BIBLIOGRAPHY

- Attewell, P. B. (1962), Response of rocks to high velocity impacts: Bull. Inst. Min. Met., p. 705-724.
- Attewell, P. B. (1963), Dynamic fracturing of rocks: Parts I, II, and III, Colliery Engineering, p. 203-210, 248-252, 289-294.
- Bacon, L. O. (1962), A method for determining dynamic tensile strength of rock at minimum loading: U.S.B.M. R.I. 6067.
- Bell, J. F. (1966), An experimental diffraction grating study of the split Hopkinson bar experiment: J. Mech. Phys. Solids, v. 14, p. 309-327.
- Brace, W. F. and Bombolakis, E. G. (1963), Note on brittle crack growth in compression: J. Geophys. Res., v. 68.
- Cook, N. G. W. and Hodgson, K. (1965), Some detailed stress-strain curves for rock: J. Geophys. Res., v. 70, p. 2883-2888.
- Davies, R. M. (1948), A critical study of the Hopkinson pressure bar: Phil. Trans. Roy. Soc., A240, p. 375-437.
- Davies, E. D. H. and Hunter, S. C. (1963), The dynamic compression testing of solids by the method of the split Hopkinson pressure bar: J. Mech. Phys. Solids, v. 11, p. 155-179.

- Friedman, M., Perkins, R. D. and Perkins, S. J. (1968), Observation of brittle-deformation feature at the maximum stress of Westerly Granite and Solenhofen Limestone: Report by Mat. Structures Lab., Manufacturing Development, G.M. Corp., to the Defense Atomic Support Agency (DA-49-146-XZ-544), no. 11, 23 p.
- Goldsmith, W., Austin, C. F., Wang, C., and Finnegan, S. (1966), Stress waves in igneous rocks.
- Green, S. J. and Perkins, R. D. (1968), Uniaxial compression tests at strain rates from 10^{-4} /sec to 10^4 /sec on three geological materials: Proc. Tenth Symposium on Rock Mech., The Univ. of Texas at Austin.
- Griffith, A. A. (1924), Theory of rupture: Proc. First Int. Congress Appl. Mech., p. 55-63.
- Hakalehto, K. O. (1967), A study of the dynamic behavior of rock using the Hopkinson split bar method: M.S. thesis, Univ. of Minnesota, 82 p.
- Hakalehto, K. O. (1969), The behavior of rock under impulse loads: ACTA Polytechnica Scandinavica, Ch. 81, 60 p.
- Hoek, E. and Bieniawski, Z. T. (1965), Brittle fracture propagation in compression: Int. J. of Fracture Mech., v. 1, p. 137-155.
- Hopkinson, B. (1914), A method of measuring the pressure produced in the detonation of bullets: Phil. Trans. Roy. Soc., A213, p. 375-457.

- Kolsky, H. (1949), An investigation of the mechanical properties of material at very high rates of loading: Proc. Phys. Soc., B62, p. 676-706.
- Kolsky, H. (1963), Stress waves in solids: Dover, New York.
- Kumar, A. (1968), The effect of stress rate and temperature on the strength of Basalt and Granite: Geophysics, v. 33, no. 3, p. 501-510.
- Lindholm, U. A. (1964), Some experiments with the split Hopkinson pressure bar: J. Mech. Phys. Solids, v. 12, p. 317-335.
- Miller, M. H. (1966), The effect of stress wave duration on brittle fracture: Int. J. Rock Mech. Min. Sci., v. 3, p. 191-203.
- Perkins, R. D. and Green, S. J. (1969), Uniaxial stress behavior of porphyritic tonalite at strain rates to 10/sec: Report by Mat. Structures Lab., Manufacturing Development, G.M. Corp. to the Defense Atomic Support Agency (NWER Subtask SB047), no. 2, 38 p.
- Rinehart, J. S. (1960), On fractures caused by explosive and impacts: C.S.M. Quarterly, v. 55, no. 4.
- Robertson, E. C. (1955), Experimental study of the strength of rocks: Geol. Soc. Amer. Bull., v. 66, p. 1275.
- Scholz, C. A. (1968), Mechanism of creep in brittle rock: J. Geophys. Res., v. 73, no. 10, p.

- Watstein, D. (1963), Effect of straining rate on the compressive strength and elastic properties of concrete: J. Amer. Concrete Inst., Title No. 49-52, p. 729.
- Wawersik, W. R. (1968), Detailed analysis of rock failure in laboratory compression tests: Ph.D. Thesis, The Univ. of Minnesota, 165 p.